TOWARD SUB-10 NM LITHOGRAPHIC PROCESSES: EPOXY-BASED NEGATIVE TONE MOLECULAR RESISTS AND DIRECTED SELF-ASSEMBLY (DSA) OF HIGH χ BLOCK COPOLYMERS

A Dissertation
Presented to
The Academic Faculty

by

Jing Cheng

In Partial Fulfillment
of the Requirements for the Degree
Doctor of Philosophy in the
School of Chemistry and Biochemistry

Georgia Institute of Technology
August 2013

TOWARD SUB-10 NM LITHOGRAPHIC PROCESSES: EPOXY-BASED NEGATIVE TONE SINGLE MOLECULE RESISTS AND DIRECTED SELF-ASSEMBLY (DSA) OF HIGH χ BLOCK COPOLYMERS

Approved by:

Dr. Laren M. Tolbert, Advisor
School of Chemistry & Biochemistry
Georgia Institute of Technology

Dr. Clifford L. Henderson, co-Advisor
School of Chemical & Biomolecular Engineering
Georgia Institute of Technology

Dr. David Collard
School of Chemistry & Biochemistry
Georgia Institute of Technology

Dr. Joseph Perry
School of Chemistry & Biochemistry
Georgia Institute of Technology

Dr. Thomas Orlando
School of Chemistry & Biochemistry
Georgia Institute of Technology

Date Approved: July 1, 2013

ACKNOWLEDGEMENTS

I wish to thank Dr. Laren M. Tolbert and Dr. Clifford L. Henderson for their invaluable support and advice throughout my PhD study. They encouraged me to pursue my ideas in the lithographic field which I found exciting. They have taught me how to think, how to criticize and how to develop new ideas. I have learnt how to be a scientific researcher from our many discussions.

Special thanks to Dr. David Collard, Dr. Joseph Perry and Dr. Thomas Orlando for their participation in my thesis committee and their helpful suggestions on my research. I also would like to thank Intel for giving advice and funding my project.

I would like to thank the Tolbert and Henderson group members. Special thanks go to Dr. Janusz Kowalik and Dr. David Noga, who spent lots of time teaching me the organic synthesis and the use of many characterization tools; and to Dr. Richard Lawson, who is so knowledgeable and always helpful when I have questions and problems. Many thanks to Dr. Wei-Ming Yeh for helping with the clean room experiments. Also I would like to thank Nathan Jarnagin and Andrew Peters for their help and collaboration on our Intel projects. I would like to thank Dr. Hua-Wei Chu for his encouragement when I had problems on my research and frustration on the job hunting. I would like to thank Juan Vargas and his wife for their warmness when I first came to Atlanta and so much help during my stay here. Thanks to Dr. Kyril Solntsev, Dr. Anthony Baldridge, Dr. EA Gould, Dr. Russell Vegh, Jose Baltazar and Brett Fellows who gave great help during my PhD study at Georgia Tech.

I would like to thank my dear friends who I made in Georgia Tech. Our friendship is my greatest treasure in my life. Many thanks to my boy friend Yuan Li who has been so supportive. Last, I would like to thank my parents for their love. They have been always giving me happiness and strength.

TABLE OF CONTENTS

LIST OF FIGURES

LIST OF SYMBOLS AND ABBREVIATIONS

χ	Flory Huggins interaction parameter
^{1}H NMR	Proton-1 nuclear magnetic resonance
AFM	Atomic Force Microscopy
ATRP	Atom Transfer Radical Polymerization
AIBN	Azobisisobutyronitrile
CAR	Chemically amplified resist
CD	Critical dimension
DCM	Dichloromethane
dNbpy	4,4'-di(5- nonyl)-2,2'-bipyridine
DNQ	Diazonaphthoquinone
DSA	Directed Self-assembly
DSC	Differential Scanning Chromatography
DUV	Deep ultraviolet
EUV	Extreme ultraviolet
FTIR	Fourier transform infrared spectroscopy
GIR	Grazing angle infrared spectroscopy
GPC	Gel permeation chromatography
IC	Integrated circuit
IPA	isopropanol
LER	Line edge roughness
LWR	Line width roughness
mCPBA	meta-Chloroperoxybenzoic acid

MDSC	Modulated Differential Scanning Chromatography
MIBK	Methyl isobutyl ketone
NRT	Normalized remaining thickness
PAB	Post-apply bake
PAG	Photoacid generator
PEB	Post-exposure bake
PGMEA	Propylene glycol monomethyl ether acetate
PHOST	Poly(p-hydroxystyrene)
PMDETA	N,N,N',N',N''-pentamethyldiethylenetriamine
RIE	Reactive ion etch
SEM	Scanning electron microscope
TBAF	tetra-n-butylammonium fluoride
TLC	Thin layer chromatography
TMAH	Tetramethylammonium hydroxide

SUMMARY

This thesis is composed of two major topics: single molecule resists for the conventional "top-down" photolithography, and block copolymers and functional materials for the new "bottom-up" block copolymer lithography – the directed self-assembly (DSA) of block copolymers. It's becoming more and more difficult to make smaller, denser, and faster computer chips. The EUV lithography is not mature enough for high volume manufacturing. There's an increasing demand to design new materials to be applied in current lithographic process to get higher patterning performance.

The single molecule resists have gained increasing interest as their smaller size and monodispersity contribute to a potentially improved LER compared to the traditional chemically amplified polymeric resists which suffer from the polydispersity caused problems. The epoxy resists based on ring opening cationic polymerization have shown better LER than the positive tone molecule resists. In this work, the aqueous developable single molecule resists are introduced, synthesized and patterned. Efforts are made to design a negative tone epoxy-based resist without swelling in aqueous base development. A new group of epoxide other than glycidyl ether, cyclohexene oxide is introduced to functionalize BHPF molecular core and the patterning performance is compared with 2-Ep and 2-Ox. The BHPF-2CHEp shows better contrast curve due to the better controlled polymerization behavior. A 15 nm resolution has been obtained.

The directed self-assembly (DSA) of block copolymers as an alternative lithographic technique has received growing interest in the last several years for performing higher levels of pitch subdivision. Thus, novel materials are needed for high

resolution patterning for this technique. A 3-step simplified process for DSA by using a photodefinable substrate is introduced by using a functionalized polyphenol with an energy switchable group and a crosslinkable group. The first generation photodefinable substrates has successfully directed the self-assembly of symmetric PS-b-PMMA into lamellar structures.

Block copolymers with high repulsive interactions (characterized by χ value) are desired to provide high resolution imaging. Two high χ block copolymers PS-b-PAA and PS-b-PHEMA are successfully designed and synthesized via ATRP with controlled Mw and PDI. PS-b-PAA undergoes thermal reaction to form anhydride, ketone, and alkane sequentially. The size of the same PS-b-PAA polymer is tunable by varying the thermal annealing time. PS-b-PHEMA shows to be a suitable block polymer for the industry-friendly thermal annealing process. This block copolymer forms 15 nm pitch size lamella by using thermal annealing.

A self-complementary hydrogen-bonding urea group as a center group is proposed to facilitate the self-assembly of polymers. In this thesis, we compare two synthetic methods to make PS-Urea-Urea-PS. Finally, “click” chemistry shows high conversion. “Click” chemistry will be used for synthesis of PS-Urea-Urea-PMMA.

CHAPTER 1

INTRODUCTION TO NANOLITHOGRAPHY

1.1 Overview of Nanolithography Process

Nanolithography is the science of printing desired patterns on silicon wafers with patterned features that scale at dimensions from 10 to 100 nm. Nanolithography is a key step in semiconductor fabrication of integrated circuits (IC). The history and mechanism of nanolithography will be introduced in this chapter.

1.1.1 Basics of Nanolithography Process

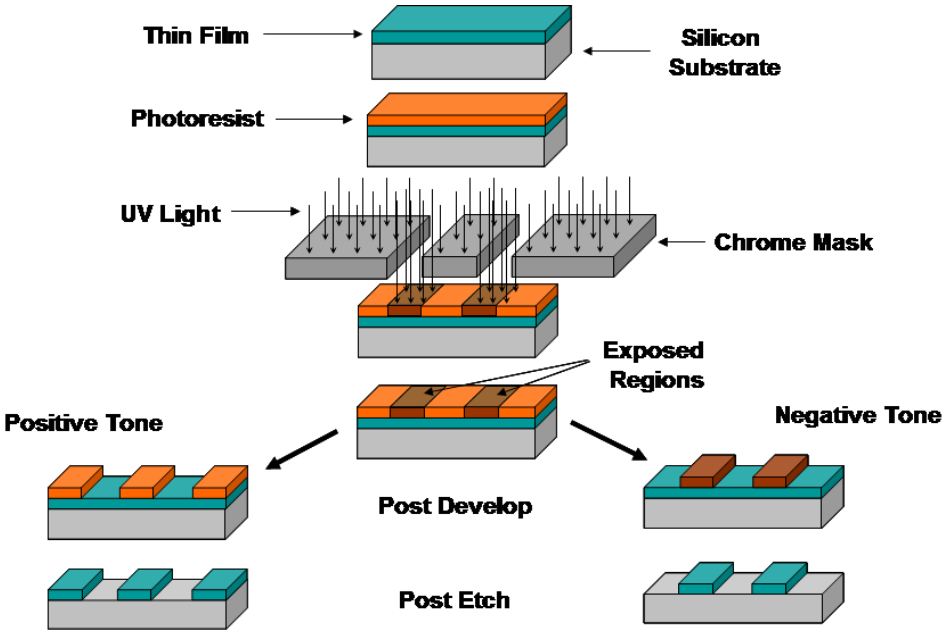

Figure 1.1 Lithographic imaging process.

Integrated circuits are fabricated by the "top-down" microlithographic process, which transfers complex micro-patterns from a single master to a number of copies **(Figure 1.1)**.[1] A radiation-sensitive material, called a "photoresist", is used to produce circuit patterns on silicon wafers in the presence of light, generally ultraviolet, and a mask. The exposed resist films are subsequently developed with a solvent. A positive-tone resist will become more soluble in the exposed region, while a negative-tone resist become less soluble in the developer. The remaining resist film after the development process must "resist" the following reactive ion etching, so that the bare areas on the silicon wafers will be etched to form desired topological patterns.

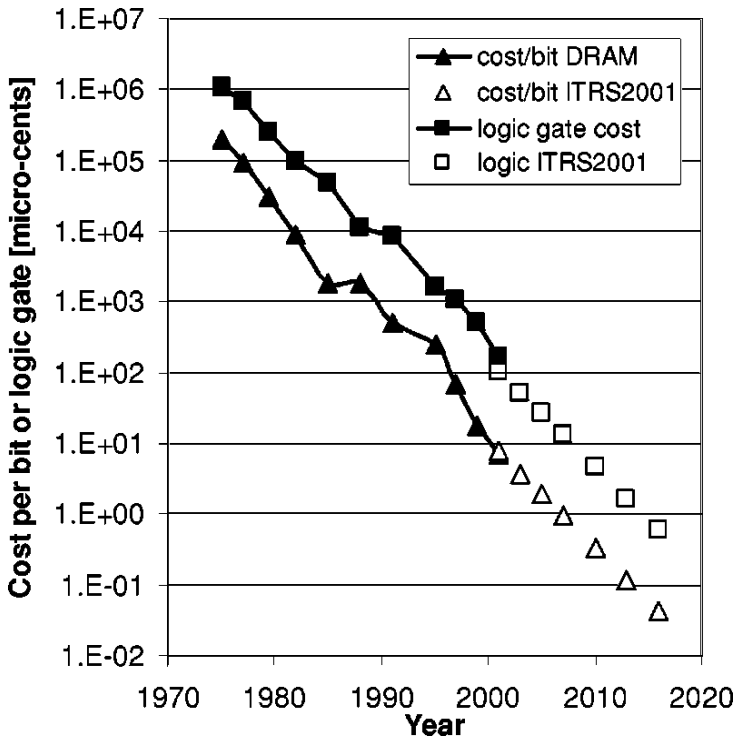

Figure 1.2 Cost decrease per DRAM bit and cost per CMOS logic gate. The roadmap projections are also shown.[2]

Moore's law has predicted that the number of transistors that can be placed inexpensively on an integrated circuit should double approximately every 18 to 24 months.[3] In other words, the cost of manufacturing both dynamic random access memory (DRAM) bits and logic gates is decreasing exponentially yearly, as shown in **Figure 1.2**.[2]

1.1.2 Exposure Tools

In an exposure tool setup, which is called the mask aligner, the photomask and the wafer are aligned to each other and the resist is exposed. The mask is aligned to the wafer in usually three different ways, contact, proximity and projection modes, see **Figure 1.3**.[4]

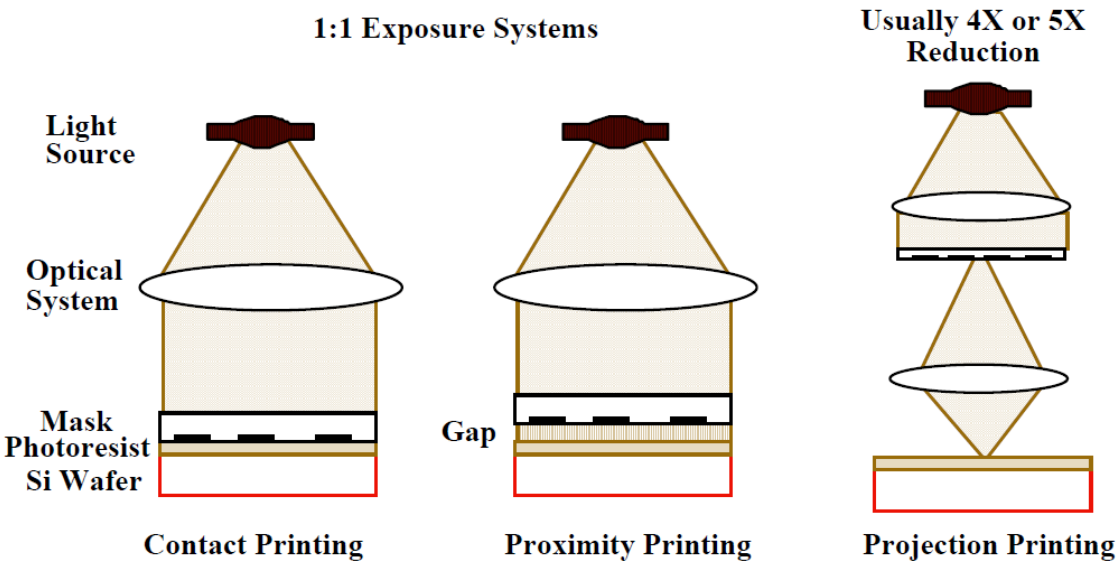

Figure 1.3 Three types of exposure systems: contact printing, proximity printing and projection printing.[4]

The incident light beam travels through the mask, creating a diffraction grating (series of lines and spaces with pitches of 2W). The radiation pattern onto the resist is an aerial image of the mask, see **Figure 1.4.**[4]

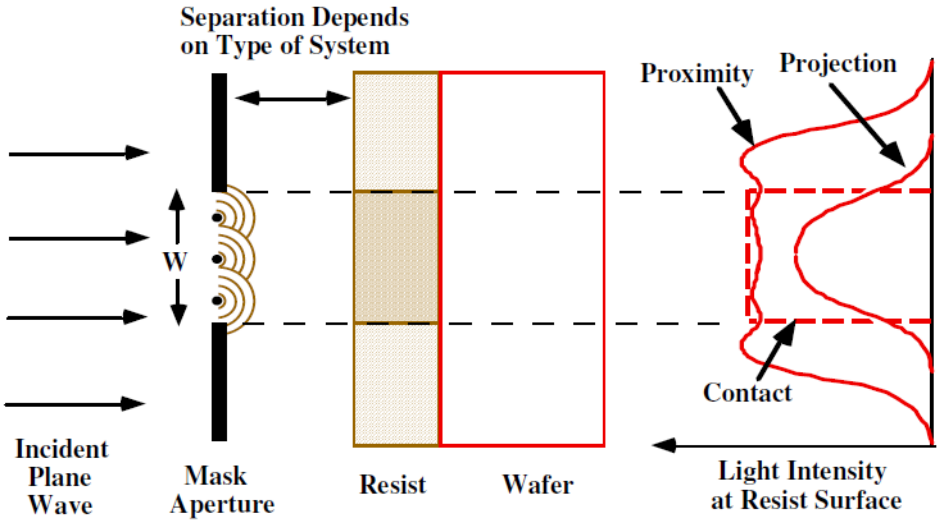

Figure 1.4. Diffraction grating aerial images produced in contact, proximity and projection exposure tools.[4]

As demonstrated by Raleigh's law, see **Equation 1.1**,

$$R=k\lambda/NA \qquad (1.1)$$

the lithographic resolution, R, is governed by the wavelength, λ, of light used during patterning. Also, the numerical aperture, NA, of the lens is another contributing factor for the feature resolution. A larger NA is needed for a smaller R, which means higher resolution. As shown in **Figure 1.5**, the NA could be expressed as:

$$NA = n \sin(\alpha) \qquad (1.2)$$

where α is the sin of the maximum refraction angle. The NA is governed by n, the refractive index of the media between the mask and the lens. The refractive index of air and water are 1.00 and 1.43, respectively. Thus, a larger n will ensure a larger NA. In 193 nm immersion lithography, the air gap between the lens and mask is replaced by high purity water. The resolution is enhanced by about 30-40% (depending on materials used).

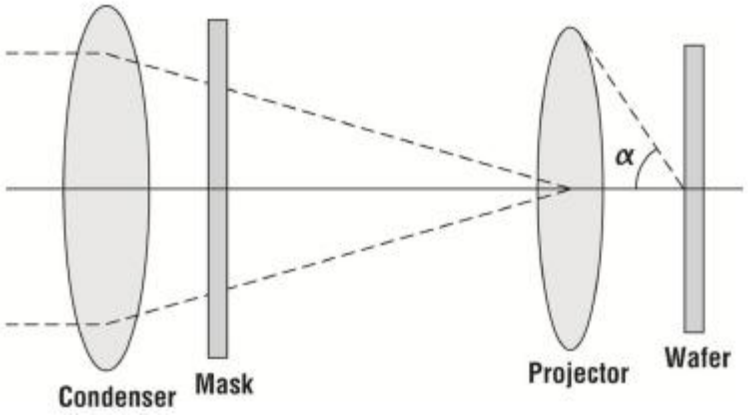

Figure 1.5. The lithographic tools set up.[4]

Unfortunately, the depth of focus, σ, is limited by NA, as shown in **Equation 1.3**.

$$\sigma = \frac{n\lambda}{NA^2} \qquad (1.3)$$

Since σ is inversely proportional to NA^2, an increasing NA would significantly affect the depth of focus. Thus, there's not too much tolerance with the numerical aperture change.

In order to meet the ever decreasing feature sizes, industry is moving to shorter wavelengths, as shown in **Figure 1.6**.[5] Next generation lithographic (NGL) techniques, such as extreme ultraviolet lithography (EUV-lithography), X-ray lithography, and electron beam lithography, are currently under active research. Resists are designed differently to meet the changes of exposure tools.

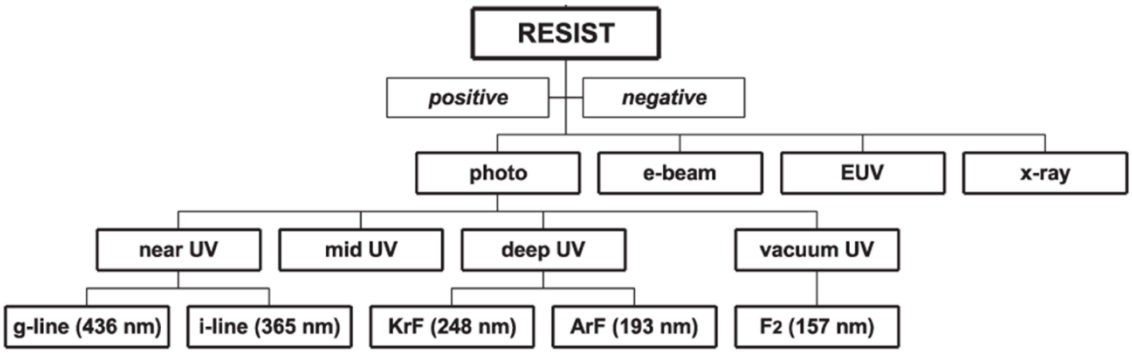

Figure 1.6. Classification of resists by exposure sources.[5]

1.2 Resists

Resists can be classified by the tone (positive or negative), exposure sources (various exposure wavelengths) or photochemical mechanisms (non-chemically amplified or chemically amplified). There are several basic requirements for all types of resists:[5]

- Good solubility switch in developing solvents
- Good film formation ability with reasonable adhesion to various substrates
- Good chemical stability for storage in solution and thermal treatment
- High dry etch resistance
- Good patterning performance (low LER, high resolution, high sensitivity and high contrast)

Those requirements must be taken into careful consideration when designing the chemical structure and formulation of resists. Other factors, like environmental safety and the cost of synthesis, must also be considered. As the semiconductor industry is driven by Moore's law, new resist designs are required to meet the increasing demand in terms of shrinking pattern size.

1.2.1 Evaluation of the Patterning Performance of Resists

In addition to the resolution of the resist patterns, other factors, such as line edge roughness (LER), line width roughness (LWR), sensitivity and contrast, are important to evaluate the patterning performance of a resist. Line width roughness (LWR) stands for the variation of the resist line width along a patterned line, see **Figure 1.7**. The variation along the line edge itself is called line edge roughness (LER).

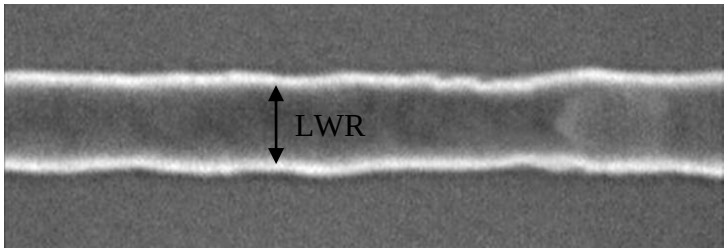

Figure 1.7. Resist line pattern.

LER becomes an important control factor when pattern features are below 100 nm, which significantly affects pattern quality. There are a number of contributing factors to the variation of LER, such as fluctuation of the incident protons/electrons from the exposure beam, the chemical distribution of the resist components, the size/molecular distribution of the resist materials along the line edge, which are mostly polymers, and the diffusion of the photoacids, which is considered the most serious problem to the

pattern quality in chemically amplified systems. The 3σ deviation value of a line edge from a straight line is used to characterize LER. For patterns below 100 nm, the 3σ value is usually about 5% of the nominal critical dimension (CD).[6]

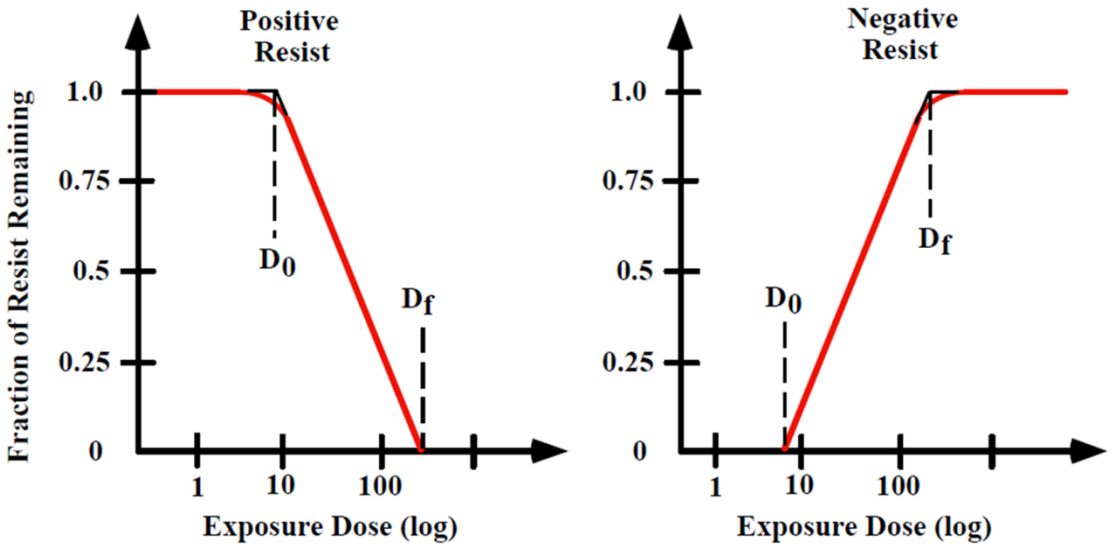

Figure 1.8. Contrast curves of positive and negative tone resists.[4]

Figure 1.8 shows the contrast curves of positive and negative tone resists.[4] The contrast curve is plotted as the remaining film thickness (normalized to the initial film thickness) of the exposed film, after development, as a function of the logarithmic exposure dose. The contrast, γ, could be calculated from the slope of the linear part of the curve, which is defined as:

$$\gamma = \frac{1}{\log_{10}\frac{D_f}{D_0}} \qquad (1.4)$$

High contrast is needed for a high resolution image to prevent any light diffraction causing the image to blur.[4]

A high resist sensitivity is needed for high throughput wafer production, although a too sensitive patterning system is to be avoided as it is unstable, temperature dependent and prone to noise.[4] For positive tone resists, the sensitivity is defined as the minimum dose that is required to completely clear the resist film to the substrate, which is D_f in **Figure 1.8.** In the case of negative tone resists, the sensitivity is generally defined as the dose when 50% of the original thickness is retained after development.[5]

1.2.2 The Concept of Chemical Amplification

Before the invention of chemically amplified resist systems, non-chemically amplified resists were used for many years. The most popular resist system used in the i-line exposure system was diazonaphthoquinone (DNQ)/novolac positive tone resist, which was invented by S üss.[7] This is a two-component system which is composed of a base soluble novolac resin, see **Figure 1.9**, and a photosensitive compound diazonaphthoquinone (DNQ). When the DNQ is evenly blended with the novolac resin, the DNQ molecule acts as a dissolution inhibitor, which prevents the dissolution of the novolac resin in aqueous base. However, once the DNQ molecule is irradiated with UV light, it decomposes by releasing N_2 gas, rearranges and reacts with ambient water to form a dissolution enhancer, which contains carboxylic acid functional group thus promotes the dissolution of novalac resin in aqueous base developer.[8]

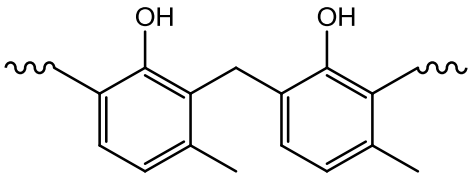

Novolac resin

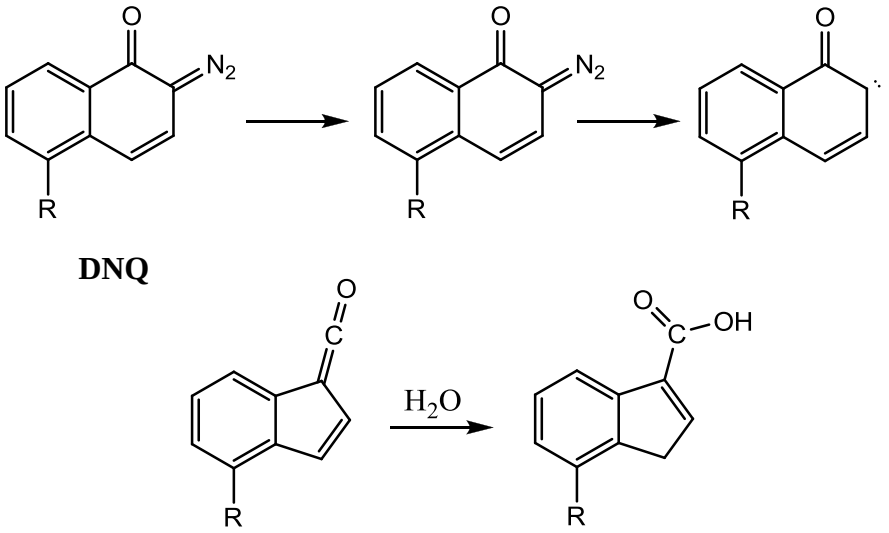

Figure 1.9 Diazonaphthoquinone (DNQ)/novolac positive tone resist.[7]

The DNQ/novolac positive tone resist was abandoned when the exposure technique moved to a shorter wavelength, the 248 nm deep UV (DUV) system. The novolac resin strongly absorbs in this region which significantly obstructs the patterning performance of this system.[5] Another use of non-amplified resists today is in e-beam lithography. There are a few commonly used resists: PMMA (polymethylmethacrylate)[9] and ZEP (a methyl styrene-chloromethyl acrylate copolymer)[10] as positive tone resists, and HSQ (hydrogen silsesquioxane)[11] as a negative tone resist. The e-beam lithographic mechanisms of the PMMA and ZEP resists are very similar: the polymer backbones

undergo high energy electron induced bond cleavage when they are exposed to the e-beam, which leads to the decomposition of the polymer into smaller molecular chains. Those smaller molecular polymer chains are more soluble in the developer (organic solvents normally). Thus the exposed area is developed to the substrate to produce a relief image. The e-beam exposed HSQ monomers ($H_8Si_8O_{12}$) undergo a redistribution reaction in which the silicon crosslinks via oxygen bridges after generating silanes (SiH_4).[12] Thus the exposed regions crosslink and form an insoluble film after development. Such resists are capable of achieving very high resolution image (half pitch ~ 10 nm) by using e-beam lithography. However, due to the low throughput of the e-beam lithography, it is only feasible for small scale research and mask design. It may take days to print a whole wafer using e-beam lithography. High volume production of wafers requires high resist sensitivity. None of those non-chemical amplified resists can meet current high demand for wafer production.

In 1982, Ito, Willson, and Fréchet developed the chemical amplification concept for high throughput resist exposure.[13, 14] In the chemically amplified system, the resist (transparent polymeric or single molecule material) is often blended with a photoacid generator which usually constitutes less than 5 wt% of the resist. Other additives may present, such as a base quencher.[5] Once the PAG is irradiated by the exposure source, it decomposes to form a super strong acid. This acid catalyzes numerous events such as the deprotection in positive tone system or crosslinking in negative tone system. The quantum yield of the photoreaction is significantly increased using this method.

Triarylsulfonium salts are common PAGs used in photolithography. They are stable up to 350 ℃ and sensitive to deep UV, e-beam, and X-ray irradiation.[5] The mechanism of the photo generation of PAGs has been well studied. **Figure 1.10** shows the mechanism for a triphenylsulfonium hexafluoroantimonate (TPS-SbF_6) salt.[15-18]

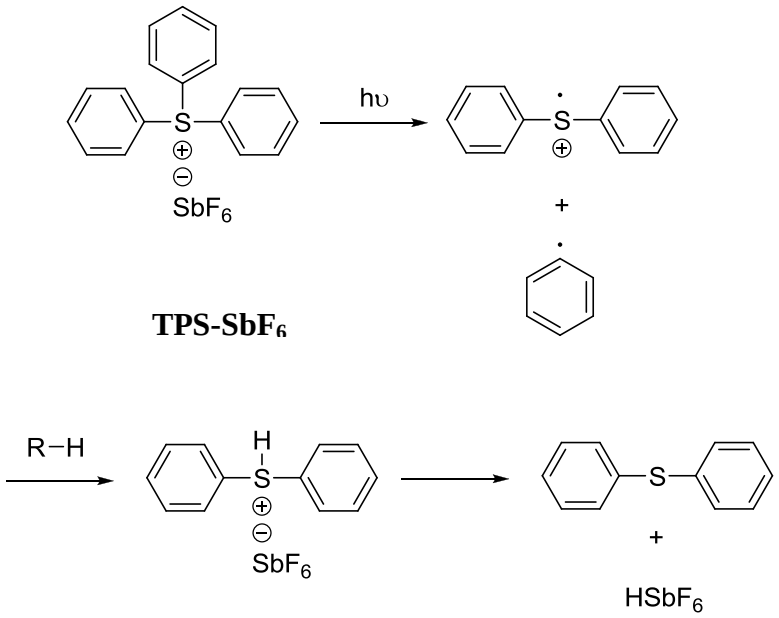

Figure 1.10 Photo generation mechanism for triphenylsulfonium hexafluoroantimonate (TPS-SbF_6) salt.

The PAG, once irradiated, will trigger numerous reactions in the resist, deprotection for positive tone resists and polymerization for negative tone resists. **Figure 1.11** shows the deprotection mechanism for the positive tone resist poly (4-tertbutoxycarbonyloxystyrene) (PBOCST).[5] PBOCST undergoes acid catalyzed deprotection to give aqueous base soluble polyphenol and a few volatile residues (CO_2 and isobutene). While the protected polyphenol PBOCST is hydrophobic and insoluble in

polar solvent such as alcohol and aqueous base, the unexposed region would be remaining on the substrate after development.

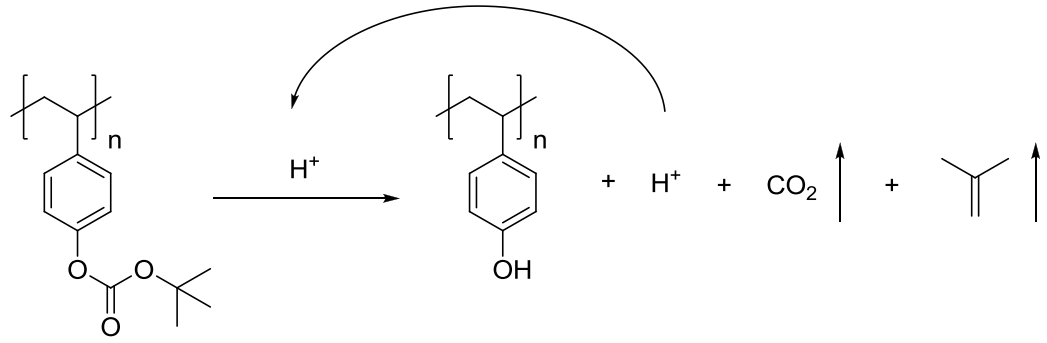

PBOCST

Figure 1.11 The deprotection mechanism for a positive tone resist poly (4-tertbutoxycarbonyloxystyrene) (PBOCST).

Figure 1.12 shows the mechanism of acid catalyzed cationic ring opening polymerization for an epoxide resist.[19] Non-nucleophilic anions such as hexafluoroantimonate and hexafluoroarsenate are chosen as PAGs to prevent the risk of nucleophilic trapping the growing cationic chain.[5] This type of reaction has been applied to a widely used negative tone resist SU-8 (see **Figure 1.12**) for micro-electromechanical systems (MEMS) fabrication.[20, 21]

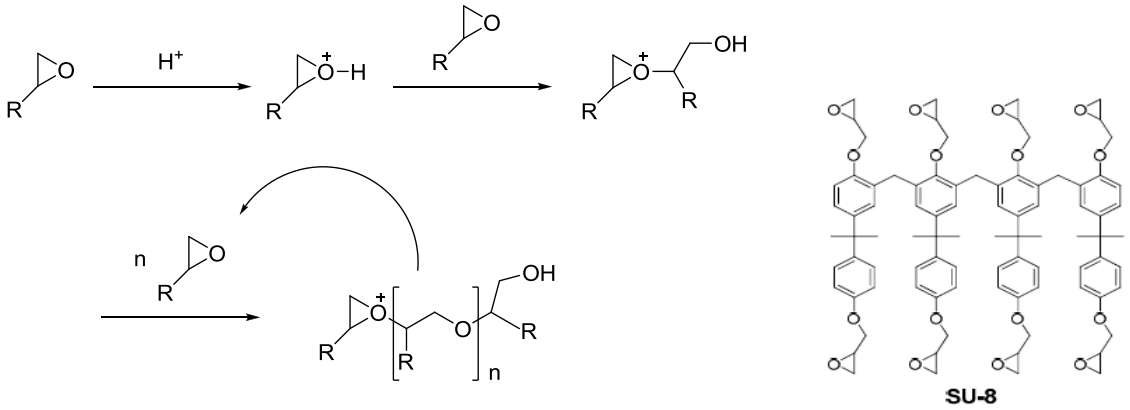

Figure 1.12 The mechanism of acid catalyzed cationic ring opening polymerization for an epoxide resist[19] and chemical structure of SU-8.

1.3 High Resolution Patterning

1.3.1 EUV Lithography

For the past several decades, the semiconductor industry has been driven by "Moore's Law". There is an increasing demand for high resolution patterning to manufacture smaller, denser and faster computer chips. By shortening the wavelength of the exposure source, higher resolution can be obtained. Lithography has evolved from 365 nm UV light to deep UV at 248 nm and 193 nm, although the 157 nm was abandoned due to the lack of lens materials; the next step is EUV (extreme ultra violet) at 13.5 nm.

There are many challenges in the application of EUV. First of all, the conventional lens can't be used in EUV system, as they absorb the light. A multilayer mirror (MLM) with a special coating must be used, see **Figure 1.13**.[22] However, these

mirrors still absorb about 30% of the light. The more mirrors the instrument uses, the less light it can transmit. Any gas in the light path, such as air or nitrogen, will also absorb the light. Thus the entire light path must be maintained inside a vacuum chamber.[22] Due to the low power of the light source, EUV is not mature enough for high volume manufacturing.[23]

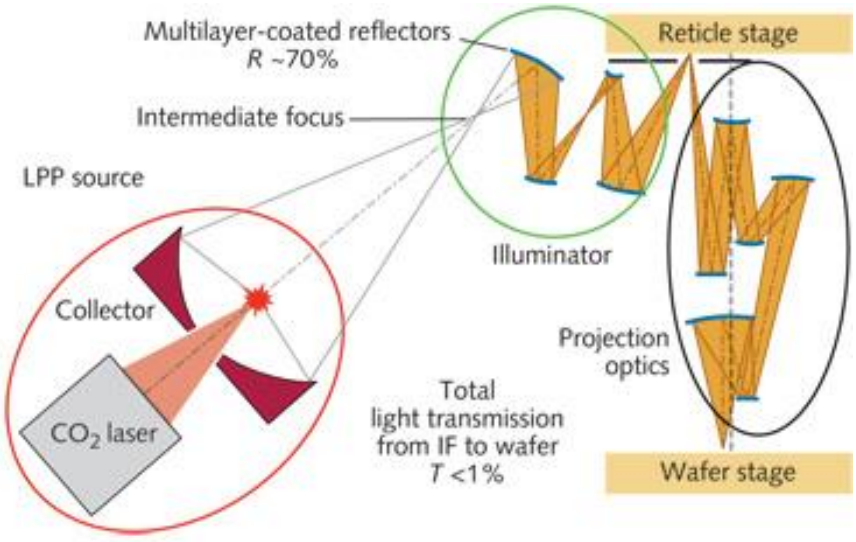

Figure 1.13. A multilayer mirror (MLM) system for EUV.[22] Pulses from the CO_2 laser illuminate droplets of tin (the red spot). 13.5 nm light is radiated in all directions. A set of mirrors collect and direct the light to focus onto the wafer stage. The overall transmission to the wafer stage is less than 1%.

1.3.2 Multiple Patterning

Multiple patterning has been introduced to be used with state-of-the-art 193 nm immersion lithography tools for the 32 nm half-pitch node and below. Although it increases the cost and complexity, multiple patterning has been adopted by the leading chip concerns and will continue to play a leading role before EUV lithography or any other techniques come to maturity. There are a few types of double patterning routes. For example, see **Figure 1.14**, one of the very first introduced paths is called a litho-etch, litho-etch (LELE) approach.[24] Another route, which is called litho-freeze process, 'freezes' the first step patterned resist and applies a second step of resist deposition and patterning, see **Figure 1.14**.[25]

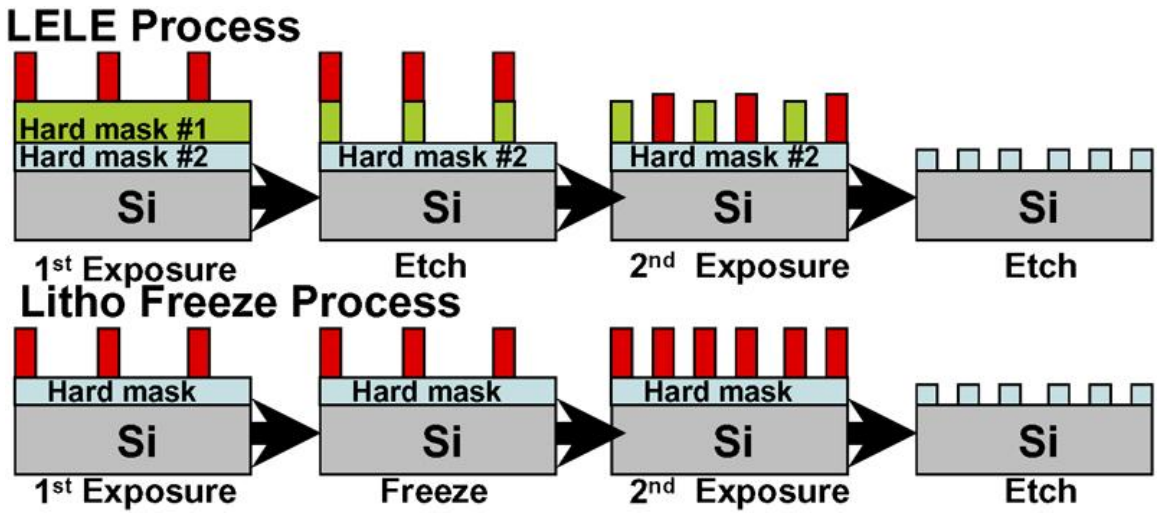

Figure 1.14. Examples of the process flow of LELE process and Litho Freeze process.[26]

1.3.3 Preview of the Thesis

The increase of complexities in exposure tool designs and lithographic process flows require better patterning materials to be developed simultaneously to release the pressure of maintaining Moore's law. This PhD work represents efforts on single molecule resist materials for conventional photolithography and on polymers for directed self-assembly (DSA) as an alternative lithographic technique.

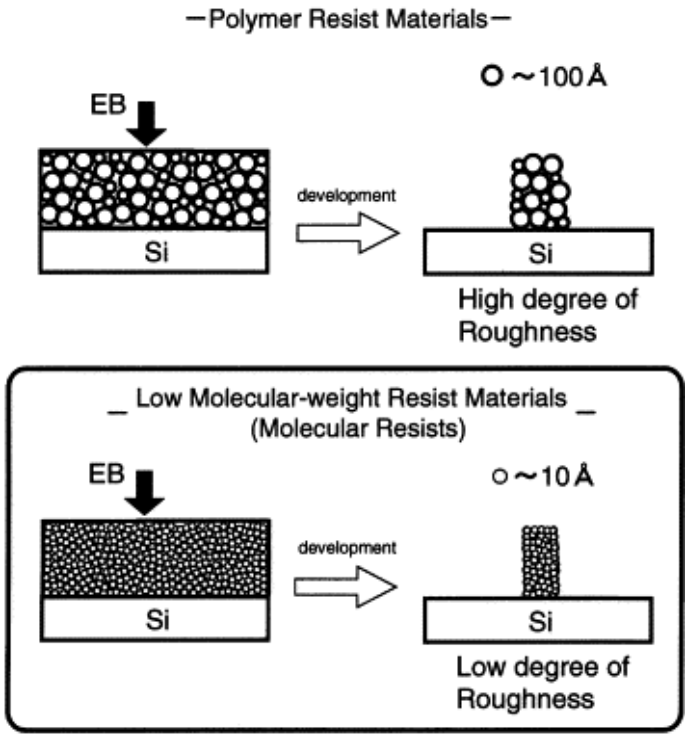

Figure 1.15. Comparison between polymeric resists and single molecule resists.[27]

Single molecule resists, as a new family of resist materials, have gained increasing interest in recent years. The monodispersity and the small size are the most attractive features compared to the conventional polymeric resists, see **Figure 1.15**.[27] This work is focusing on developing epoxy-based negative tone single molecule resists with advanced patterning performance. A 15 nm line resolution is achieved by using a cyclohexene oxide based resist. Also, a dual-developable (organic solvent/aqueous base) resist is successfully synthesized and patterned, without swelling.

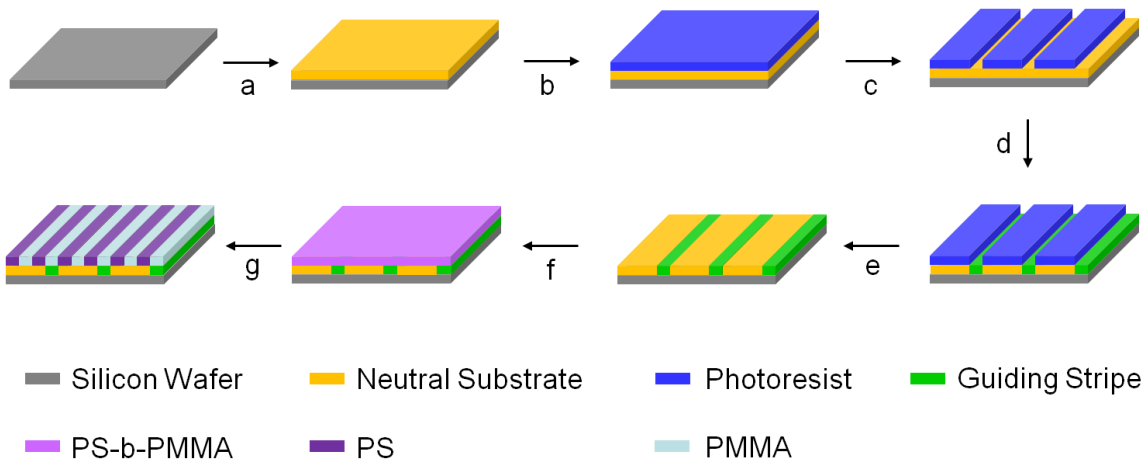

Figure 1.16. A typical DSA process. a. neutral underlayer deposition; b. photoresist deposition; c. photoresist patterning; d. surface decoration (eg. O_2 plasma); e. photoresist removal; f. block copolymer deposition; g. annealing (by solvent or heat)

Another field that falls within the purview of this thesis is block copolymer lithography (BCPL) utilizing directed self assembly (DSA). This alternative lithographic technique has received growing interest in the last several years for performing higher levels of pitch subdivision. We have designed a directly photodefinable substrate

material to simplify the current DSA process. We report the synthesis of PS-b-PAA and PS-b-PHEMA as high Flory-Huggins interaction parameter block copolymer for high resolution patterning. The last part of this thesis work is developing a robust synthetic method for PS-Urea-Urea-PS, which has a bis-urea linking group. This introduces a potential synthetic method for PS-Urea-Urea-PMMA, which may have a smoother LER due to the H-bonding the urea groups provide. This thesis has provided solutions for new materials design used in lithography. The results have shown that high resolution patterning has been achieved.

1.4 References

1. Thompson, L. F.; Willson, C. G.; Bowden, M. J. *Introduction to Microlithography, 2nd ed., ACS, Washington, DC* **1994**.
2. Brunner, T. A. *J. Vac. Sci. Technol. B* **2003,** 21, (6), 2632-2637.
3. *Excerpts from A Conversation with Gordon Moore: Moore's Law. Video Transcripts. Intel Museum.*
4. Plummer, J. D.; Deal, M.; Griffin, P. D. *Pearson Education* **2009**.
5. Ito, H. *Adv Polym Sci* **2005** 172, 37-245.
6. Mack, C. A. *Field Guide to Optical Lithography, SPIE Press, Bellingham, WA* **2006**.
7. Süss, O. *Liebigs Ann Chem* **1944**, 556:65.
8. Pacansky, J.; Lyerla, J. *IBM J Res Dev* **1979**, 23-42.
9. Hu, W.; Bernstein, G. H.; Sarveswaran, K.; Lieberman, M. *J. Vac. Sci. Technol. B.* **2004,** 22, 1711.
10. S.Hosaka; Sano, H.; Shirai, M.; Sone, H. *Appl. Phys. Lett.* **2006,** 89, 223131.

11. Baek, I. B.; Yang, J. H.; Cho, W. J.; Ahn, C. G.; Im, K.; Lee, S. *J. Vac. Sci. Technol. B.* **2005,** 23, 3120.

12. Olynicka, D. L.; Cord, B.; Schipotinin, A.; Ogletree, D. F.; Schuck, P. J. *J. Vac. Sci. Technol. B* **2010,** 28, (3), 581-587.

13. Iwayanagi, T.; Ueno, T.; Nonogaki, S.; Ito, H.; Wilson, C. G. *Materials and Processes for Deep UV Lithography," in ACS Advances in Chemistry Series 218*.

14. *"Electronic and Photonic Applications of Polymers," NI. J. Bowden and S. R. Turner, eds., American Chemical Society, Washington, D. C.* **1988**, 109.

15. Crivello, J.; Lam, J. *J Polym Sci Polym Lett Ed* **1979,** 17, 759.

16. Pappas, S. *J Imaging Technol* **1985,** 11, 146.

17. Dektar, J.; Hacker, N. *J Am Chem Soc* **1990,** 112, 6004.

18. Pohlers, G.; Scaiano, J.; Sinta, R.; Brainard, R.; Pai, D. *Chem Mater* **1997,** 9, 1353.

19. Ortiz, R. A.; Cisneros, M. d. L. G.; Garc á, G. A. *Polymer* **2005,** 46, (24), 10663–10671.

20. Ito, H.; Willson, C. *In: Davidson T (ed) Polymers in electronics. ACS Symposium Series 242, American Chemical Society, Washington, D.C.* **1984**, 11.

21. LaBianca, N.; Gelorme, J. *Proc 10th International Conference on Photopolymers* **1994**, 239.

22. Cymer. *http://www.cymer.com/euv_lithography/*.

23. ASML. *http://www.asml.com EUV: Questions and answers*.

24. Drapeau, M.; Wiaux, V.; Hendrickx, E.; Verhaegen, S.; Machida, T. *Proc. SPIE* **2007,** 6521, 652109.

25. Hori, M.; Nagai, T.; Nakamura, A.; Abe, T.; Wakamatsu, G.; Kakizawa, T.; Anno, Y.; Sugiura, M.; Kusumoto, S.; Yamaguchi, Y.; Shimokawa, T. *Proc. SPIE* **2008,** 6923, 69230H.

26. Zimmerman, P. *http://spie.org/x35993.xml#B4 Micro/Nano Lithography* **2009**.

27. Kadotaa, T.; Kageyamaa, H.; Wakayab, F.; Gamob, K.; Shirota, Y. *Materials Science and Engineering: C* **2001,** 16, (1-2, 20), 91-94.

CHAPTER 2

EPOXY-BASED CHEMICALLY AMPLIFIED NEGATIVE-TONE SINGLE MOLECULE RESISTS WITH ADVANCED PATTERNING PERFORMANCE

2.1 Introduction

New imaging materials may be required to meet the increasing manufacturing demands. Conventional resists, such as diazonaphthoquinone (DNQ)/novolac resists for i-line lithography and polymethacrylate-based one component resists for deep UV technique, suffer from low sensitivity.[1] The chemical amplification concept proposed in 1982 by Ito, Willson, and Fréchet well supports high resolution resist systems.[2, 3] The acid-catalyzed reactions triggered by photochemical generation of acid provide extremely high sensitivities and high throughput patterning. Current polymeric chemically amplified resists (CAR) are developed with new functional groups and chemistry suited to the emerging shorter wavelength. They are able to form stable thin film at high temperatures due to their high glass transition temperature (T_g) and amorphous properties. However, in the polymeric resist system, polymer molecular weight, molecular weight distribution (MWD),[4, 5] and polymer aggregation[6] are the main causes to the poor lithographic performance, such as the poor line edge roughness (LER) and line width roughness (LWR) as the smallest feature sizes move to 32 nm and below. Further, acid diffusion in polymeric CAR is a potential resolution limiter as too much diffusion reduces chemical contrast, leading again to more roughness.[7] The imaging resolution is hampered, where

the acid, generated during exposure, diffuses outside of the patterned area during the post-exposure bake (PEB), thus blurring the final resist image.[8]

In recent years, molecular glass (MG) resists have received significant attention as potential replacements for polymer based resists in high resolution lithography. Such small molecules possess structural features that render high T_g, despite their small size. Their monodispersity and reduction of "pixel" size have directly correlated to the decrease of LER compared to conventional polymeric resists **(Figure 2.1)**[9]. Also, as recent stochastic simulation studies show, the smaller segments of free volume in molecular glass systems can, to some extent, inhibit the diffusion of acid molecules.[10]

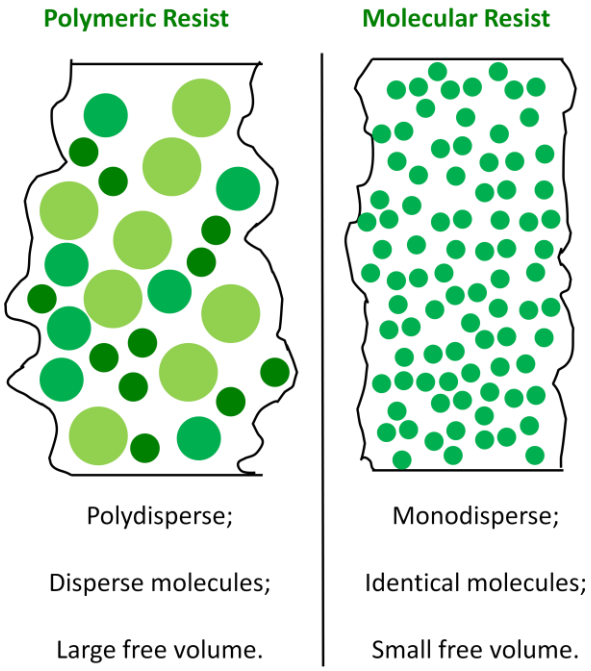

Figure 2.1 Comparison between molecular glasses and polymeric resists.

Ober *et al.* have conducted research on positive tone molecular CARs based on acid catalyzed deprotection of acid-labile protected phenolic compounds.[11] However, to

normal molecular CARs, LER persists as a problem due to photoacid diffusion. Reduced mechanical strength and integrity compared to polymeric resists are also considered as their disadvantages in patterning. We currently study high resolution chemically amplified molecular resists based on cationic polymerization, such as epoxide polymerization, to achieve solubility switching by cross-linking of monomers in the resist film.[12] Cationic polymerization, as an imaging mechanism different from an acid catalyzed deprotection based mechanism, provides several potential advantages.[12] Among these advantages, the negative tone resists should have superior mechanical strength compared to positive tone molecular resists because they could form cross-linked high molecular weight films upon acid catalysis. There is an additional benefit due to their polymerization mechanism: in cationic polymerization resists, the photoacid is only active for the protonation of an epoxide. After the epoxide is protonated and polymerization initiates, the active site is attached to the end of a rapidly growing chain or network. This is in contrast to the acid catalyzed deprotection mechanism in positive tone resists, in which the acid is active to each deprotection process. Finally, another potential advantage of these types of resists is that the cationic polymerization is a zero mass loss process, which should contribute to very low or negligible levels of outgassing.

Cationic polymerization and cross-linking of epoxy-based polymer resists have been used for several years in both electron-beam and deep-UV (DUV) applications, such as the widely-used commercially available oligomeric resist SU-8.[13] The Henderson group has studied a series of epoxy-based fully functional molecular resists – 2-Ep, 3-Ep, and 4-Ep.[12] These molecular resists have high patterning performance: high sensitivity with low line edge roughness and excellent resolution. Additionally, they all show superior performance compared to SU-8 in high resolution dense patterns **(Figure 2.2)**. It has been proposed that the better imaging of molecular resists is due to significantly more

cross-links forming in the film. This leads to a denser film which is hardly subject to swelling like SU-8 during development.[12]

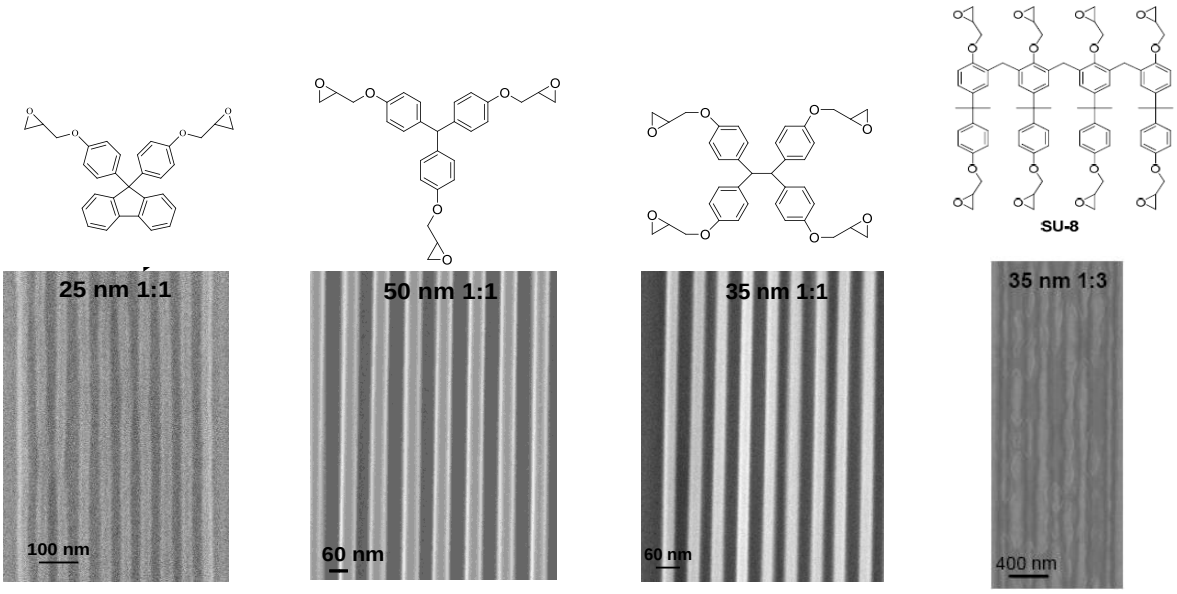

Figure 2.2. SEM of e-beam (100 keV) patterning of epoxy-based resists with a PEB of 60 ℃ for a variety of line/space patterns.

2.2 Synthesis Methods for Epoxy-Based Single Molecules

Three different synthetic routes were used for the synthesis of epoxide compounds: direct alkylation of poly-phenol by epichlorohydrin, epoxidation of alkenes by oxone ($2KHSO_5 \cdot KHSO_4 \cdot K_2SO_4$) or mCPBA. In the case of the alkene substrates, rate of epoxidation increases with the number of electron-donating substituents on the double bond, which determines the ease of the experimental procedure and reaction work-up. There are two kinds of alkene substrates in this study: aryl cyclohexenyl ether and aryl allyl ether. The former is a better substrate for epoxidation, which could be easily epoxidized by either mCPBA (see synthesis of SBI-2CHEp) or oxone (see synthesis of

BHPF-2CHEp) under mild conditions. However, epoxidaion of an aryl allyl ether is retardant due to its electron-deficiency property.

The two epoxidation reagents are compared. mCPBA, with modest epoxidation strength, epoxidizes aryl cyclohexenyl ethers to full conversion with a relatively short reaction time at RT. Also, it does not oxidize phenol, as indicated in our model reaction in which p-cresol remains intact after mCPBA treatment. However, it fails to epoxidize aryl allyl ethers at RT. Only 30% conversion at 70 ^{o}C is obtained, though high temperature can't be used in the synthesis because the epoxide shows decomposition when exposed to long heating times. So, mCPBA epoxidation is successful for phenol-containing aryl cyclohexenyl ethers, such as SBI-2CHEp.

Oxone shows an epoxidation ability superior to mCPBA. It epoxidizes an aryl allyl ether in a 30% conversion at RT. However, it oxidizes p-alkyl phenol to p-hydroxyl quinine[14] though does not react with carboxylic acids. As a result, aryl allyl ether DPA-2Ep (containing a carboxylic acid) and TPOE-3Ep (containing a phenol) are synthesized through different schemes.

2.3 Base Developable Single Molecule Resists

2.3.1 Introduction

Polarity change of resists plays an important role in the development. So does the selection of developer solvent. Several organic solvent systems have been studied as developers, such as MIBK, IPA and PGMEA. However, as millions of gallons of waste solvents from semiconductor processing facilities are treated annually, resist design has

to meet the requirement of an environmentally friendly and economical process for semiconductor fabrication. Currently, industry still focuses on aqueous base TMAH (tetramethylammonium hydroxide) as developer which is less hazardous than organic solvent. The patterning performance of epoxy-based fully functional molecular resists, 2-Ep, 3-Ep and 4-Ep, have shown results superior to SU-8.[12] Since they are only organic solvent (e.g. MIBK) developable, they are not suitable in industry production. Incorporation of acidic groups into epoxy-based resist could achieve base developability while retaining excellent patterning performance. This design might also increase the T_g of molecular resist due to hydrogen-bonding from the acidic groups.

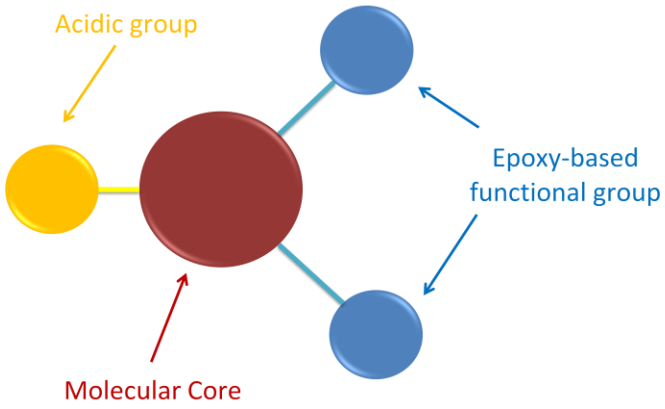

Figure 2.3. Epoxy-based base developable molecular negative-tone resists.

Other than the successful patterning performance of glycidyl ether type molecular resists mentioned above, base developability could also be achieved if acidic groups, such as carboxylic acids or phenols, are incorporated into this resist structures **(Figure 2.3)**. Another type of epoxides – cyclohexyl epoxides, which is easier to make than glycidyl ethers, will be also synthesized and patterned. The molecular core should have etch

resistance and amorphous property. There should be at least two epoxy groups per molecule to facilitate cross-linking. However, since epoxides are sensitive to base, acid and heat, specific care should be taken in synthesis. In this study, several epoxide molecules, which include SBI-2CHEp, SBI-2Ep, DPA-2Ep and TPOE-3Ep, are designed as candidates for the base-developable systems, as shown in **Figure 2.4**.

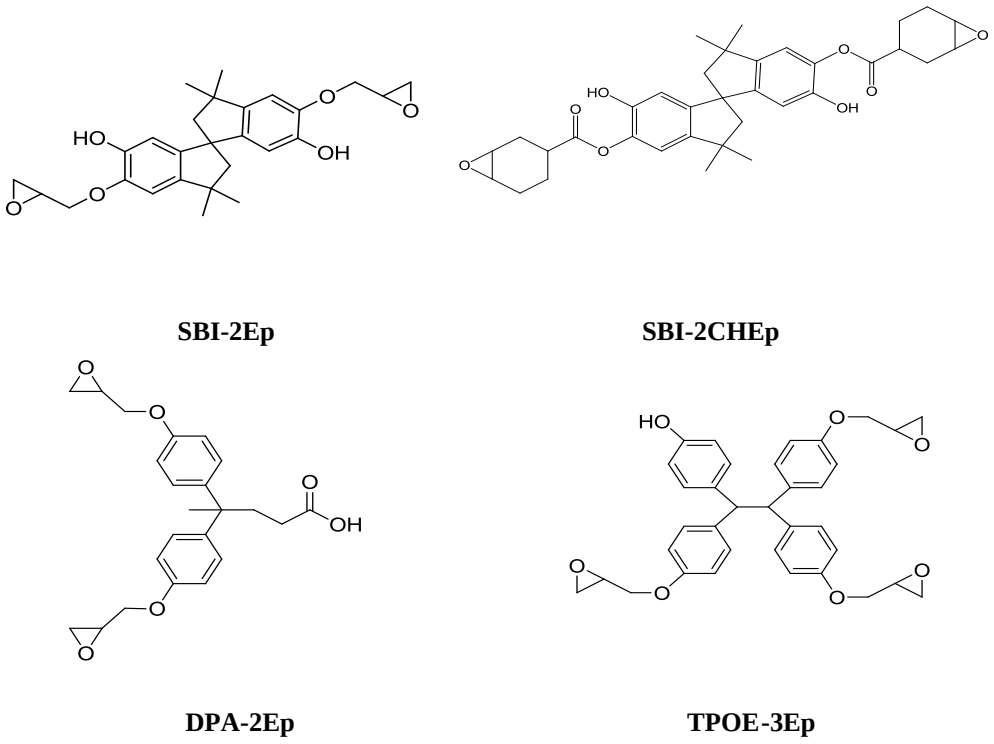

SBI-2Ep **SBI-2CHEp**

DPA-2Ep **TPOE-3Ep**

Figure 2.4. Candidates for epoxy-based base developable molecular negative-tone resists

2.3.2 Experimental

A series of different functionalized epoxide resists are initially proposed to make, which include BHPF-2CHEp, SBI-2CHEp, SBI-2Ep, DPA-2Ep and TPOE-3Ep. Their lithographic performance was also evaluated and discussed.

2.3.2.1 Materials and Instruments

Unless otherwise noted, all reagents and solvents were purchased from Sigma-Aldrich, TCI America, or Alfa-Aesar and used as received. Triphenylsulfonium hexafluoroantimonate (TPS-SbF_6) photoacid generator (PAG) was purchased from Midori Kagaku Co., Ltd.

A Varian Mercury Vx 300 was used to collect NMR. Deep ultraviolet (DUV) exposures were performed using an Oriel Instruments 500W Hg-Xe arc lamp with a 248 nm band-pass filter. Film thicknesses were measured using a M-2000 spectroscopic ellipsometer (J.A. Woolam, Inc.) over the wavelength range of 350 to 1000 nm using a Cauchy layer to model the resist film. E-beam lithography was performed using a JEOL JBX-9300FS electron-beam lithography system with 100 keV acceleration voltage, 8 nm beam diameter, 2 nA current, and 10 nm single-pixel shot pitch. The patterns produced by e-beam lithography were imaged using a Carl Zeiss Ultra60 SEM with 5 keV acceleration voltage.

2.3.2.2 Resists Synthesis

<u>2.3.2.2.1 SBI-2Ep</u>

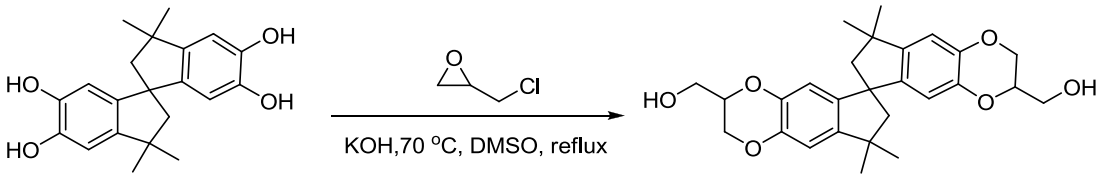

Figure 2.5. Reaction scheme for direct alkylation of poly-phenol by epichlorohydrin

Synthesis of SBI-2Ep is proposed with direct alkylation of poly-phenol by epichlorohydrin (**Figure 2.5**). However, the desired product is not obtained through this route. In contrast, a ring closing product is obtained as confirmed by NMR. An internal etherification could open the preformed epoxide, as ortho-OH could easily attack the epoxy ring when deprotonated by base. A proposed decomposition mechanism is shown in **Figure 2.6**.

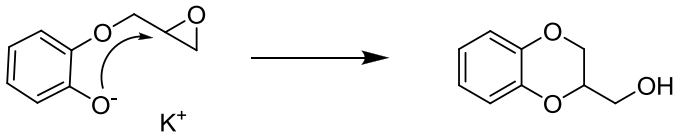

Figure 2.6. Proposed decomposition mechanism for internal etherification of ortho-OH glycidyl ether

2.3.2.2.2 SBI-2CHEp

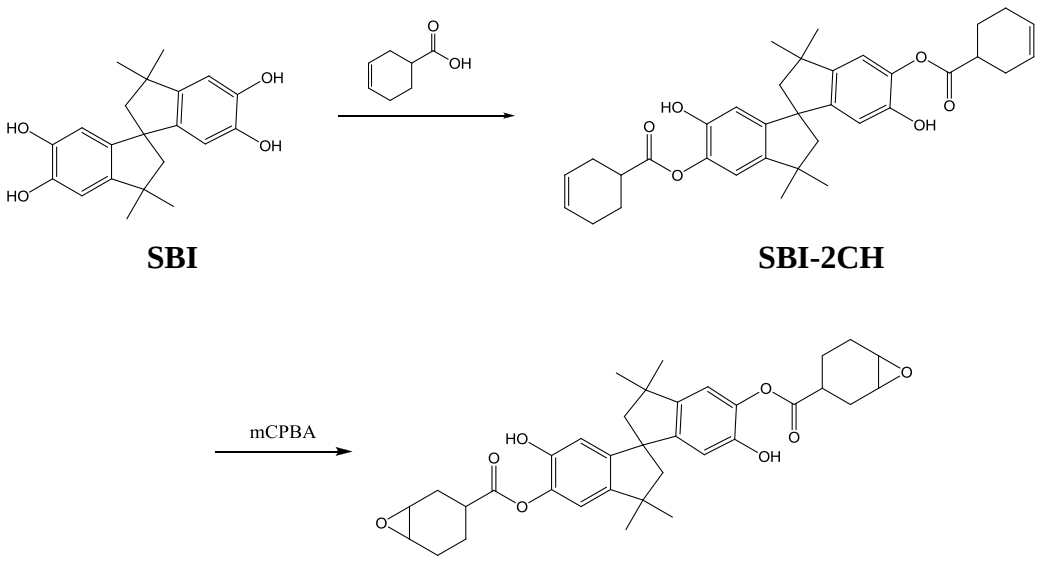

SBI **SBI-2CH**

SBI-2CHEp

Figure 2.7. Synthesis scheme of SBI-2CHEp.

The synthesis of SBI-2CHEp is very straightforward, see **Figure 2.7**. The aryl cyclohexenyl ether is electron-richer. It is a better substrate for epoxidation, which could be easily epoxidized by either mCPBA under mild conditions.

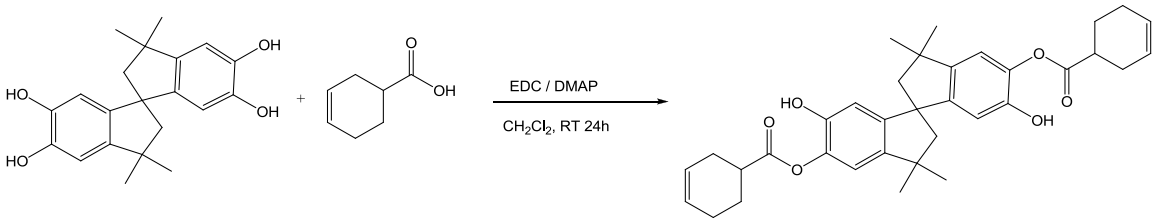

SBI **SBI-2CH**

Figure 2.8. Synthesis scheme of SBI-2CH.

5,6-dicyclohex-3-enecarboxylate -5',6'-dihydroxy-3,3,3',3'-tetramethyl- 1,1'-spirobisindane (SBI-2CH). 3-Cyclohexene-1-carboxylic acid (2.45 g, 19.39 mmol, 2.20 equiv.) and 1-Ethyl-3-(3-dimethyllaminopropyl)carbodiimide hydrochloride (EDC.HCl, 3.72 g, 19.39 mmol, 2.20 equiv.) were dissolved in 50 mL dried CH_2Cl_2. The mixture was stirred at ice bath temperature for 30 min under nitrogen atmosphere. To the solution was then added 4-Dimethylaminopyridine (DMAP, 0.236 g, 1.94 mmol, 0.22 equiv.), 5,5',6,6'-tetrahydroxy-3,3,3',3'-tetramethyl- 1,1'-spirobisindane (SBI, 3.00 g, 8.81 mmol, 1.00 equiv.) and 50 mL dried CH_2Cl_2. The solution was stirred at room temperature for 48 h. The solution was washed 1x with 10% $NaHCO_3$, 2x with 5% HCl and 2x with DI H_2O, filtered and the filtrate was dried over $MgSO_4$, and evaporated to dryness to afford 3.55 g dark green solid, which was a mixture of SBI-nCH. Separation of the crude mixture by flash chromatography (Hexane/Ethyl Acetate: 3/1) provided SBI-2CH (consists of three isomers) as a light yellow solid (0.76 g, 16%) The spectral data were: ^{1}H-NMR (300 MHz, Acetone-d6) δ (ppm) 1.31 (m, 6H), 1.36 (d, 6H), 1.52-2.95 (m, 18H), 5.70 (d, 4H), 6.22-7.08 (12 s, 4H), 8.20 (sb, 2H)

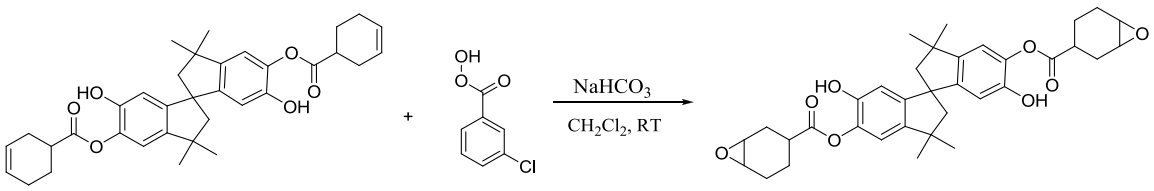

SBI-2CH **SBI-2CHEp**

Figure 2.9. Synthesis scheme of SBI-2CHEp.

5,6- diyl bis(7-oxabicyclo[4.1.0]heptane-3-carboxylate) -dihydroxy-3,3,3',3'-tetramethyl- 1,1'-spirobisindane (SBI-2CHEp). SBI-2CH (750 mg, 1.35 mmol, 1.00

equiv.) was dissolved in 100 mL dried CH_2Cl_2. To the solution was then added $NaHCO_3$ (362 mg, 4.31 mmol, 3.20 equiv.) and *meta*-Chloroperoxybenzoic acid (mCPBA, 929 mg, 4.04 mmol, 3.00 equiv.) at ice bath temperature. The mixture was stirred at room temperature for 6 h. Then the solution was washed 3x with 10% $Na_2S_2O_3$, 2x with 10% $NaHCO_3$, 1x with DI H_2O, filtered and the filtrate was dried over $MgSO_4$, and evaporated to dryness to afford ~ 750 mg dark brown solid. Purification of the crude mixture by flash chromatography (Hexane/Acetone: 2/1) provided SBI-2CHEp as a light yellow solid (250 mg, 32%) The spectral data were: ^{1}H-NMR (300 MHz, Acetone-d6) δ (ppm) 1.30 (s, 6H), 1.35 (s, 6H), 1.45-2.31 (m, 18H), 3.02-3.25 (m, 4H), 6.34 (m, 1H), 6.45 (m, 1H), 6.78 (m, 1H), 6.86 (m, 1H), 8.10 (sb, 2H)

2.3.2.2.3 DPA-2Ep

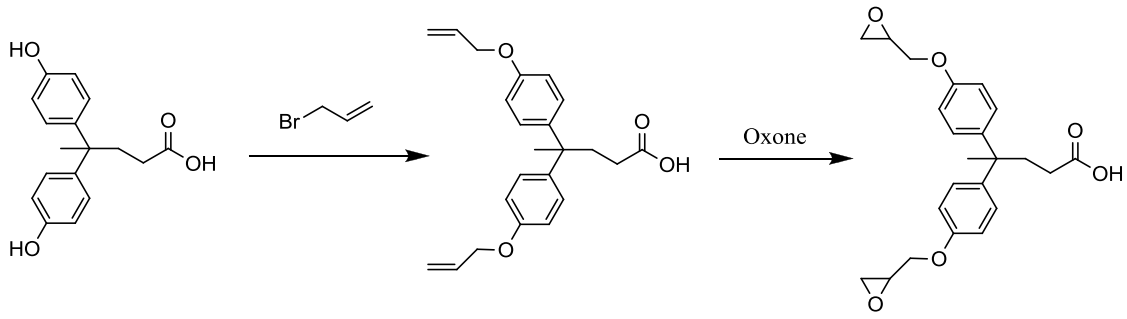

DPA **DPA-2OAllyl** **DPA-2Ep**

Figure 2.10. Synthesis scheme of DPA-2Ep.

Since Oxone does not react with carboxylic acids. So in this synthetic route, Oxone was used as epoxidation reagent for the electron-deficient aryl allyl ether DPA-2OAllyl.

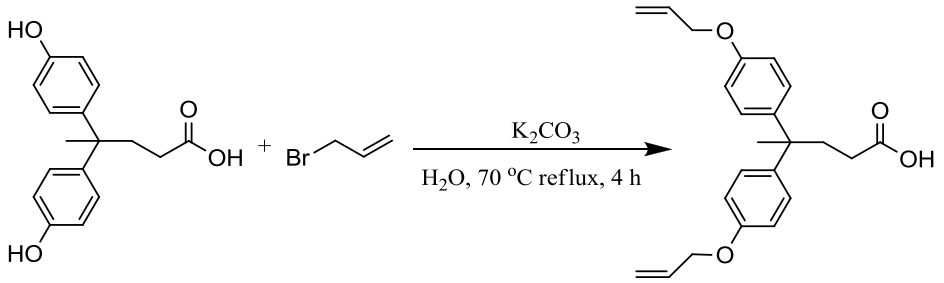

DPA **DPA-2OAllyl**

Figure 2.11. Synthesis scheme of DPA-2OAllyl.

4, 4-bis(4- allyloxyphenyl)pentanoic acid (DPA-2OAllyl). 4, 4-bis(4-hydroxyphenyl)pentanoic acid (DPA, 4.00 g, 13.97 mmol, 1.00 equiv.) was dissolved in 60 mL DI H_2O, KOH (3.14 g, 55.88 mmol, 4.00 equiv.) was added to the solution and the mixture was stirred for 0.5 h. Allyl bromide (3.72 g, 30.73 mmol, 2.20 equiv.) was added dropwise to the mixture over 10 minutes. Then the reaction mixture was heated up to 70 ^oC and refluxed for 4 h. The solution was washed 1x with 3% HCl, 2x with H_2O, filtered and the filtrate was dried over $MgSO_4$, and evaporated to dryness to afford 2.44 g yellow viscous oil, which was a mixture of DPA-2OAllyl (87%) and DPA-3OAllyl (13%) confirmed by ^1H-NMR. Purification of the crude mixture by flash chromatography (Hexane/Ethyl Acetate: 2/1) provided DPA-2OAllyl as a yellow viscous oil (1.51 g, 29%) The spectral data were: ^1H-NMR (300 MHz, $CDCl_3$) δ (ppm) 1.58 (s, 3H), 2.16 (m, 2H), 2.40 (m, 2H), 4.52 (dt, 2H), 5.28 (dq, 2H), 5.39 (dq, 2H), 5.97-6.14 (m, 2H), 6.80 (m, 4H), 7.10 (m, 4H)

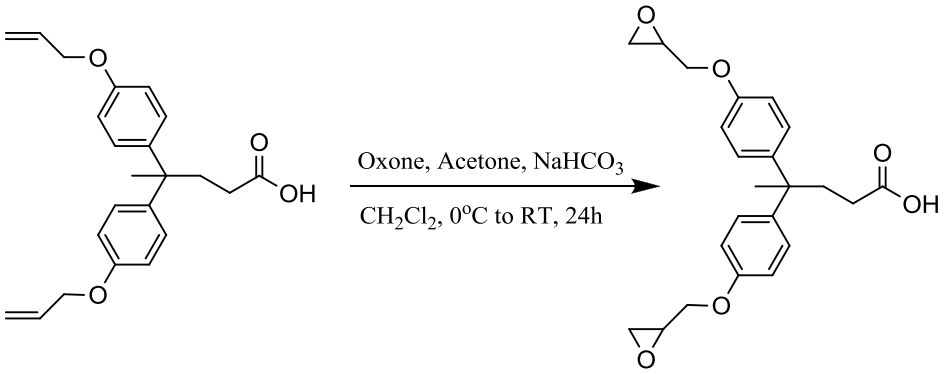

DPA-2OAllyl **DPA-2Ep**

Figure 2.12. Synthesis scheme of DPA-2Ep.

4,4-bis(4-(oxiran-2-ylmethoxy)phenyl)pentanoic acid (DPA-2Ep). A solution of oxone ($2KHSO_5 \cdot KHSO_4 \cdot K_2SO_4$, 20.09 g, 32.72 mmol, 8.00 equiv.) in water (80 mL) was added dropwise to a vigorously stirred mixture of DPA-2OAllyl (1.50 g, 4.09 mmol, 1.00 equiv.), acetone (20 mL), $NaHCO_3$ (8.25 g, 98.16 mmol, 24.00 equiv.) in CH_2Cl_2 (60 mL) at ice bath temperature. The mixture was stirred at room temperature for 24 h. Then the same epoxidation procedure was repeated for 4 times until the aryl allyl ether was fully converted to glycidyl ether. The solution was washed 2x with brine, filtered and the filtrate was dried over $MgSO_4$, and evaporated to dryness to afford 1.45 g yellow viscous oil. Purification of the crude material by flash chromatography (Hexane/Ethyl Acetate: 2/1) provided DPA-2Ep as a slightly yellow viscous oil (1.02 g, 63%) The spectral data were: ^{1}H-NMR (300 MHz, $CDCl_3$) δ (ppm) 1.57 (s, 3H), 2.13 (m, 2H), 2.40 (m, 2H), 2.75 (dd, 2H), 3.34 (m, 2H), 3.94 (dd, 2H), 3.18 (dd, 2H), 6.82 (m, 4H), 6.09 (m, 4H)

2.3.2.2.4 TPOE-3Ep

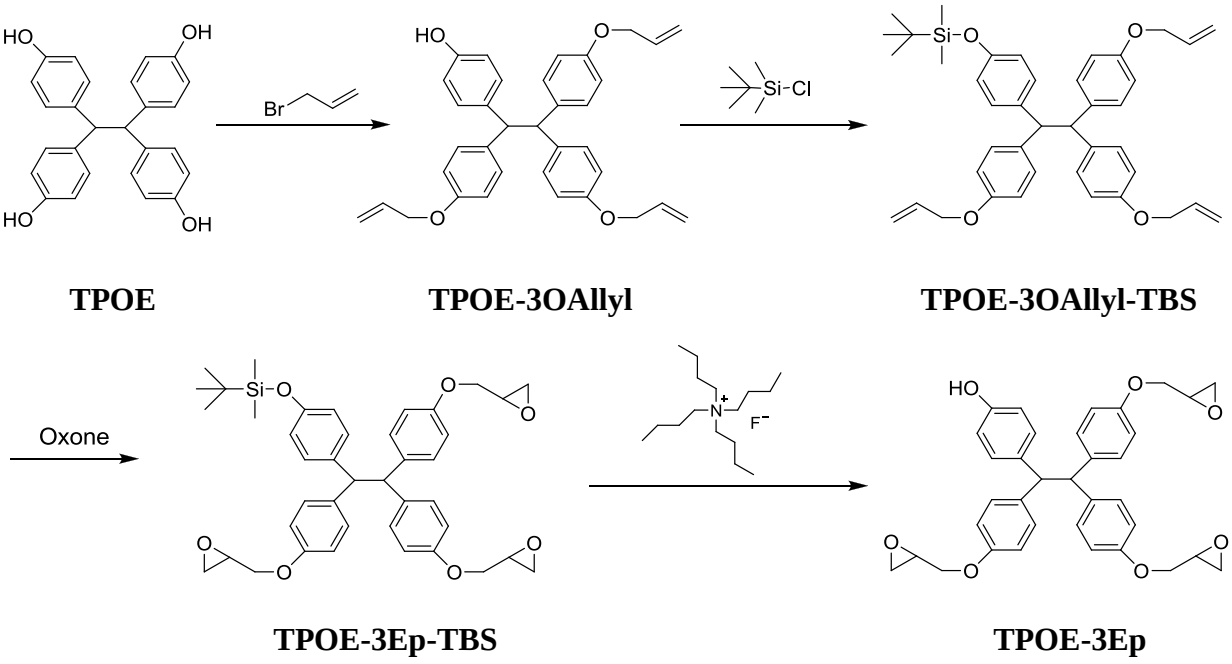

Figure 2.13. Synthesis scheme of TPOE-3Ep.

The synthesis of TPOE-3Ep was accomplished by protecting one of the phenolic groups, allylation, epoxidation, and deprotection.

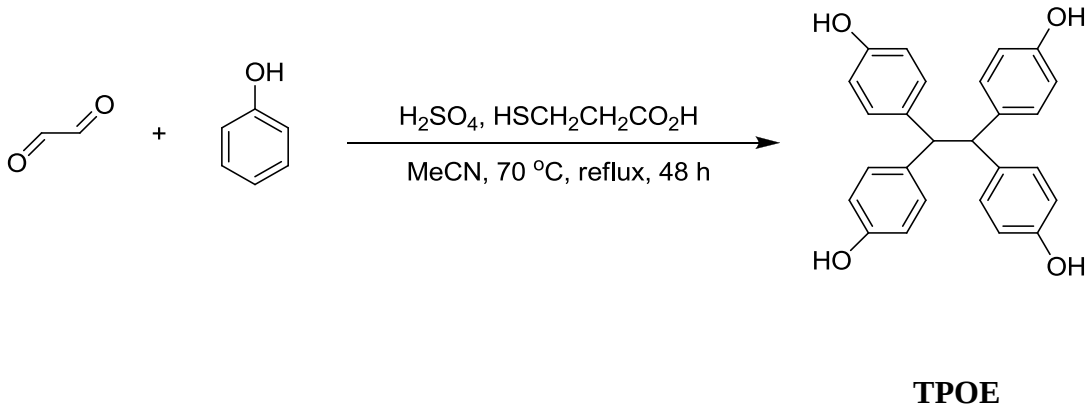

Figure 2.14. Synthesis scheme of TPOE.

1,1,2,2-Tetra(hydroxyphenyl)ethane (TPOE). Glyoxal (40 wt% in water, 7.50 g, 51.7 mmol, 1.00 equiv.), phenol (58.41 g, 620.3 mmol, 12.00 equiv.) and MPA (3-mercaptopropionic acid, 0.45 mL, 5.2 mmol, 0.10 equiv.) were dissolved in 60 mL acetonitrile. H_2SO_4 (98%, 5.51 mL, 103.4 mmol, 2.00 equiv.) was slowly added and the mixture was stirred and heated to reflux at 70 ℃ for 48 h. The solution gradually turned into dark brown. A white solid gradually formed and precipitated from the solution. The solution was cooled down and poured into 400 mL acetone. More white solid precipitated, and the solution was filtered. The filtered solid was washed with H_2O to neutrality and dried in a vacuum oven at 50 ℃ for 10 h, and collected to yield 4.21 g (20%). The ^{1}H-NMR (300 MHz, CD_3OD) were: δ (ppm) 4.53 (s, 1H), 6.55 (d, 4H), 6.99 (d, 4H).

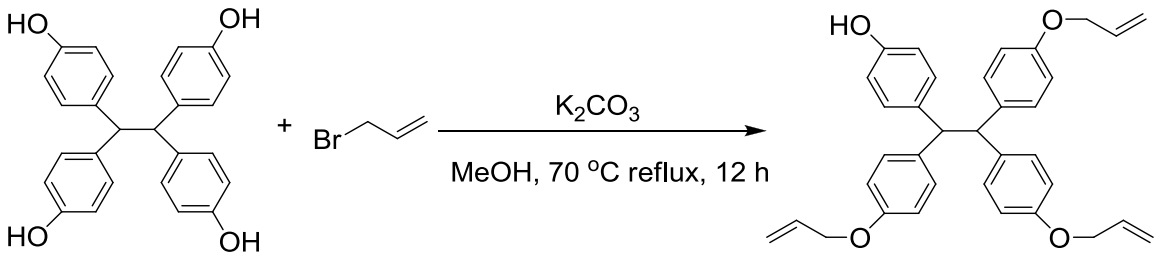

TPOE **TPOE-3OAllyl**

Figure 2.15. Synthesis scheme of TPOE-3OAllyl.

1,2,2-Tris(allyloxyphenyl)-2-hydroxyphenylethane (TPOE-3OAllyl). TPOE (4.00 g, 14.0 mmol, 1.00 equiv.) was dissolved in 120 mL methanol, and K_2CO_3 (3.47 g, 25.1 mmol, 2.50 equiv.) was added and the mixture stirred for 0.5 h. Allyl bromide (2.55 g, 21.1 mmol, 2.10 equiv.) was added dropwise to the mixture over 10 min. The reaction mixture was heated at reflux (70 °C) for 12 h. The solution was washed with 3% HCl, twice with H_2O, filtered, the filtrate dried over $MgSO_4$, and evaporated to dryness to afford 4.21 g of yellow solid. Purification of the crude product by flash chromatography

(hexane/ethyl acetate: 2/1) provided **TPOE-3OAllyl** as a yellow solid (1.17 g, 29%). The spectral data were: ^{1}H-NMR (300 MHz, CD_3OD) δ (ppm) 4.38 (dt, 6H), 4.63 (s, 2H), 5.17 (dq, 3H), 5.32 (dq, 3H), 5.90-6.06 (m, 3H), 6.52 (dt, 2H), 6.65 (dt, 6H), 7.01 (dt, 2H), 7.09 (dt, 6H).

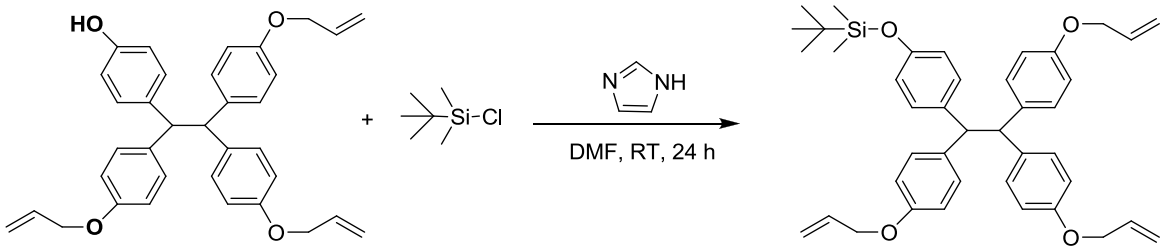

TPOE-3OAllyl **TPOE-3OAllyl-TBS**

Figure 2.16. Synthesis scheme of TPOE-3OAllyl-TBS.

1,1,2-Tris(allyloxyphenyl)-2-*t*-butyldimethylsilyloxyphenylethane TPOE-3OAllyl-TBS. TPOE-3OAllyl (1.00 g, 1.93 mmol, 1.00 equiv.) and *tert*-butyldimethylsilyl chloride (TBS-Cl, 0.45 g, 2.89 mmol, 1.50 equiv.) were dissolved in 60 mL dimethylfuran. Imidazole (0.393 g, 5.78 mmol, 3.00 equiv.) was added and the mixture was stirred at room temperature for 24 h. The solution was washed with 3% HCl, twice with H_2O, extracted with ethyl acetate, dried over $MgSO_4$, and evaporated to dryness to afford 0.92 g (75%) of a yellow solid which was used without further purification. The spectral data were: ^{1}H-NMR (300 MHz, $CDCl_3$) δ (ppm) 0.11 (s, 6H), 0.92 (s, 9H), 4.40 (dt, 6H), 4.52 (s, 2H), 5.23 (dq, 3H), 5.35 (dq, 3H), 5.92-6.06 (m, 3H), 6.56 (dt, 2H), 6.65 (dt, 6H), 6.92 (dt, 2H), 7.01 (dt, 6H).

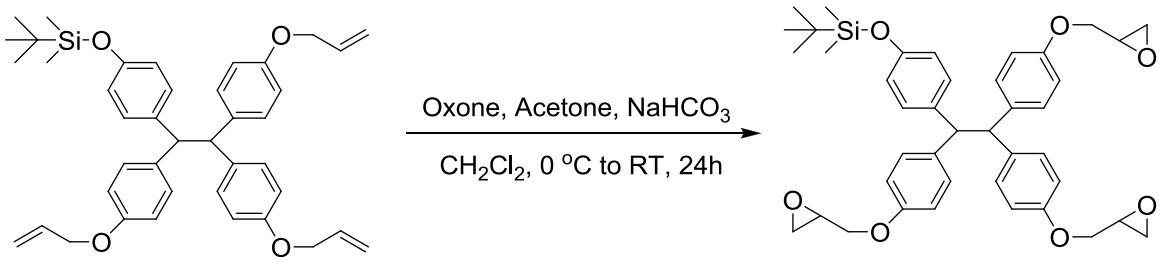

TPOE-3OAllyl-TBS **TPOE-3Ep-TBS**

Figure 2.17. Synthesis scheme of TPOE-3Ep-TBS.

1,1,2-Tris(glycidyloxyphenyl)-2-hydroxyphenylethane (TPOE-3Ep-TBS). A solution of oxone ($2KHSO_5 \cdot KHSO_4 \cdot K_2SO_4$, 9.30 g, 15.16 mmol, 12.0 equiv.) in water (40 mL) was added dropwise to a vigorously stirred mixture of TPOE-3OAllyl-TBS (0.80 g, 1.26 mmol, 1.00 equiv.), acetone (10 mL), $NaHCO_3$ (3.82 g, 45.5 mmol, 36.0 equiv) in CH_2Cl_2 (40 mL) in an ice bath. The mixture was stirred at room temperature for 24 h. The same epoxidation procedure was repeated until the aryl allyl ether groups were fully converted to glycidyl ether groups, as monitored by NMR. The solution was washed twice with brine, filtered, the filtrate dried over $MgSO_4$, and evaporated to dryness to afford 0.72 g (84%) of a yellow solid which was used without further purification. The spectral data were: ^{1}H-NMR (300 MHz, $CDCl_3$) δ (ppm) 0.09 (s, 6H), 0.91 (s, 9H), 2.68 (dd, 3H), 2.86 (dd, 3H), 3.27 (m, 3H), 3.84 (dd, 3H), 4.08 (dd, 3H), 4.51 (s, 2H), 6.56 (dt, 2H), 6.65 (dt, 6H), 6.92 (dt, 2H), 7.00 (dt, 6H).

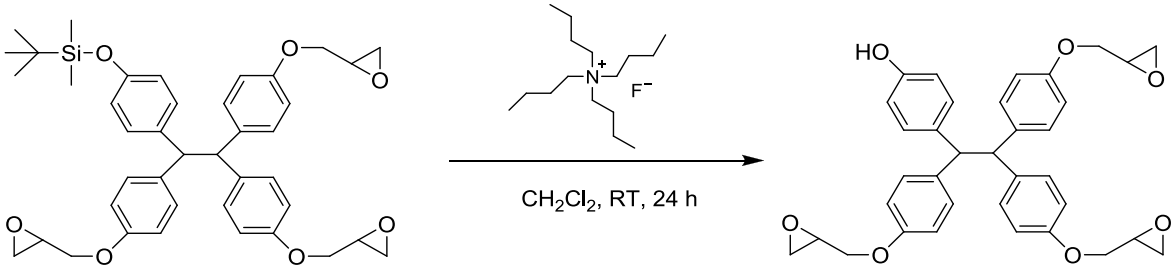

TPOE-3Ep-TBS **TPOE-3Ep**

Figure 2.18. Synthesis scheme of TPOE-3Ep.

1,1,2-Tris(glycidyloxyphenyl)-2-hydroxyphenylethane (TPOE-3Ep). TPOE-3Ep-TBS (0.70 g, 1.03 mmol, 1.00 equiv.) was dissolved in 60 mL dichloromethane. Tetrabutylammonium fluoride (TBAF, 1.0 M in THF, 3.08 mmol, 3.00 equiv) was added dropwise. The mixture was stirred for 24 h. The solution was washed twice with H_2O, extracted with dichloromethane, dried over $MgSO_4$, and concentrated. The concentrated solution was dropped in cold hexane, and the yellow solid which precipitated was collected and dried under vacuum overnight to yield 0.45 g (77%) of the presumed product TPOE-3Ep as yellow solid. The spectral data were: ^{1}H-NMR (300 MHz, $CDCl_3$) δ (ppm) 2.68 (dd, 3H), 2.84 (dd, 3H), 3.26 (m, 3H), 3.82 (dd, 3H), 4.06 (dd, 3H), 4.54 (s, 2H), 6.55 (dt, 2H), 6.65 (dt, 6H), 6.94 (dt, 2H), 6.99 (dt, 6H).

2.3.3 Patterning Performance of the Base-Developable Resists

2.3.3.1 Patterning Performance of SBI-2CHEp

SBI-2CHEp is chosen as base-developable resist because that it is relatively easier to synthesize than the glycidyl ether version SBI-2Ep, as cyclohexene is an e-rich

substrate for epoxidation which allows mild epoxidation condition by using mCPBA. DUV patterning performance of SBI-2CHEp is evaluated with both organic solvent and aqueous base as developers (**Figure 2.19**).

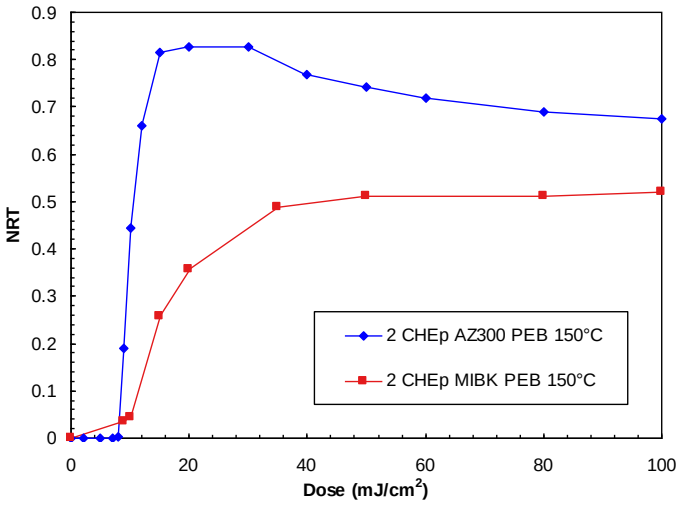

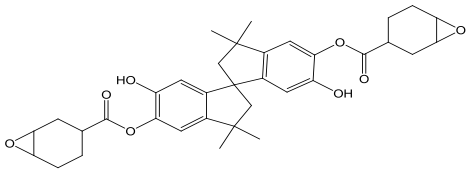

SBI-2CHEp

Figure 2.19. DUV (248 nm) contrast curves for SBI-2CHEp with different developers: red – MIBK, blue – AZ300 (aqueous base 0.26 N TMAH). Patterning condition: 5 mol% TPS-SbF_6, PAB 90 ℃ 2 min, PEB 150 ^{o}C 60 sec. NRT stands for normalized remaining thickness.

Higher dose and PEB temperature are required, while the normal PEB temperature for the glycidyl ether type resist is 90 ^{o}C. When expanding to higher doses, unusual behavior is found in base development: the normalized remaining thickness is higher at intermediate dose than at higher dose. However, solvent development shows expected behavior. Development behavior in base suggests swelling of the resist with TMA (tetramethylammonium) cation during development, and this behavior persists after rinse. As the extent of cross-linking increases (at higher dose), penetration of the

developer is reduced and the extent of OH cross-linking increases. Further high resolution patterning and imaging of SBI-2CHEp is not performed due to the poor film remaining and swelling issue.

2.3.3.2 Patterning Performance of DPA-2Ep.

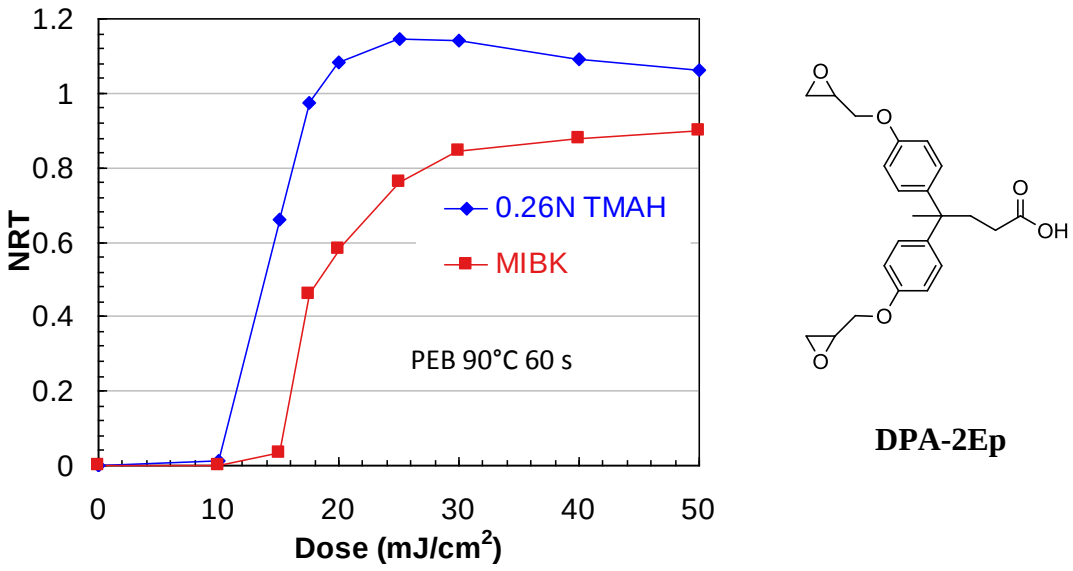

Figure 2.20. DUV (248 nm) contrast curves for DPA-2Ep with different developers: red dots – MIBK, blue dots – AZ300 (0.26 N TMAH), PEB 90 ^{o}C 60 s, 5 mol% TPS-SbF_6, PAB 90 ℃ 2 min.

Carboxylic acid groups incorporated DPA-2Ep is obtained as a viscous melt at room temperature, which should allow patterning at a lower PEB temperature based on the previous observation that high mobility of molecular resist in glass would render relatively high cross-linking. Due to this, improved resolution might be obtained because the acid diffusion rate is lowered at low PEB temperature. DPA-2Ep shows what could be the most important result toward improving EUV performance of these systems – shift

of E_0 away from 0 mJ/cm^2 (**Figure 2.20**). Since DPA-2Ep is not so sensitive at lower dose, the image might not be affected by out of band irradiation. However, DPA-2Ep shows severe swelling problem (**Figure 2.21**) due to the uptake of TMA by RCOOH during TMAH development, which is not shown in MIBK development.

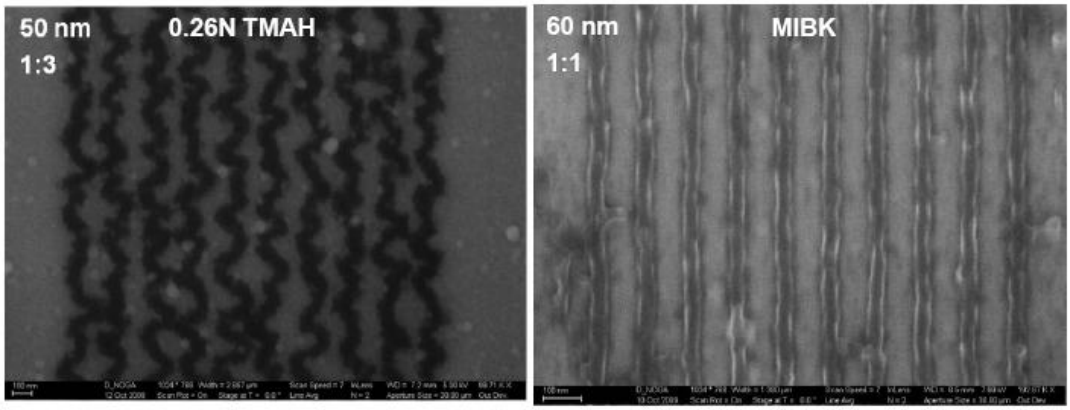

Figure 2.21. DPA-2Ep SEM images with developer (a) AZ 300 (0.26 N TMAH); (b) MIBK.

2.3.3.3 Patterning Performance of TPOE-3Ep.

TPOE-3Ep shows excellent contrast in TMAH (see **Figure 2.22**). E_0 is shifted away from 0 mJ/cm^2 due to different crosslinking kinetics, but not shifted as far as DPA-2Ep (see **Figure 2.20**). Though there is one phenol group in the molecule, the contrast curve does not show an up-then-down trend as other base developable resists, which indicates there is no immediate swelling. The PEB condition needs to be improved to get more complete crosslinking, which will be studied later. The formulated TPOE-3Ep is patterned by E-beam lithography. Development in TMAH shows resolution of 40 nm 1:3 line:spacing, significantly better than other base developable system, see **Figure 2.23a**.

Other 1:1 line: spacing patterns, such as 100 nm 1:1 and 60 nm 1:1 are shown here as well, see **Figure 2.23b and c**.

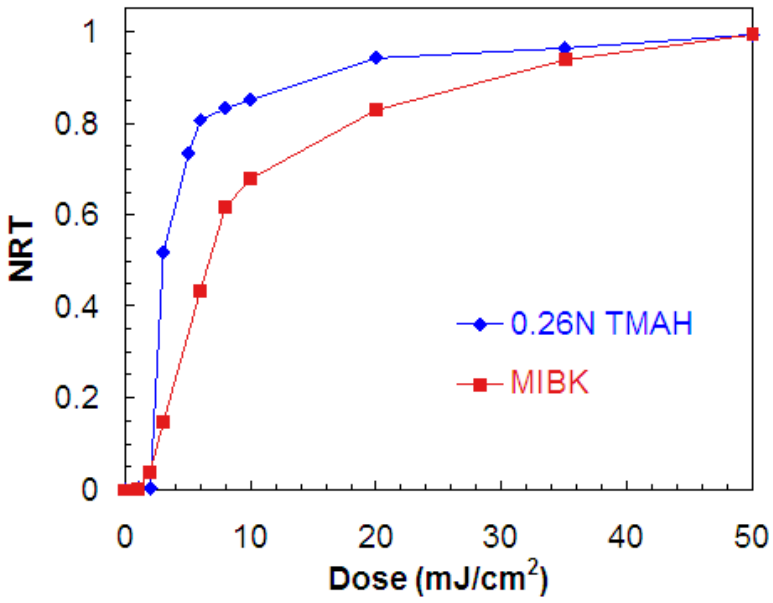

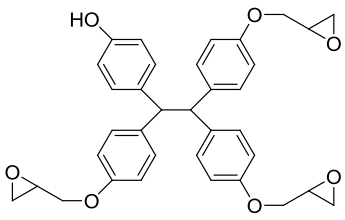

TPOE-3Ep

Figure 2.22. DUV (248 nm) contrast curve for TPOE-3Ep with different developers: red dots – MIBK, blue dots – AZ300 (0.26 N TMAH), PEB 90 ^{o}C, 5 mol% TPS-SbF_6, PAB 90 ℃ 2 min.

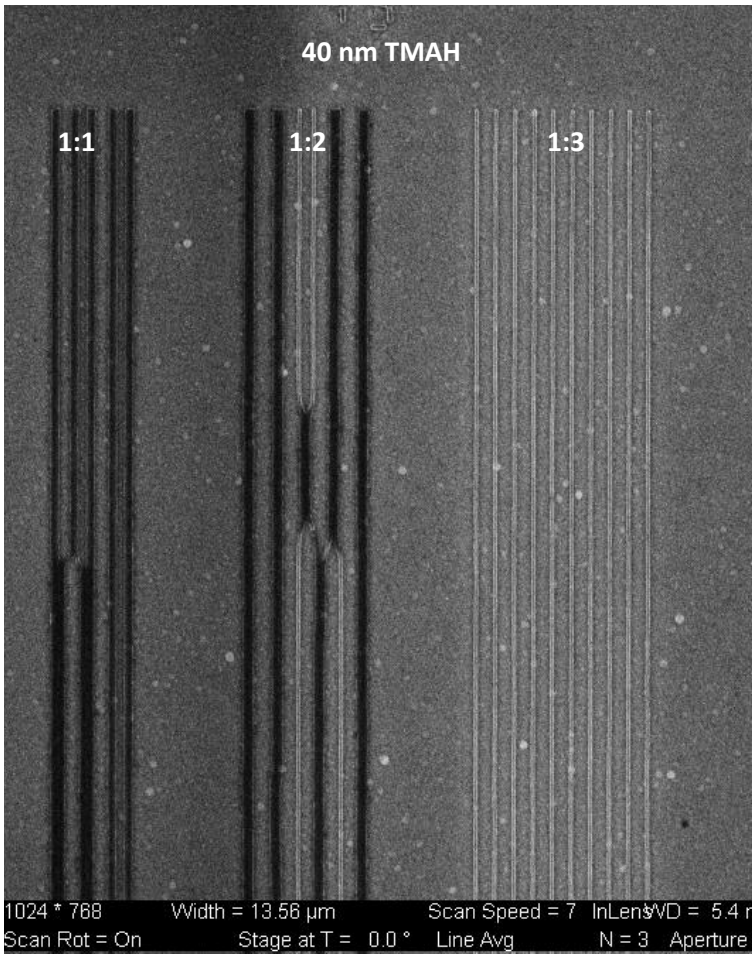

(a)

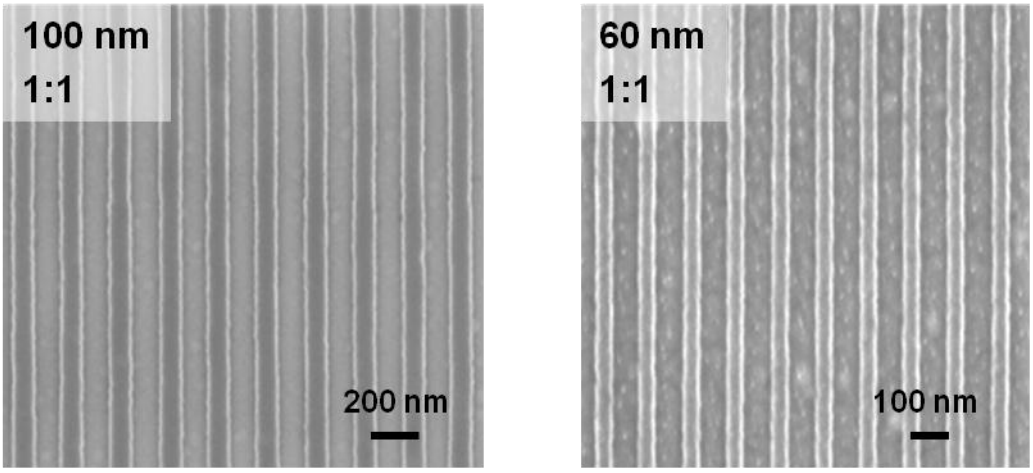

(b) **(c)**

Figure 2.23. SEM images of e-beam patterned TPOE-3Ep with 40 nm 1:1, 1:2 and 1:3 line:spacing patterns, developed in TMAH.

Development in MIBK shows slightly better resolution than TMAH. 35 nm 1:2 line: spacing resolution is achieved, as shown in **Figure 2.24**. **Figure 2.25** shows the patterning size at 40 nm with 1:1, 1:2 and 1:3 line: spacing. The 1:2 and 1:3 patterns are able to be resolved. Thus, TPOE-3Ep has been successfully invented and utilized as base/organic solvent dual developable resist. It resolves at 40 nm by using TMAH development, without swelling.

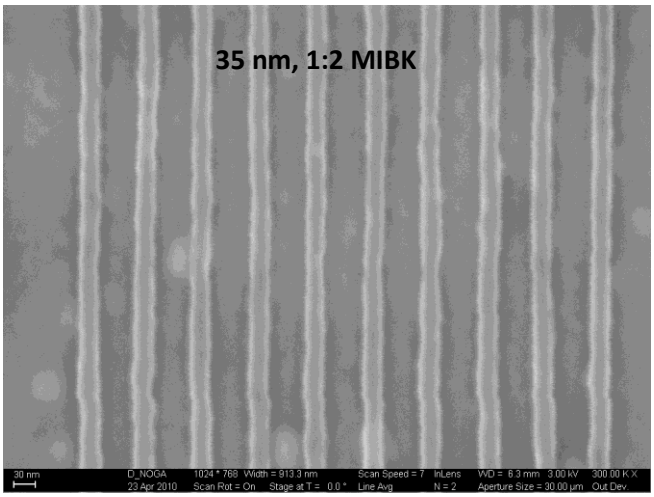

Figure 2.24. SEM images of e-beam patterned TPOE-3Ep with 35 nm 1:2 line:spacing patterns, developed in MIBK

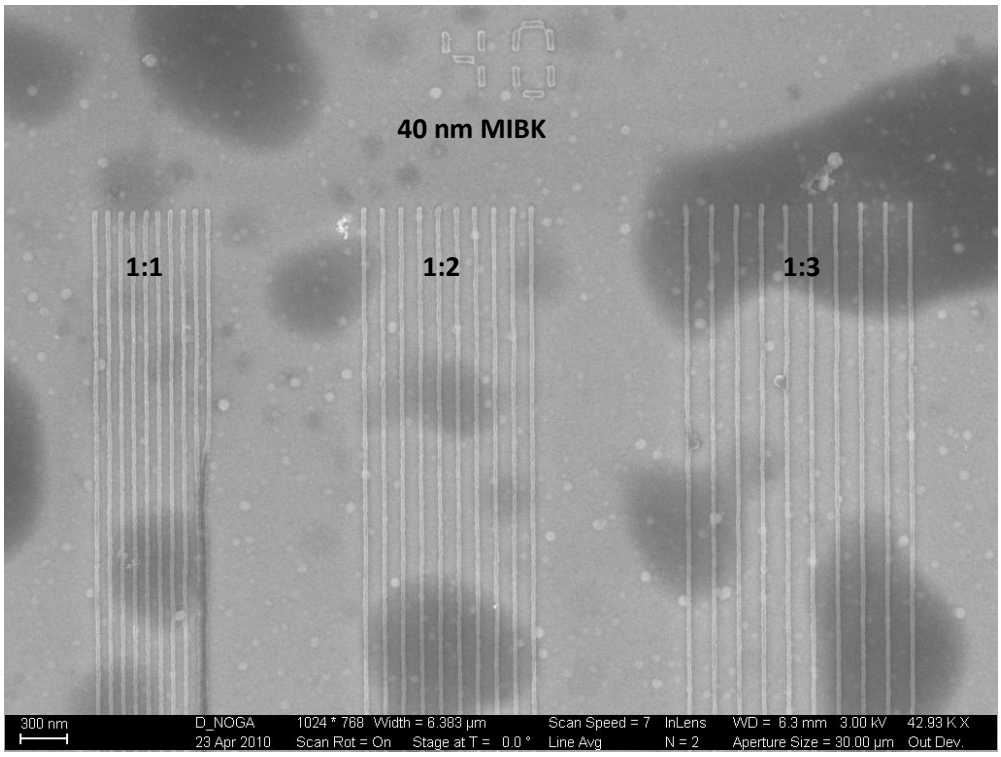

Figure 2.25. SEM images of e-beam patterned TPOE-3Ep with 40 nm 1:1, 1:2 and 1:3 line:spacing patterns, developed in MIBK.

2.4 Cyclohexene Oxide Based Single Molecule Resists

2.4.1 Introduction

The initiation and propagation rates determine the polymerization. A faster initiation rate and a slower propagation rate are needed for controlled polymerization. The cyclohexene oxide has a more rigid structure than glycidyl ether, thus it possesses a slower propagation rate in solid state. The cyclohexene oxide type resists are expected to form more uniform crosslinking network than glycidyl ether type resists. The patterning

performance would be improved by using this type of epoxide. BHPF-2CHEp is designed as cyclohexene based resist, see **Figure 2.26**. Like 2-Ep and 2-Ox,[15] BHPF-2CHEp shares the same molecular core. The patterning performance will be compared among those three resists.

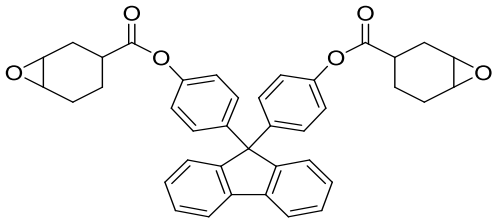

Figure 2.26. Chemical structure of BHPF-2CHEp.

2.4.2 Synthesis of BHPF-2CHEp

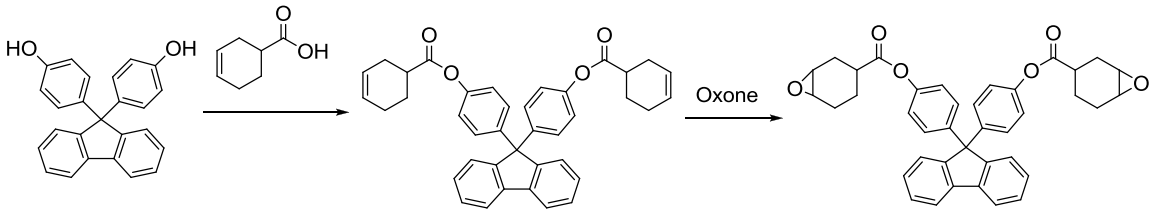

BHPF **BHPF-2CH** **BHPF-2CHEp**

Figure 2.27. Synthesis scheme of BHPF-2CHEp.

The BHPF-2CHEp is synthesized through oxone oxidation on a cylcohexene substrate. The final material is characterized by NMR and elemental analysis. The synthesis scheme is shown in **Figure 2.27**.

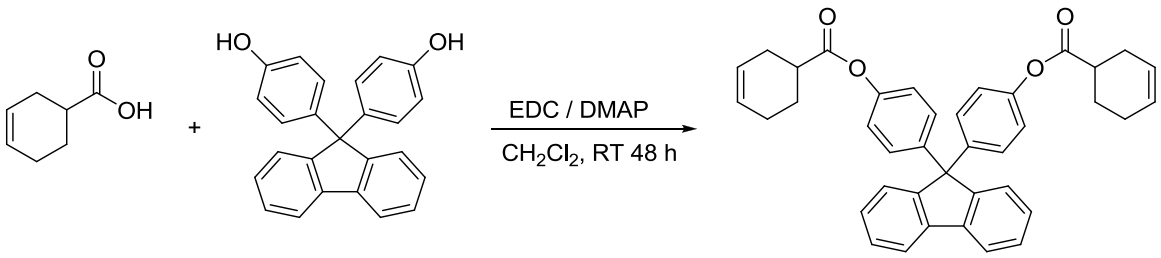

BHPF **BHPF-2CH**

Figure 2.28. Synthesis scheme of BHPF-2CH.

4,4'-(9H-fluorene-9,9-diyl)bis(4,1-phenylene) dicyclohex-3-enecarboxylate (BHPF-2CH). 3-Cyclohexene-1-carboxylic acid (2.70 g, 21.4 mmol, 2.50 equiv.) and 1-Ethyl-3-(3-dimethyllaminopropyl)carbodiimide hydrochloride (EDC.HCl, 4.10 g, 53.5 mmol, 2.50 equiv.) were dissolved in 50 mL dried CH_2Cl_2. The mixture was stirred at ice bath temperature for 30 min under nitrogen atmosphere. To the solution was then added 4-Dimethylaminopyridine (DMAP, 0.26 g, 5.35 mmol, 0.25 equiv.), 9,9-bis(4-hydroxyphenyl) fluorene (BHPF, 3.00 g, 8.56 mmol, 1.00 equiv.) and 50 mL dried CH_2Cl_2. The solution was stirred at room temperature for 48 h. The solution was washed 1X with 10% $NaHCO_3$, 2X with 5% HCl and 2X with DI H_2O, filtered and the filtrate was dried over $MgSO_4$, and evaporated to dryness to afford 4.55 g yellow solid. The crude produce was recrystalized from cold diethyl ether and gave BHPF-2CH as a light yellow solid (3.52 g, 73%) The spectral data were: ^{1}H-NMR (300 MHz, $CDCl_3$) δ (ppm) 1.75-2.39 (m, 6H), 2.79 (m, 1H), 5.72 (s, 2H), 6.95 (dt, 2H), 7.22 (dt, 2H), 7.25-7.41 (m, 3H), 7.77 (d, 1H).

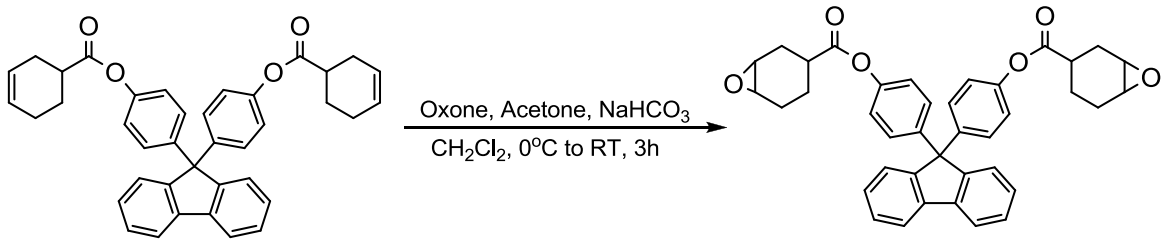

BHPF-2CH **BHPF-2CHEp**

Figure 2.29. Synthesis scheme of BHPF-2CHEp.

4,4'-(9H-fluorene-9,9-diyl)bis(4,1-phenylene) bis(7-oxabicyclo[4.1.0]heptane-3-carboxylate) (BHPF-2CHEp). A solution of oxone ($2KHSO_5 \cdot KHSO_4 \cdot K_2SO_4$, 28.89 g, 47.04 mmol, 8.00 equiv.) in water (100 mL) was added dropwise to a vigorously stirred mixture of BHPF-2CH (3.33 g, 5.88 mmol, 1.00 equiv.), acetone (10 mL), $NaHCO_3$ (11.86 g, 141.12 mmol, 24.00 equiv.) in CH_2Cl_2 (100 mL) at ice bath temperature. The mixture was stirred at room temperature for 3 h. The solution was washed 2X with brine, filtered and the filtrate was dried over $MgSO_4$, and evaporated to concentrate the solution. Purification of the crude material by recrystalization from cold acetone provided BHPF-2CHEp as a slightly yellow solid (2.80 g, yield was 80%). The spectral data were: ^{1}H-NMR (300 MHz, $CDCl_3$) δ (ppm) 1.46-2.81 (m, 7H), 3.24 (m, 2H), 6.91 (dt, 2H), 7.19 (dt, 2H), 7.23-7.39 (m, 3H), 7.75 (d, 1H). Elemental analysis: C (77.63%), H (5.71%), O (16.17%).

By doing TLC test of BHPF-2CHEp, it is found that there are three active spots on the TLC plate. There are three isomers, as shown in **Figure 2.30**. The presence of isomers might not affect the patterning performance.

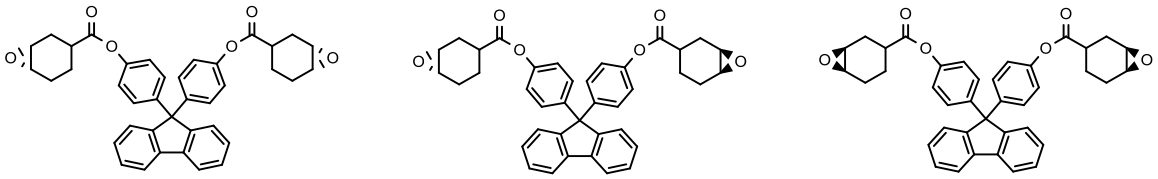

(trans, trans) (trans, cis) (cis, cis)

Figure 2.30. Isomer structures of BHPF-2CHEp.

2.4.3 Patterning Performance of BHPF-2CHEp

Since the cyclohexene oxide is expected to show slower propagation than glycidyl ether in solid state, the polymerization behavior is more controlled. DUV patterning performance of 2-CHEp is compared with 2-Ep and 2-Ox,[15] which are all derived from the 9,9-Bis(4-hydroxyphenyl)fluorene **(**BHPF) molecular core (**Figure 2.31**).

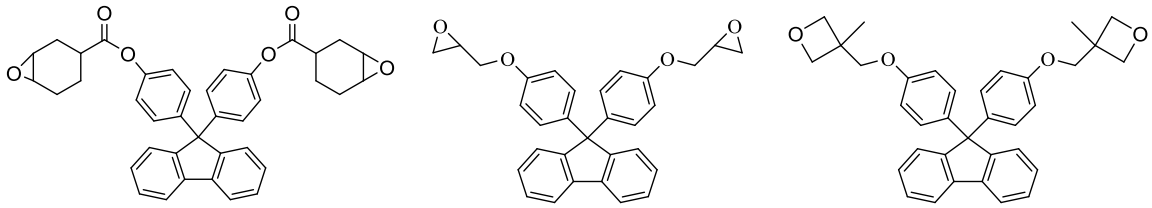

2-CHEp **2-Ep** **2-Ox**

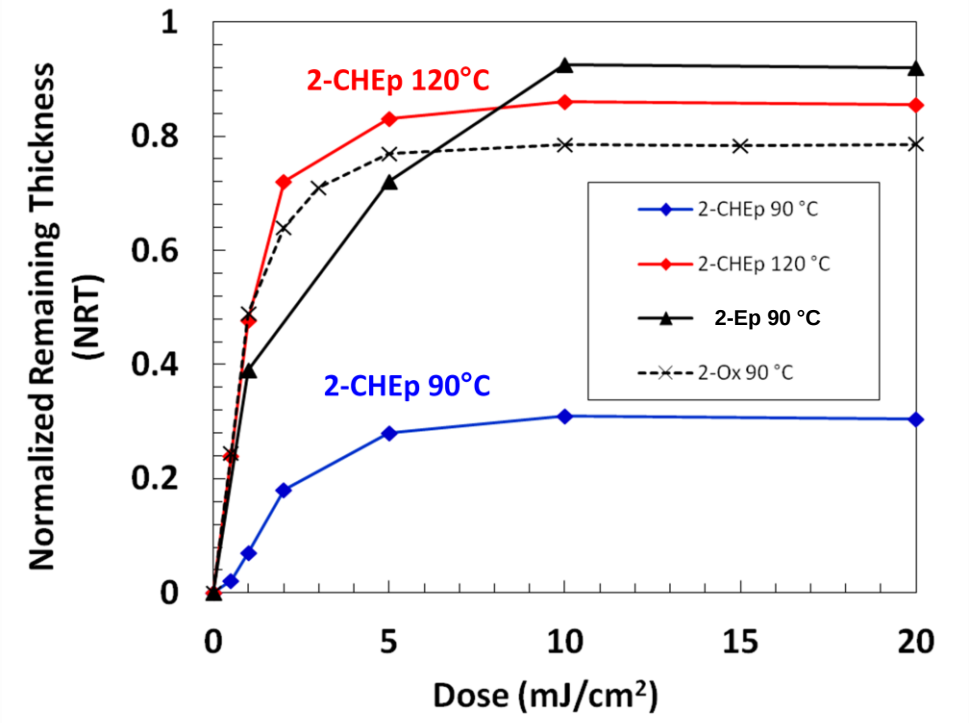

Figure 2.31. DUV (248 nm) contrast curves for 2-CHEp, compared with 2-Ep and 2-Ox based on BHPF core at different PEB temperatures. Patterning condition: 5 mol% TPS-SbF_6, PAB 90 ℃ 2 min, PEB 60 sec., developed in MIBK

The patterning performance of 2-CHEp at PEB 90 ℃ is much worse than 2-Ep and 2-Ox, which might be due to the slower polymerization rate of cyclohexyl epoxide as it has more substituents on the epoxide ring.[16] When patterning of 2CHEp is repeated at a higher PEB temperature, 120 ℃, similar results to 2-Ep and 2-Ox are obtained, even higher contrast is observed. Higher PEB temperature increases mobility of photo-acid and resist, which renders high polymerization rate. High resolution patterning of BHPF-2CHEp is carried out using 100 keV e-beam lithography. Patterns are resolved down to 15 nm 1:3 line/space with PEB at 120 ℃, which is smaller than what have been obtained

from 2-Ep patterning,[15] see **Figure 2.35**. From **Figure 2.32** to **Figure 2.34**, the patterning performance at lower resolution are shown (35 nm, 25 nm, and 20 nm line width).

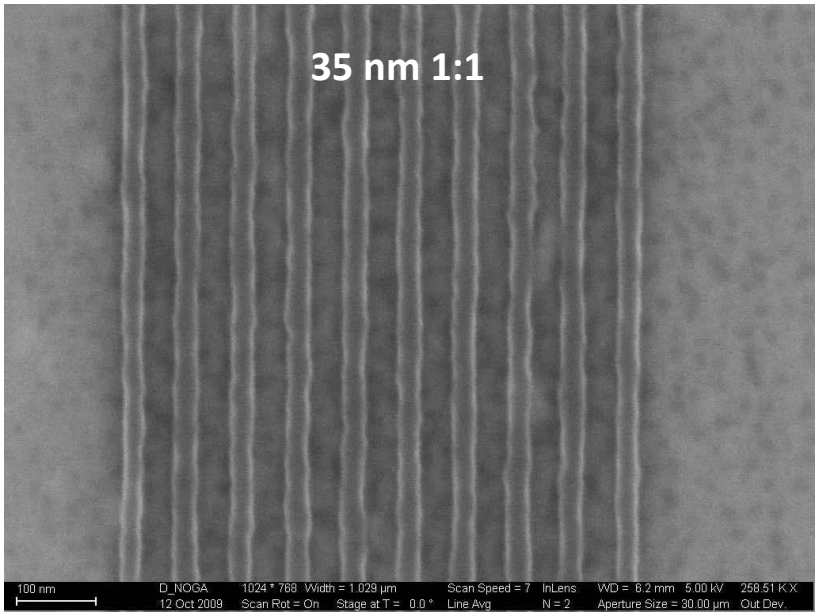

Figure 2.32. SEM images of e-beam patterned BHPF-2CHEp with 35 nm 1:1 line:spacing patterns, developed in MIBK.

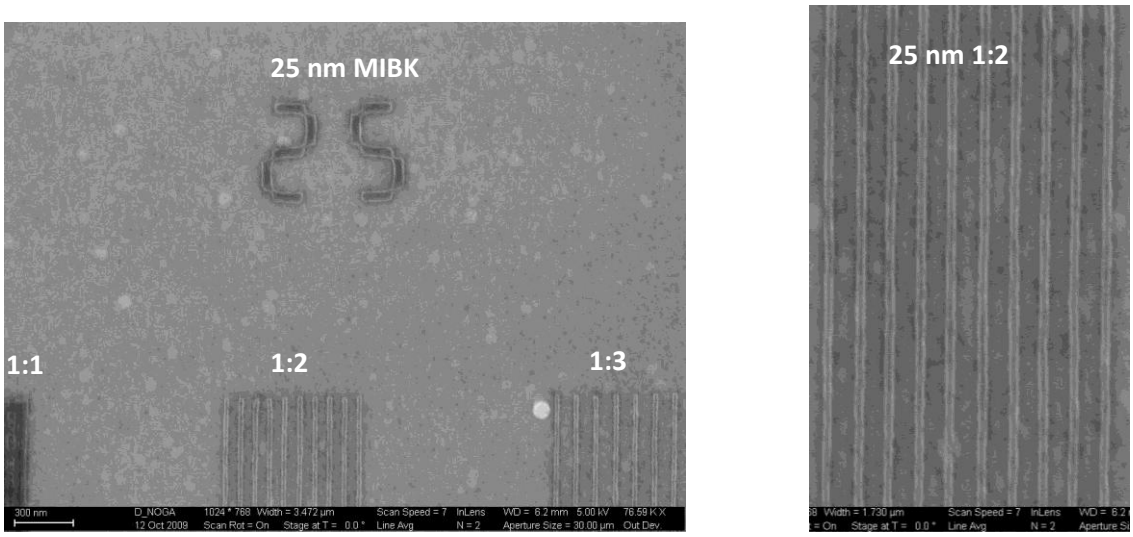

Figure 2.33. SEM images of e-beam patterned BHPF-2CHEp with 25 nm 1:2 line:spacing patterns, developed in MIBK.

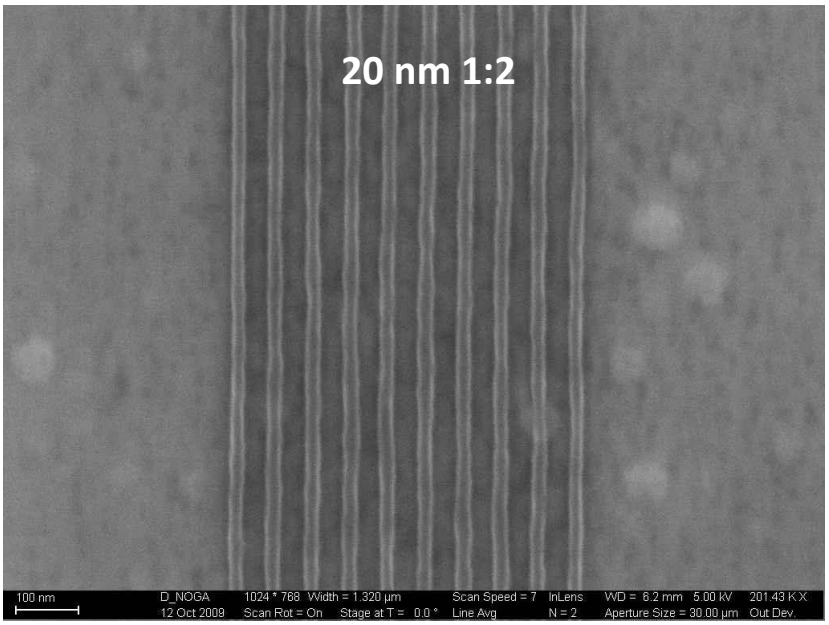

Figure 2.34. SEM images of e-beam patterned BHPF-2CHEp with 20 nm 1:2 line:spacing patterns, developed in MIBK.

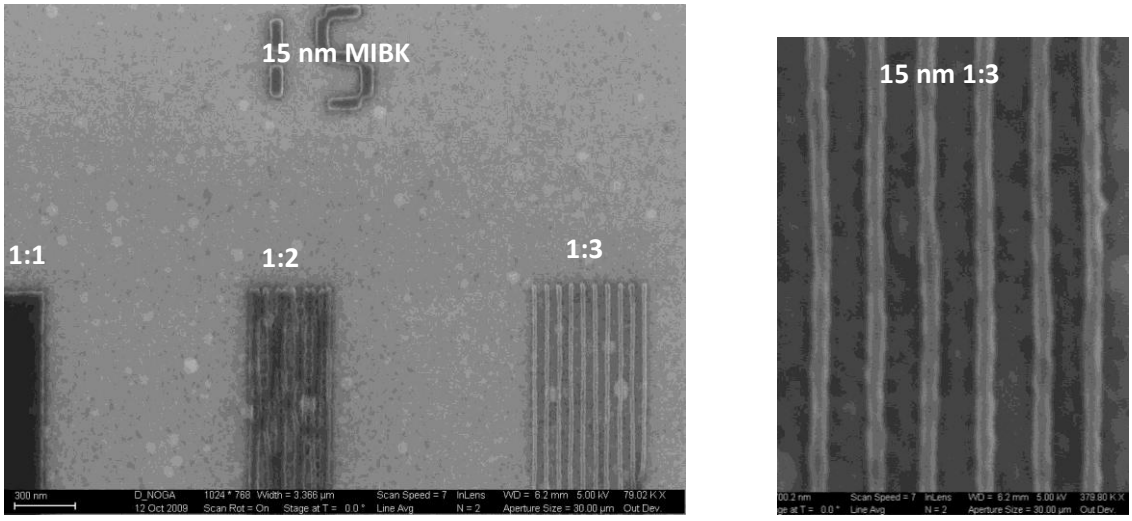

Figure 2.35. SEM images of e-beam patterned BHPF-2CHEp with 15 nm 1:3 line:spacing patterns, developed in MIBK.

2.5 Conclusion

Epoxy-based negative tone molecule resists shows superior patterning performance to traditional polymeric resists. Higher resolution and lower LER are obtained by using single molecule resists. The ring opening cationic polymerization of the epoxy resists during PEB suffer less from photoacid diffusion. Thus, the LER is even better than positive tone molecule resists.

In this work, the aqueous developable single molecule resists are introduced, synthesized and patterned. DPA-2Ep, which is based on a carboxylic acid functional group, shows severe swelling problem during base development due to the uptake of tetramethylammonium ion. TPOE-3Ep, which is based on a less acidic phenol functional group, shows proper patterning behavior, without swelling, after base development.

A new group of epoxide functional group, cyclohexene oxide functionalized BHPF is introduced and compared with 2-Ep and 2-Ox. The BHPF-2CHEp shows better contrast curve due to the better controlled polymerization behavior. 15 nm resolution with 1:3 line:spacing is obtained.

2.6 References

1. Ito, H. *Adv Polym Sci* **2005** 172, 37-245.
2. Iwayanagi, T.; Ueno, T.; Nonogaki, S.; Ito, H.; Wilson, C. G. *Materials and Processes for Deep UV Lithography," in ACS Advances in Chemistry Series 218*.
3. *"Electronic and Photonic Applications of Polymers," NI. J. Bowden and S. R. Turner, eds., American Chemical Society, Washington, D. C.* **1988**, 109.
4. Shiraishi, H.; Yoshimura, T.; Sakamizu, T.; Ueno, T.; Okazaki, S. J. *Vac. Sci. Technol., B* **1994,** 12, (6), 3895-3899.
5. Yoshimura, T.; Shiraishi, H.; Yamamoto, J.; Okazaki, S. *Appl. Phys. Lett.* **1993,** 63, (6), 764–766.
6. Yamaguchi, T.; Namatsu, H.; Nagase, M.; Yamazaki, K.; Kurihara, K. *Appl. Phys. Lett.* **1997,** 71, (16), 2388–2390.
7. Steenwinckel, D. V.; Lammers, J. H.; Koehler, T.; Brainard, R. L.; Trefonas, P. *J. Vac. Sci. Technol. B* **2006,** 24, (1), 316-320.
8. Wallraff, G. M.; Medeiros, D. R. *Proc. SPIE* **2005,** 309, 5753.
9. Silva, A. D.; Felix, N. M.; Ober, C. K. *Adv. Mater.* **2008,** 20, 3355–3361.
10. Drygiannakis, D.; Patsis, G. P.; Raptis, I.; Niakoula, D.; Vidali, V.; Couladouros, E.; Argitis, P.; Gogolides, E. *Microelectron. Eng.* **2007,** 84, 1062.

11. Silva, A. D.; Lee, J.-K.; Andr é, X.; Felix, N. M.; Cao, H. B.; Deng, H.; Ober, C. K. *Chem. Mater.* **2008,** 20, 1606–1613.

12. Lawson, R. A.; Tolbert, L. M.; Younkin, T. R.; Hendersona, C. L. *Proc. of SPIE* **2009,** 7273, 72733E-1.

13. *U.S. Patent No. 4882,245.*

14. Carreo, M.; Gonzlez-Lpez, M.; Urbano, A. *Angew. Chem. Int. Ed.* **2006,** 45, 2737 –2741.

15. Lawson, R. A.; Noga, D. E.; Younkin, T. R.; Tolbert, L. M.; Henderson, C. L. *J. Vac. Sci. Technol. B* **2009,** 27, 2998.

16. Bailey, F. E., Jr.; France, H. G. *Journal of Polymer Science* **1960,** 45, 243.

CHAPTER 3

DIRECTLY PHOTO-DEFINABLE GUIDING LAYER FOR BLOCK COPOLYMER DSA PATTERNING

3.1 Introduction

The pitch of single layer resist (SLR) processes has essentially reached a plateau at approximately 45 nm in terms of the smallest practical pitch achievable using 193 nm immersion lithography. In order to achieve smaller pitch patterning and continue to increase device densities on a single layer, alternative lithographic technologies are needed. One option to achieving smaller pitch patterning is to transit to lower wavelength exposure technologies (i.e. EUVL or e-beam lithography) that are directly capable of patterning such smaller pitches. However, EUVL technology is not yet ready for manufacturing due to a variety of issues such as low source powers that can enable high wafer throughputs. Likewise, direct write e-beam lithography technologies have also not demonstrated sufficient throughputs to be practical for high volume manufacturing.

A second option is to utilize alternative lithographic processes other than SLR methods that can provide a means for subdividing the pitch achieved in the primary lithographic exposure step to provide final patterns at a tighter pitch. Such methods are of course already receiving significant attention in the form of so-called "double patterning" methods and side-wall spacer patterning techniques. In double patterning, two separate exposure steps at relaxed pitch are overlaid to achieve a final patterned result at half of the primary exposure pitch. In this way, sub 40 nm pitch patterning can be achieved with 193 nm immersion lithography.[1]

If one assumes that for the near future exposure tools are limited still to 193 nm light as the smallest practical exposure wavelength, the issue becomes one of how to achieve final pitches smaller than this 40 nm pitch available with double patterning. One obvious option is to go to a much higher level of complexity of these multiple exposure processes. This leads to so-called "triple patterning" or "quad patterning" which involve overlaying 3 or 4 separate exposure steps to further subdivide the primary pitch available by the optical exposure tool. However, the expense and overlay requirements of such methods make these options less than desirable.

An option that has instead received growing interest in the last several years for performing such higher levels of pitch subdivision is block copolymer lithography (BCPL) utilizing directed self assembly (DSA). Block copolymers naturally undergo microphase separation into periodic domains that range in size from only a few nanometers to the order of hundreds of nanometers depending on the molecular weight of the polymer blocks themselves. This ability to control the length scale of the pattern formed from such a block copolymer by controlling the molecular weight of the BCP offers an interesting new method for controlling the size of very small scale patterns. The propensity for such block copolymers to microphase separate is determined by difference between the strength of the attractive interactions of the blocks with blocks of their own type versus the strength of the attractive interactions with blocks of the opposite type. This difference in interaction energies is typically characterized by the product χN, where χ is the Flory-Huggins interaction parameter and N is total number of monomers in the diblock copolymer. According to theory, microphase separation can occur when this value χN exceeds 10.4 which is the critical value for the order-disorder transition.[2-4] The resulting phase separated structure formed from such a diblock copolymer can itself be quite varied, including lamellar, gyroidal, cylindrical, and spherical microsturctures, and which is controlled by the relative volume fractions of the two blocks in the copolymer.[2]

Unfortunately, left to self assemble into phase separated domains on their own in bulk, such diblock copolymers generally form relatively defective, polycrystalline structures that are not suitable for high resolution lithographic applications. Therefore, methods for guiding this block copolymer phase separation process to achieve long range order and low numbers of defects in the final phase separated morphologies has been the focus of such work in the lithographic community. Researchers have used chemically[5] or topographically[6] patterned substrates, combined with thermal or solvent annealing, to direct the assembly of such microphase separated films into the desired ordered patterns. **Figure 3.1** shows an example of a primary lithographic pattern that has been used to chemically pattern an underlying surface and the subsequent block copolymer pattern that results after phase separation of a thin film of block copolymer on top of this chemically patterned surface.

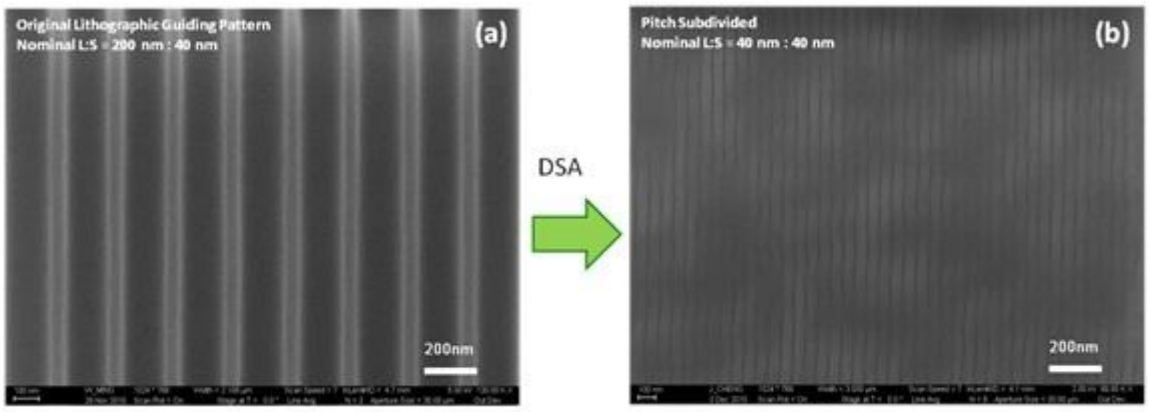

Figure 3.1. SEM of PS-b-PMMA (L_0 = 80 nm) DSA on larger pitch size guiding layer (patterned ZEP 520A resist on crosslinked PS-r-PMMA-r-PGMA neutral layer); (a) Original optical lithography result of ZEP e-beam resist pattern used to produce chemically patterned surface at relaxed pitch, nominal line: space sizes = 200 nm: 40 nm; (b) PS-b-PMMA block copolymer pattern after DSA on the surface produced from the

pattern shown in (a) demonstrating pitch subdivision by a factor of 3 to a nominal line: space size = 40 nm: 40 nm.

3.1.1. Directed Self Assembly (DSA) via Chemoepitaxy

There are three critical steps to the basic block copolymer DSA process (see **Figure 3.2**):

1. Guiding layer deposition and patterning: While block copolymers will naturally phase separate under certain conditions, they tend to form randomly oriented, polycrystalline morphologies. By providing an underlying surface that possesses a non-uniform energetic landscape (i.e. a "Guiding Layer" or GL) on which to anneal the block copolymer film, the phase separation process can be forced to produce well ordered and aligned structures. Guiding layers using both topographically and chemically textured surfaces have been demonstrated. Chemically textured guiding layer surfaces that can achieve chemoepitaxial block copolymer alignment are likely to be the most general solution to this problem.

2. Block copolymer film deposition and annealing: The block copolymer thin film is spun cast onto the guiding layer from organic solvent to form an amorphous, disordered film. The film is then annealed using either baking at elevated temperature or solvent vapor annealing (or some combination of the two) to allow the block copolymer to phase separate and order, which in the presence of a guiding layer produces patterns with long range order and registration.

3. Selective removal of block copolymer domains: The phase separated block copolymer pattern formed during the annealing process is not immediately useful as a lithographic

mask. One of the two copolymer block domains must be removed selectively. This has traditionally been achieved using plasma etch (e.g. in PS-b-PDMS) or selective chain scission and dissolution of one block (e.g. in PS-b-PMMA).

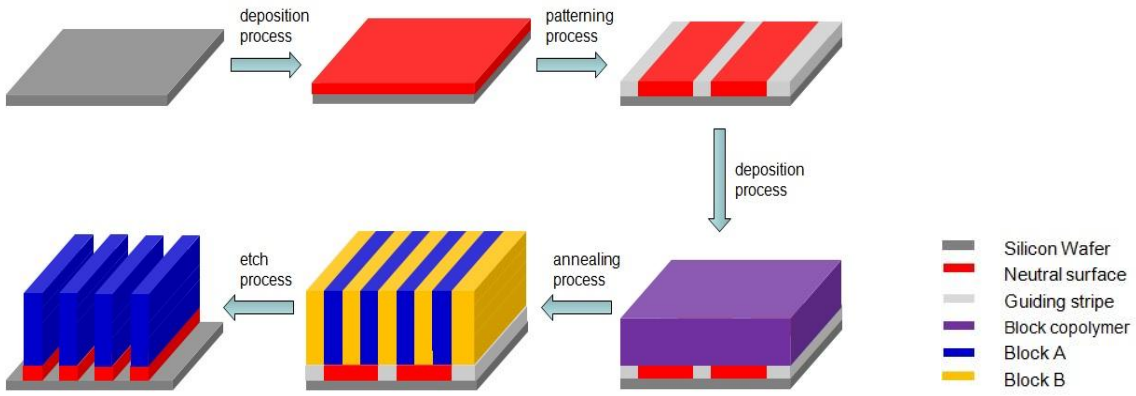

Figure 3.2. Scheme of the BCP directed self assembly (DSA) process using a chemically patterned surface (i.e. chemoepitaxy).

3.1.2. Design of Guiding Layers and Processes

Currently, the vast majority of chemoepitaxial guiding layers demonstrated and used in literature are based on deposition and subsequent patterning of self-assembled monolayers or grafted polymer monolayers. Such monolayer approaches suffer from a number of disadvantages including: (1) methods for forming monolayers are time consuming and not "fab friendly" in many cases, (2) a completely separate lithographic step including resist deposition, exposure, development, and etch is commonly required to achieve chemical patterns on the surface, and (3) the "background" chemical nature of monolayer can not be easily tuned and requires a new material to maintain overall surface neutrality as patterning requirements change. Compared to the lengthy and complex multi-step process currently used for forming chemoepitaxial guiding layers (see **Figure**

3.3), a directly photodefinable guiding layer that could be deposited by spin coating and processed on a standard lithography cell track system would greatly simplify the process and reduce chances for defectivity.

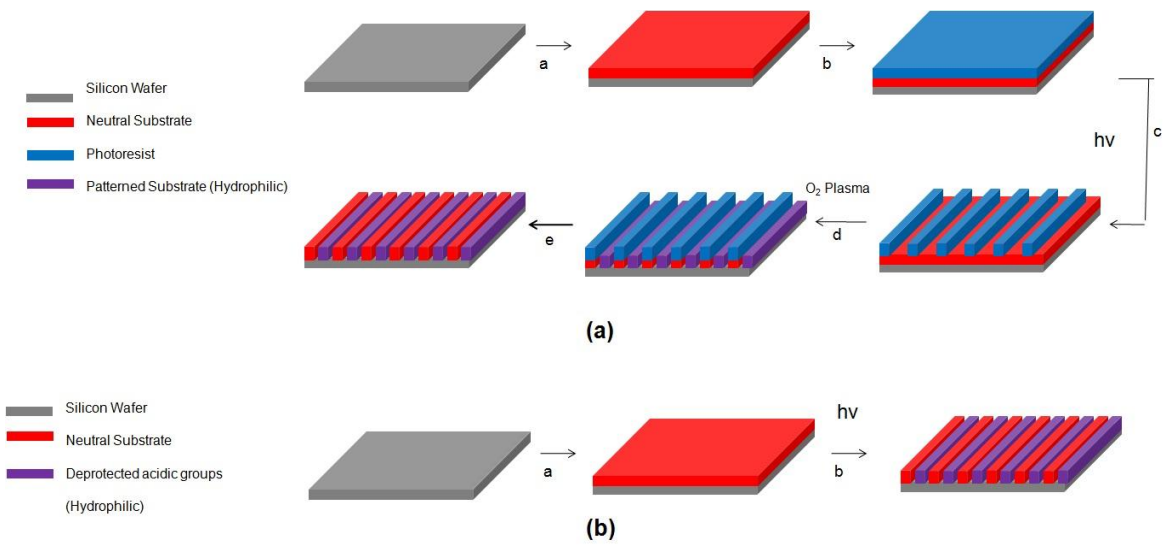

Figure 3.3. Comparison between: (a) Conventional chemical epitaxy process; (b) Photodefinable guiding layer process.

3.1.3. Directly Photodefinable Guiding Layers

Based on the overall DSA process, the requirements for a directly photodefinable guiding layer are: (1) it provides a simple and fast method for Guiding Layer (GL) deposition, (2) it provides a simple method for producing chemical contrast on the GL surface, and (3) it produces a GL layer that does not swell or deform during coating of BCP film from organic solution, and (4) it produces a GL layer that does not change significantly chemically during thermal or solvent annealing of BCP film.

To achieve these goals, a terpolymer design (**Figure 3.4.a**) is proposed in our work that functions in a manner similar to a chemically amplified resist in that it can: (1) be spin coated from organic solvent, (2) cross-linked during post-apply bake, (3) exposed using conventional optical lithography tools, (4) made to form a chemically patterned top surface during post-exposure bake, and (5) survive subsequent spin coating and annealing of the BCP film without change. Selection of a polymer backbone and functional groups to satisfy the first two goals is relatively easy. Acrylate groups can be polymerized radically by thermally generated radicals from initiators like AIBN during post apply bake. However, selecting a protecting group to meet all these requirements is a bit more of an unusual challenge.

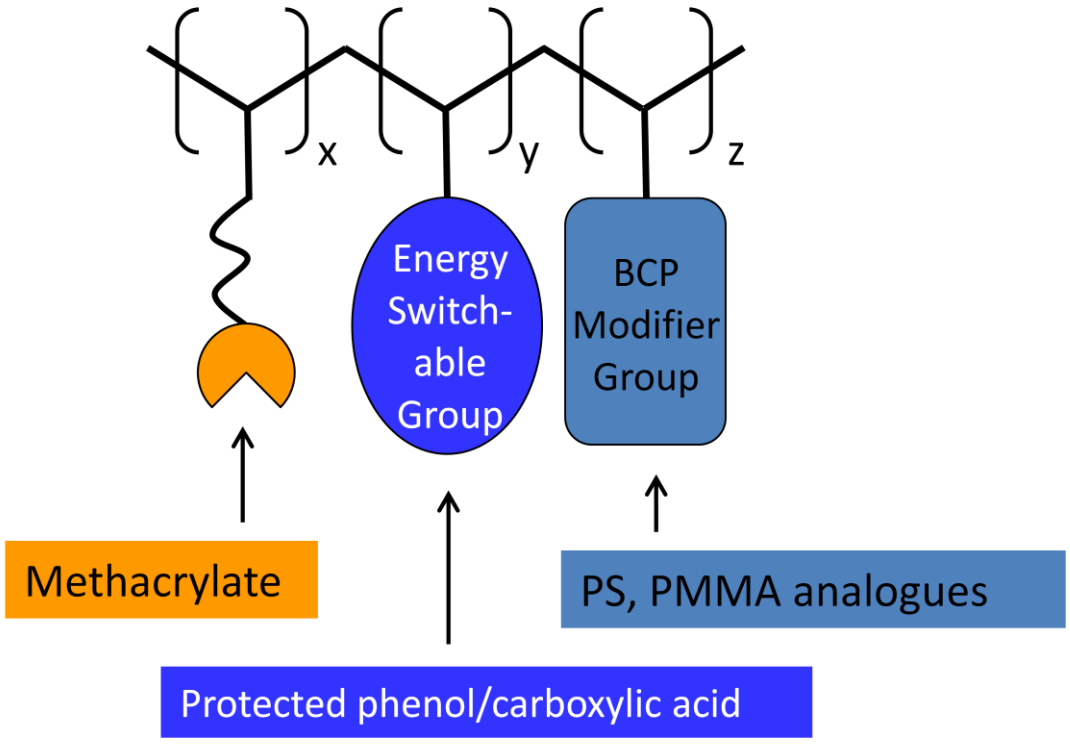

(a)

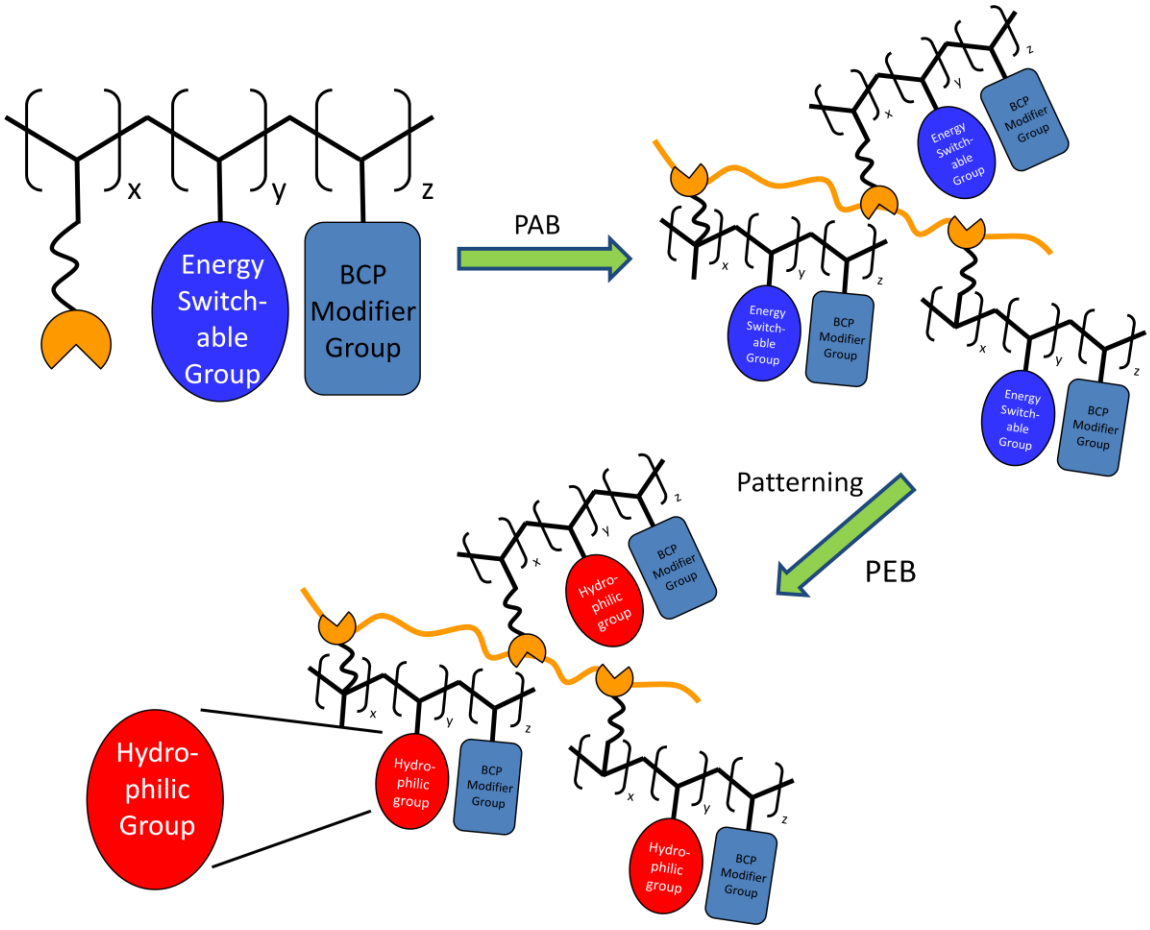

(b)

Figure 3.4. (a) Schematic design of the directly photodefinable guiding layer polymer being developed in this work. (b) Example of such a polymer that utilizes an acrylate functional group to provide the ability to radically cross-link and harden the GL after coating.

3.1.4. Selection of Protecting Group Chemistry for a Photodefinable BCP Guiding Layer

The current photodefinable guiding layer design being studied in this work is based on a functionalized polyhydroxystyrene backbone since it is useful for both the

model BCP system (PS-b-PMMA) and other potentially higher resolution BCP systems. The initial design approach has been to utilize protecting groups that can be removed by acid catalyzed deprotection during PEB to unmask polar alcohol groups (e.g. phenol) or carboxylic acids. The challenge is identifying a protecting group that can be thermally stable in the absence of photoacid at the high temperatures required for BCP thermal annealing (i.e. up to 250 ℃) but which shows good acid catalyzed deprotection rates at reduced temperatures. A number of different protecting groups have been studied to find such a suitable group.

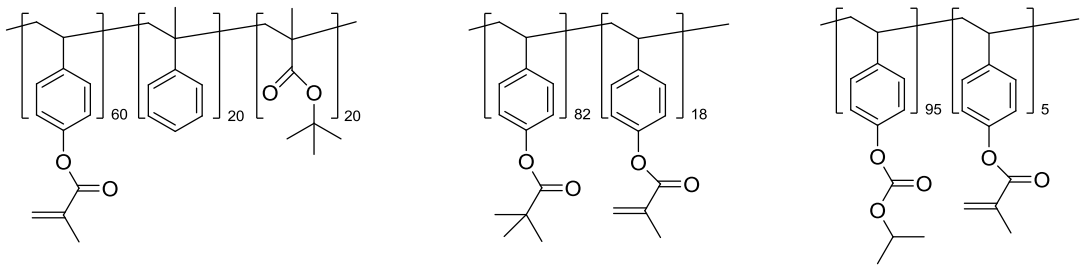

ESCAP-1-MA **PHOST-Pv-MA** **PHOST-iPOC-MA**

Figure 3.5. Materials studied as photodefinable guiding layer

Three materials are synthesized for the initial studies on protecting group behavior in cross-linkable resins (see **Figure 3.5**): a t-butyl ester protecting group in a crosslinkable ESCAP-type resist (ESCAP-1-MA), a pivolate (Pv) ester group in a functionalized polyhydroxystyrene (PHOST-Pv-MA), and an isopropyloxycarbonyl (iPOC) group in a functionalized polyhydroxystyrene (PHOST-iPOC-MA). Previous study has shown that styrene fractions between 0.48 and 0.63 in PS-r-PMMA random copolymers can provide neutral surfaces for the assembly of vertically oriented lamellae in PS-b-PMMA.[7] Thus, all of the materials used in this initial study are designed based on PS and PMMA analogues. They are expected to provide materials within this range of

neutrality required in the underlayer for the desired vertical lamellae PS-b-PMMA self-assembly. Direct modification of commercially available resist resin ESCAP-1 is conducted due to the ease of synthesis and its proven high resolution patterning capability. PHOST-Pv-MA and PHOST-iPOC-MA are made based on the modification of poly(p-hydroxystyrene). Pv has high stability toward acid catalyzed deprotection. It is normally deprotected only with a strong base or nucleophile.[8] The iPOC protecting group is reported to be much less acid sensitive and thermally labile than the traditional CAR protecting group tBOC. While it has been shown that a completely tBOC protected polyhydroxystyrene (PHOST-tBOC) is thermally stable up to 180 ℃ in the absence of photoacids, a partially protected PHOST-tBOC has much lower thermal stability because the free phenols are sufficiently acidic at elevated temperature to catalyze the deprotection of the tBOC group.[9] The superior stability of the iPOC group is because it forms a secondary isopropyl carbocation after the acid catalyzed deprotection which is less stable than the tertiary t-butyl carbocation formed from tBOC deprotection. This means that the acid catalyzed iPOC deprotection is less favorable than tBOC.[10] Therefore, it is expected that both the Pv and iPOC groups could provide reasonable thermal stability during the BCP thermal annealing process (e.g. up to 250 ℃) as will be discussed later.

3.2 Experimental

3.2.1 Materials and Instruments

Unless otherwise noted, all reagents and solvents were purchased from Sigma-Aldrich, TCI America, or Alfa-Aesar and used as received. Poly(p-hydroxystyrene)

(PHOST) with Mw 11,800 g/mol was donated by TriQuest, LP. ESCAP-1 resist resin (a poly-hydroxystyrene-styrene-*t*-butyl methylmethacrylate terpolymer with a molar ratio of 0.6:0.2:0.2, 74 wt% in PGMEA) was supplied by JSR and Intel. Azobisisobutyronitrile (AIBN) was recrystallized from methanol. Triphenylsulfonium hexafluoroantimonate (TPS-SbF6) photoacid generator (PAG) was purchased from Midori Kagaku Co., Ltd. Symmetric poly(styrene-*b*-methacrylate) (PS_{80}-*b*-$PMMA_{80}$, 80 kg/mol for PS and 80 kg/mol for PMMA, PDI = 1.09, L_0 = 80 nm) diblock copolymer was purchased from Polymer Source, Inc. and used without further purification.

A Varian Mercury Vx 300 was used to collect NMR. TGA analysis was performed using a TA Instruments Q500 TGA using a 20 ℃/min heating rate. Deep ultraviolet (DUV) exposures were performed using an Oriel Instruments 500W Hg-Xe arc lamp with a 248 nm band-pass filter. Film thicknesses were measured using a M-2000 spectroscopic ellipsometer (J.A. Woolam, Inc.) over the wavelength range of 350 to 1000 nm using a Cauchy layer to model the resist film. E-beam lithography was performed using a JEOL JBX-9300FS electron-beam lithography system with 100 keV acceleration voltage, 8 nm beam diameter, 2 nA current, and 10 nm single-pixel shot pitch. The patterns produced by e-beam lithography were imaged using a Carl Zeiss Ultra60 SEM with 2 keV acceleration voltage. The block copolymer film was etched with an Oxford End-point RIE tool; oxygen was used as etching gas at a flow rate of 10 sccm at 50 W.

3.2.2 Polymer Synthesis

3.2.2.1 ESCAP-1-MA

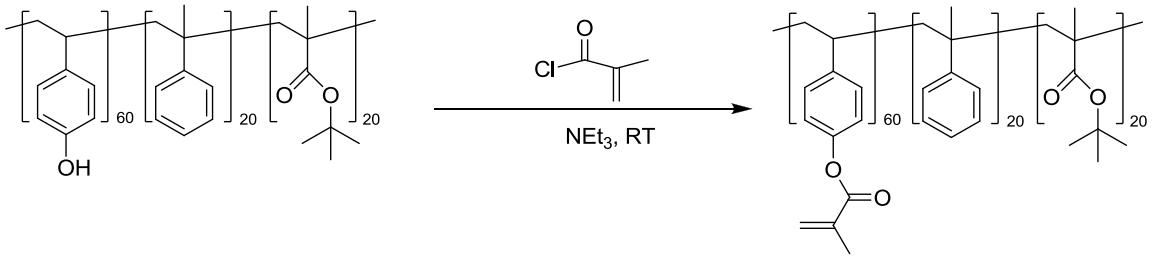

ESCAP-1 **ESCAP-1-MA**

Figure 3.6 Synthesis scheme of ESCAP-1-MA.

ESCAP-1-MA was synthesized by reacting methacryloyl chloride (1.0 equivalent) with ESCAP-1 resist in the presence of triethylamine (TEA, 2.0 equivalents) in THF at room temperature. After stirring for 24 h, the solution was washed twice with 3% HCl solution, three times with DI water, extracted with dichloromethane, dried over anhydrous $MgSO_4$, and dried using a rotary evaporator. The residual solution was precipitated in cold methanol and filtered. A white solid was obtained and dried under vacuum overnight. **Figure 3.7** shows the ^{1}H NMR of ESCAP-1-MA.

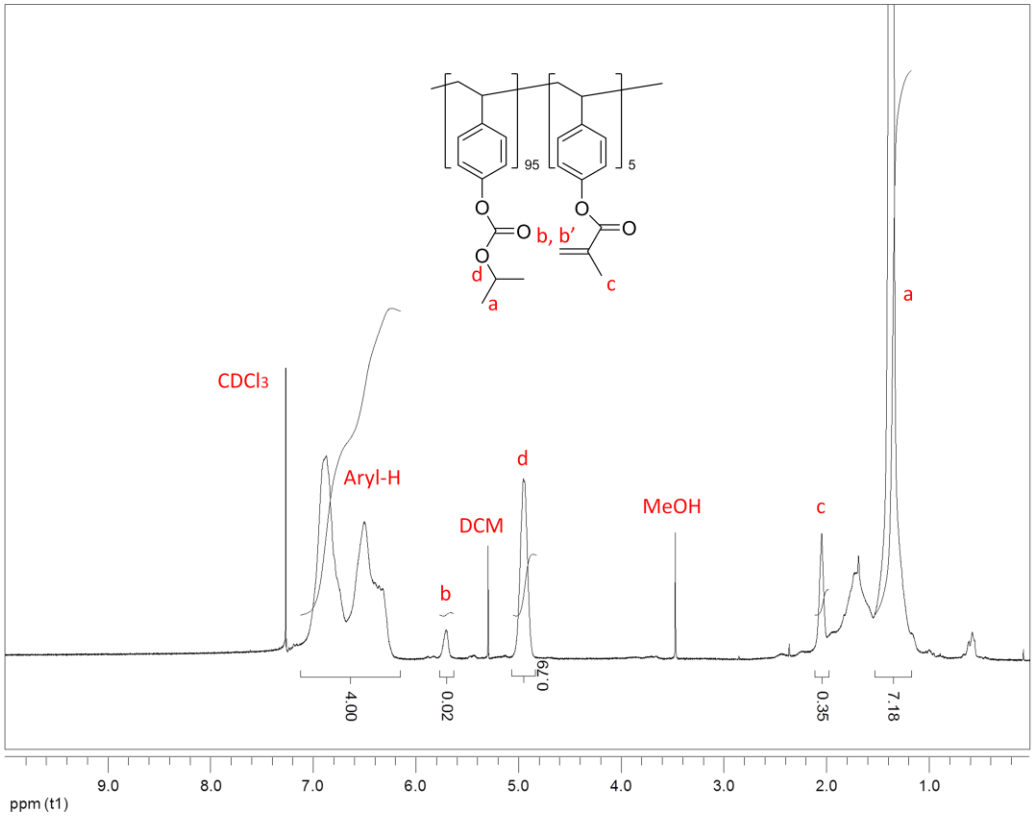

Figure 3.7. ^{1}H NMR of ESCAP-1-MA (in $CDCl_3$).

3.2.2.2 PHOST-Pv-MA

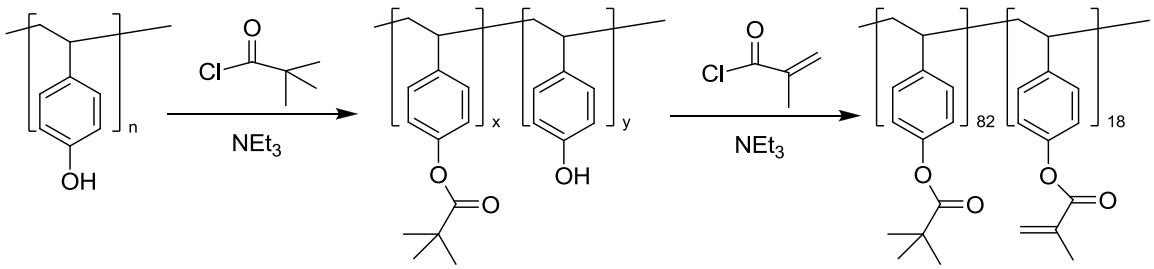

PHOST **POST-Pv** **PHOST-Pv-MA**

Figure 3.8 Synthesis scheme of PHOST-Pv-MA.

PHOST-Pv-MA was synthesized by reacting pivaloyl chloride (0.8 equivalent) with poly(p-hydroxystyrene) in the presence of triethylamine (TEA, 5.0 equivalents) in THF at room temperature. After stirring for 24 hrs, methacryloyl chloride (1 equivalent) was added in and the solution was stirred for another 24 h. The solution was washed twice with 3% HCl solution, three times with DI water, extracted with dichloromethane, dried over anhydrous $MgSO_4$, and dried using a rotary evaporator. The residual solution was precipitated in cold methanol and filtered. A light yellow solid was obtained and dried under vacuum overnight. **Figure 3.9** shows the ^{1}H NMR of PHOST-Pv-MA.

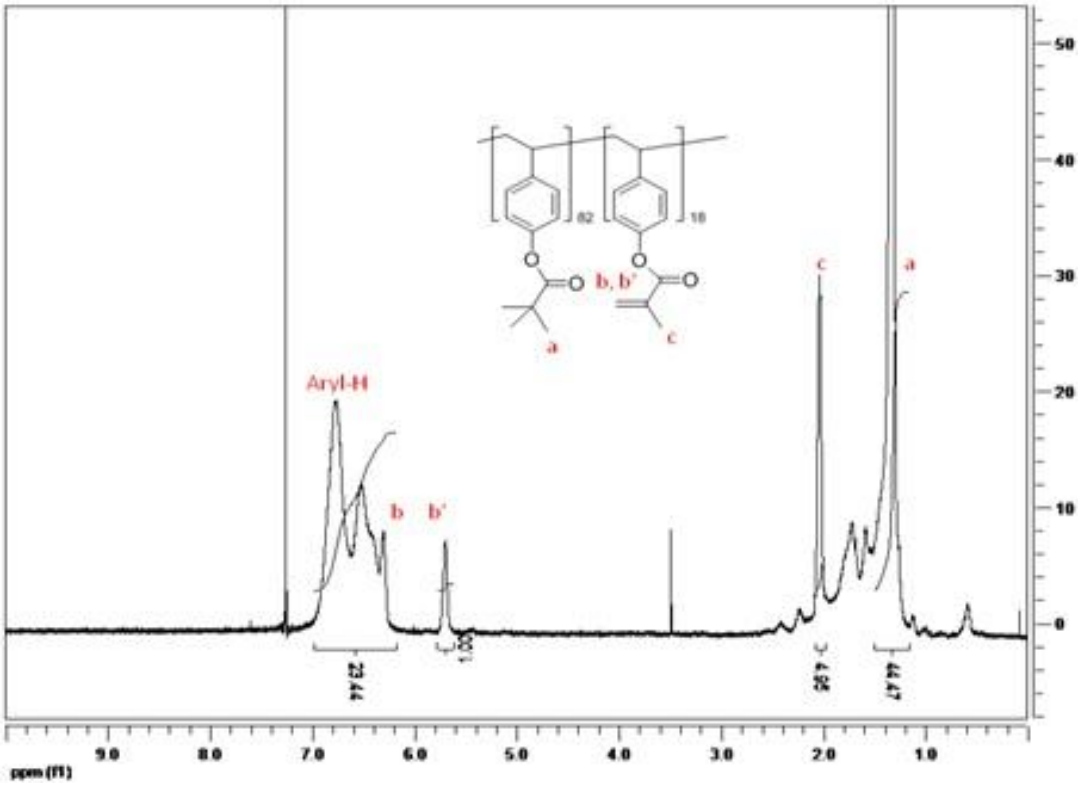

Figure 3.9. ^{1}H-NMR of PHOST-Pv-MA (in $CDCl_3$)

3.2.2.3 PHOST-iPOC-MA

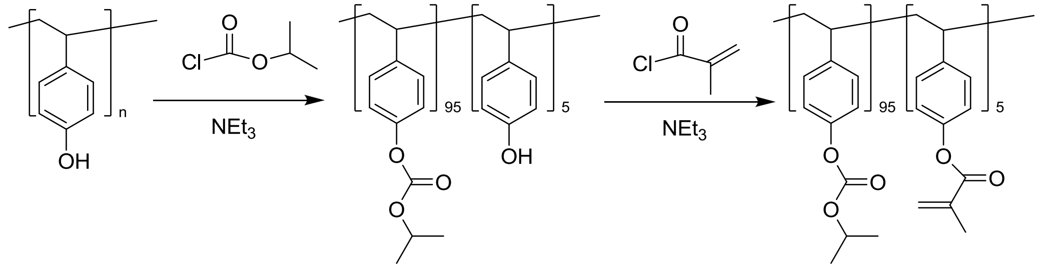

PHOST **POST-iPOC** **PHOST-iPOC-MA**

PHOST-iPOC-MA was synthesized by the similar way as PHOST-Pv-MA. The feed amount of isopropylchloroformate was 0.9 equivalents. The product is a light yellow solid. **Figure 3.10** shows the [1]H NMR of PHOST-iPOC-MA.

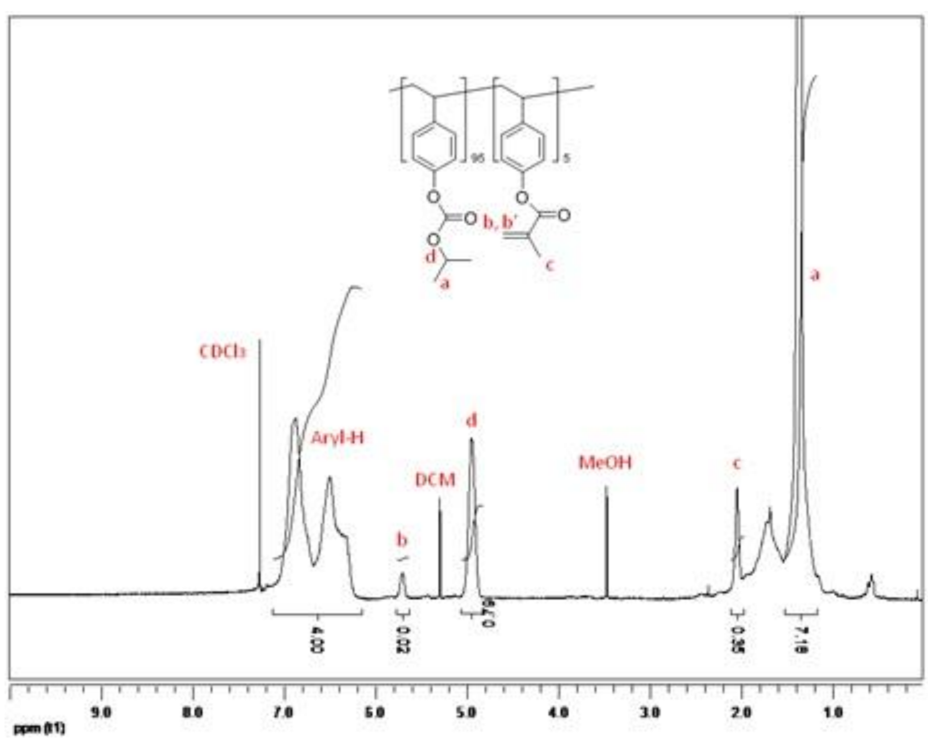

Figure 3.10. ^{1}H-NMR of PHOST-iPOC-MA

3.2.3 Lithography and DSA Processing

After testing the thermal stability of these three materials, PHOST-iPOC-MA was chosen as the first generation photodefinable guiding layer for further evaluation as will be discussed later. A multi-component system was blended using PHOST-iPOC-MA with 5 wt% TPS-SbF_6 (with respect to polymer), 20 mol% AIBN (relative to MA). The solids were dissolved in PGMEA to make a homogeneous solution. After spin-coating, the film was dried with a N_2 gun without heat to prevent the decomposition of AIBN. Different film thicknesses were obtained by varying spin speeds as well as concentration of the solution. The wafer sample was heated at 250 ℃ under nitrogen flow for 10 min to crosslink the methacrylate functional groups. After patterning with e-beam exposure from 50 μC/cm^2 to 1280 μC/cm^2 and PEB at 170 ^{o}C for two minutes, sonication for 10 min in PGMEA was performed to remove uncrosslinked polymer, as well as any residues after deprotection. A blank film exposure by DUV and wash by solvent test suggested that the film remained ~ 40% after the treatment.

E-beam lithography was used to produce a 40 nm 1:1 line:space pattern on a PHOST-iPOC-MA crosslinked film. After sonication, a 40 nm thick film of PS_{80}-*b*-$PMMA_{80}$ (L_0 ~ 80 nm) was spincoated on top of the patterned iPOC film and thermally annealed at 250 ^{o}C under N_2 for 30 min. SEM imaging was performed to evaluate the DSA performance.

3.3 Results and discussion

3.3.1 Thermal Stabilities of the Materials

Three materials (**Figure 3.5 and Figure 3.11**) were synthesized and screened for use as a photodefinable guiding layer for BCP DSA. They are all expected to form a chemically patterned surface that could be capable of guiding BCP self-assembly, and they were subsequently tested to see if they could survive the spin coating and harsh annealing conditions (e.g. 250 ^{o}C) required for many BCP self-assembly processes without significant change.

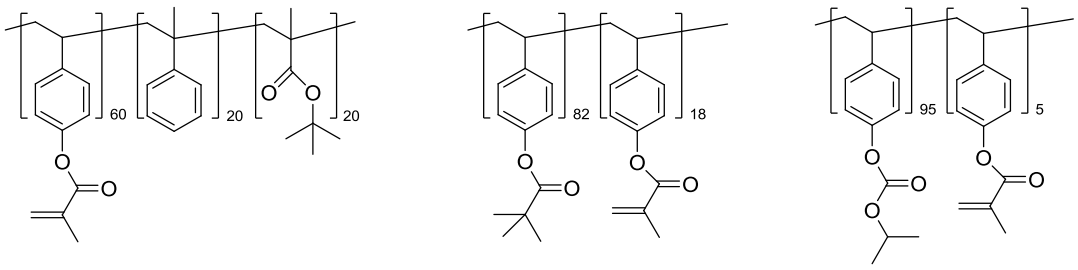

ESCAP-1-MA **PHOST-Pv-MA** **PHOST-iPOC-MA**

Figure 3.11. Materials studied as photodefinable guiding layer

Thermogravimetric Analysis (TGA) was performed to test the thermal stability of the three materials and is shown in **Figure 3.12.** TGA shows that traditional CAR protecting groups such as the t-butyl ester in ESCAP-1-MA are not sufficiently thermally stable and start to decompose as low as 150 ℃. In contrast, groups such as the pivolate group investigated are too thermally stable. PHOST-Pv-MA only shows one plateau during thermal decomposition which indicates that the polymer back bone is cleaved before or simultaneously with the deprotection of protecting group. The secondary

carbonate of the iPOC protecting group possesses the desired thermal properties. It starts to decompose at 250 - 260 ^{o}C. Also, the PHOST-iPOC-MA film water contact angle remains constant after >1 h heating at 250 ℃ in N_2, suggesting the material is stable for thermal BCP annealing treatments.

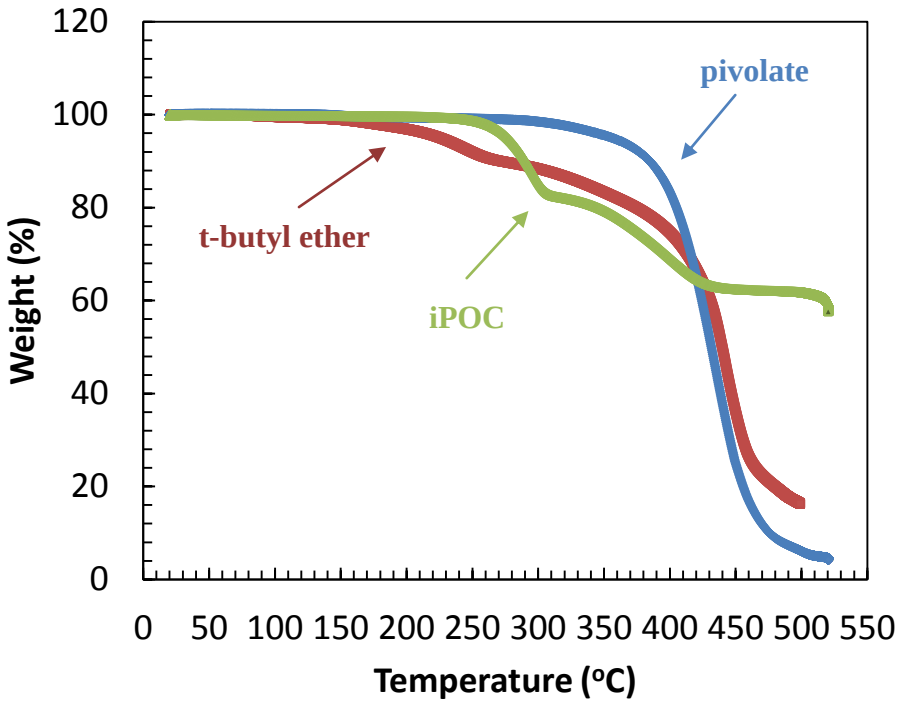

Figure 3.12. TGA for ESCAP-1-MA, PHOST-Pv-MA and PHOST-iPOC-MA.

3.3.2 Patterning Performance

Thus, PHOST-iPOC-MA was selected as a potential photodefinable guiding layer material. The initial study was based on a multi-component system: PHOST-iPOC-MA was blended with 5 wt% TPS-SbF_6 (with respect to polymer), 20 mol% AIBN (relative to MA). The first test was to measure the thermal cross-linking ability of the methacrylate functional groups of PHOST-iPOC-MA in the presence of AIBN. The polymer film was

baked at 250 ℃ under N_2 for 10 min. After cooling down, it was sonicated in PGMEA for 10 min to remove the uncrosslinked polymer. The normalized remaining film thickness is 0.43, which means about 57% of the polymer was lost during solvent sonication. Although the crosslinking extent is low, it might be still appropriate as a guiding layer. Future optimization on the polymer structure composition and the blended system formulation is being conducted to provide materials that retain 100% of their post-exposure film thickness during subsequent processing.

Tests were performed to determine the optimal post-exposure bake (PEB) conditions for the deprotection reaction in PHOST-iPOC-MA. After the coating and crosslinking the films, the film thickness was measured, and the wafers were exposed to 100 mJ/cm^2 (248 nm) to convert the majority of the PAG to photoacid. The samples were then baked at different PEB temperatures for 2 min to deprotect the iPOC groups. The resulting contact angle and normalized remaining film thickness were measured without developing the polymer. **Figure 3.13** shows the contact angle change and film thickness change with different PEB temperatures. The film becomes thinner and more hydrophilic (shown by decreasing contact angle) after the exposure because of the deprotection of iPOC group to form volatile reaction products and regenerate phenolic sites on the polymer. A PEB of ~170 ℃ appears to be optimal for PHOST-iPOC-MA to provide the largest change in contact angle which should provide the largest chemical contrast and driving force for PS-b-PMMA DSA. **Figure 3.14** shows the DUV (248 nm) dose response curve for contact angle and remaining film thickness for PHOST-iPOC-MA with a PEB of ~170 ℃. It suggests that PHOST-iPOC-MA has good sensitivity, allowing for low exposure doses to DUV and potentially e-beam radiation.

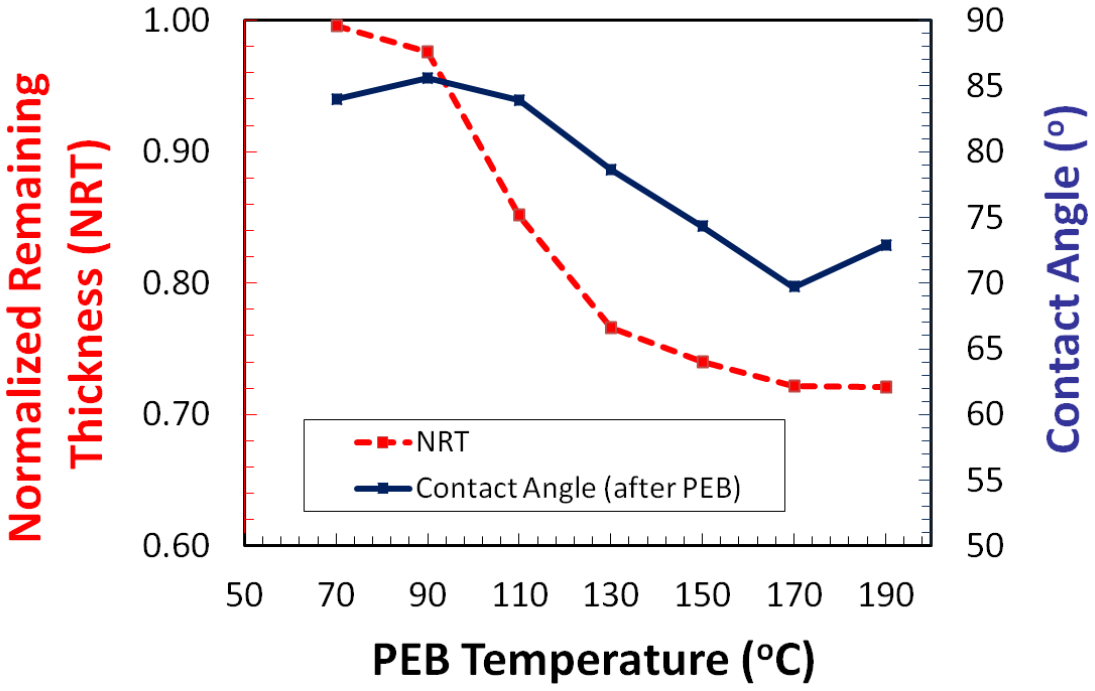

Figure 3.13. Effect of PEB temperature on PHOST-iPOC-MA exposed to 100 mJ/cm^2 containing 5 wt% TPS-SbF_6 (with respect to polymer) and 20 mol% AIBN (relative to MA).

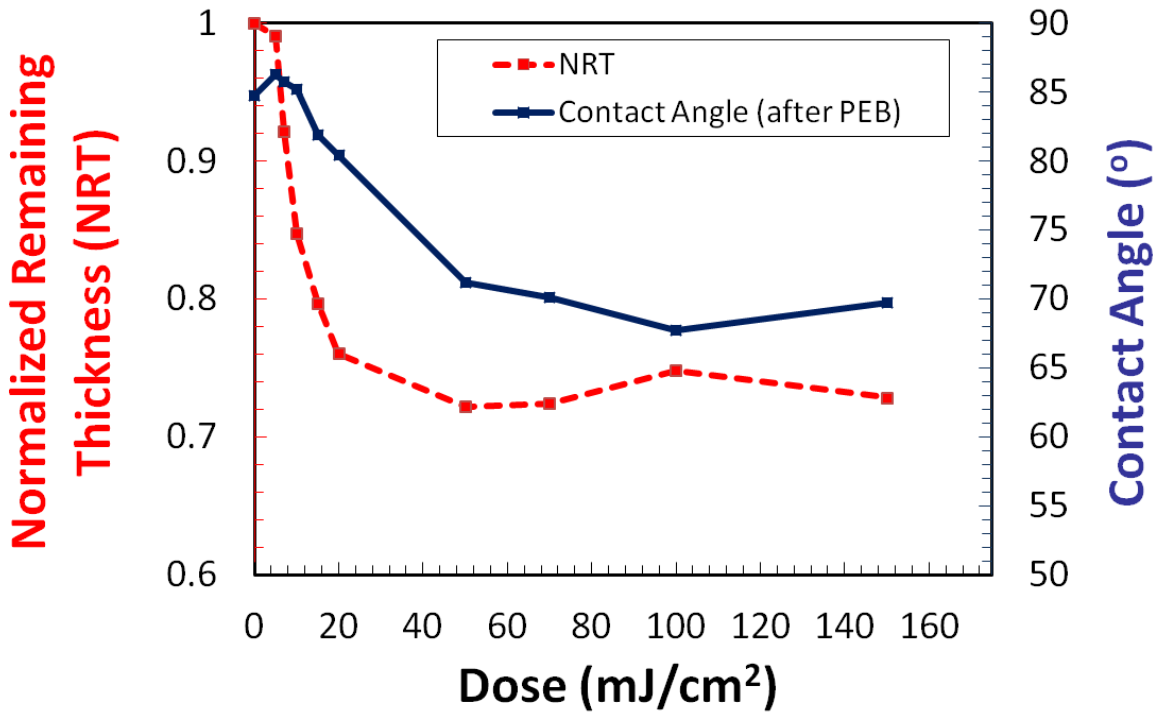

Figure 3.14. DUV dose response curve for PHOST-iPOC-MA with a PEB of 170 ℃ containing 5 wt% TPS-SbF_6 (with respect to polymer) and 20 mol% AIBN (relative to MA).

PHOST-iPOC-MA formulated with TPS-SbF_6 and AIBN was patterned using 100 keV e-beam to render surfaces suitable for chemoepitaxial guiding of PS-b-PMMA self-assembly. The crosslinked PHOST-iPOC-MA was patterned with e-beam exposure from 50 μC/cm^2 to 1280 μC/cm^2 and PEB was taken at 170 ℃ for two minutes. An AFM study of the 40 nm 1:1 line:space pattern suggested that the PHOST-iPOC-MA had been successfully patterned into desired size, see **Figure 3.15.**

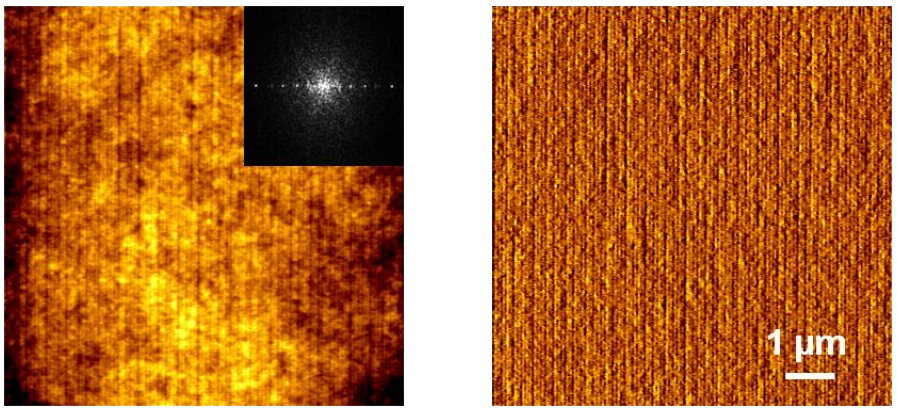

(a) **(b)**

Figure 3.15. AFM of e-beam patterned PHOST-iPOC-MA film to form 40 nm 1:1 line:space pattern. a. Topography image with inset of 2D FFT; b. Phase image.

3.3.3 DSA of PS-b-PMMA: Change of Substrate Thickness

Even though the original PHOST-iPOC-MA substrate was preferential to PMMA, and top "dots" like morphology was formed from a symmetric PS_{80}-*b*-$PMMA_{80}$ (L_0 ~ 80 nm), the DSA of PS-b-PMMA could be controlled by several experimental conditions. As mentioned earlier,[11] the PHOST-iPOC-MA could reach ~ 20 °contact angle drop after patterning, which indicates a more hydrophilic surface is formed through deprotection of iPOC functionalized polyphenols. However, the thickness of the substrates influences the DSA of PS-b-PMMA to a greater extent. As shown in **Figure 3.16**, the PS-b-PMMA was directed to self-assemble from aligned top "dots" into aligned lamella as the substrate thickness increased.

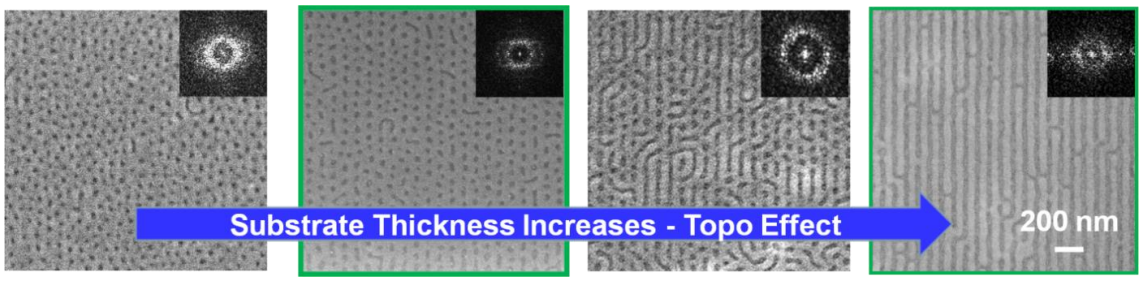

Figure 3.16. SEM of DSA of PS_{80}-*b*-$PMMA_{80}$ (L_0 ~ 80 nm) on substrates with increased film thickness, from left to right (the original thickness is 30, 38, 45 and 58 nm). All substrate films were patterned with same e-beam dose. The inset image is the 2D FFT; when more ordered lamellae are formed, the FFT appears brighter.

The effect of the substrate thickness was investigated by using AFM. Due to the low film remaining (NRT=0.4 after patterning and solvent wash) of those substrates, if deposited too thin, the substrate might not be able to form a continuous surface. The original thicknesses of the substrate shown in Figure 3.16 were 30, 38, 45 and 58 nm. However, after the e-beam patterning and solvent wash, the substrates only remained about 13, 16, 19 and 25 nm by estimation. When scanning those substrates after solvent wash, significant difference in terms of the surface topography was found, shown in **Figure 3.17**. There were pinholes found on the thinner substrate, which was the original 38 nm film that remained 16 nm after wash. The pinholes of the thin substrate lead to a more hydrophilic surface (the Si substrate), which was more preferential to PMMA. In contrast, the thicker substrate, the original 58 nm which remained 25 nm after wash, was smooth and no pinholes were found.

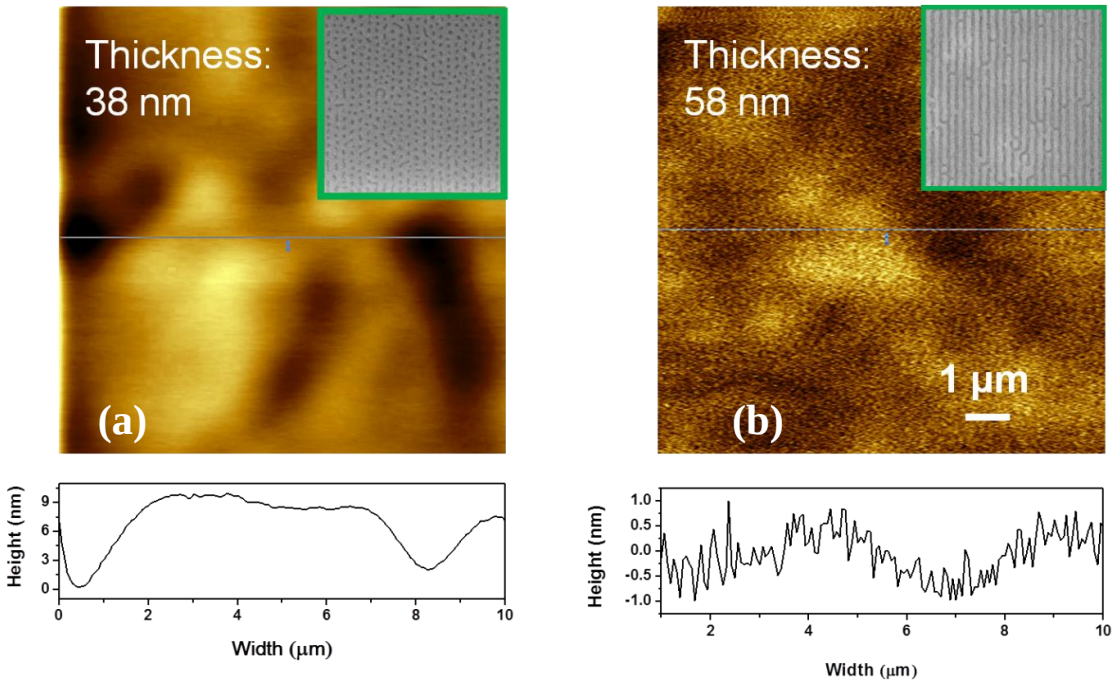

Figure 3.17. AFM of the substrate materials after e-beam patterning and solvent wash. The bottom images show the cross section of the cut line. There were pinholes found on the thinner substrate, which was the original 38 nm film (a) that remained 16 nm after wash. The pinholes of the thin substrate lead to a more hydrophilic surface (the Si substrate), which was more preferential to PMMA. In contrast, the thicker substrate, the original 58 nm (b) which remained 25 nm after wash, was smooth and no pinholes were found.

Thus, the AFM study suggested that the pinholes induced substrate surface energy increase might be the reason that caused the formation of the top "dots" morphology on the thinner substrate.

3.3.4 DSA of PS-b-PMMA: Dose Response

With the same substrate thickness, e-beam patterning did also plays an important role to the DSA of PS-b-PMMA, see **Figure 3.18**. When either underdosed or overdosed, the substrate lost commensurability with the PS-b-PMMA. Both of these events created more defects on the block copolymer film after DSA. Only in a discrete dose window were aligned lamellae seen, as the substrate reached the optimal guiding stripe size.

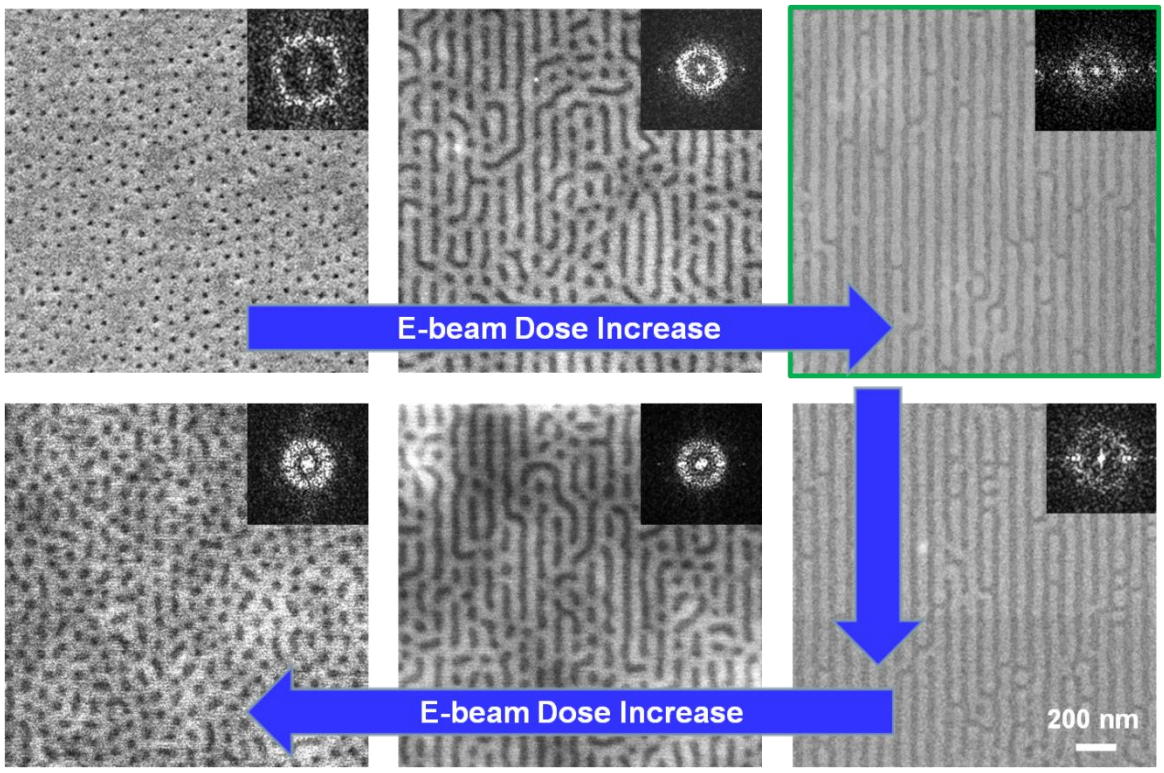

Figure 3.18. SEM of DSA of PS_{80}-*b*-$PMMA_{80}$ (L_0 ~ 80 nm) on the same substrates with increased e-beam dose. The 2D FFT shows brighter spikes when more ordered lamella are formed.

3.4 Conclusion

Photodefinable polymeric guiding layers (GL) can greatly simplify block copolymer DSA processes as compared to the multi-step guiding layer fabrication procedures currently used. A first generation photodefinable GL has been synthesized and characterized based on a PHOST polymer that has been functionalized with methacrylate and iPOC groups. It has been shown to successfully guide PS-b-PMMA directed self assembly. Radical polymerization of acrylate functional groups can be used to insolubilize such photodefinable guiding layers without interference with or from PAGs or the protecting groups on the polymer. Introduction of PAGs into these polymers then allow for deprotection based schemes to be used for generating chemical patterns on the polymer surface. The iPOC protecting group has been found to be ideal in terms of its resistance to uncatalyzed thermal deprotection during thermal BCP annealing and its resistance to thermal deprotection from weak acids. This material functions chemically to guide the PS-b-PMMA into aligned lamellae. The iPOC protected polyphenols have been shown to be a suitable energy switchable group, as the film produces a ~ 20 °contact angle drop after patterning. These types of photodefinable GLs provide promise as a method for guiding DSA processes that can easily be implemented using current lithographic tools and processes.

3.5 References

1. *International Technology Roadmap for Semiconductors, http://www.itrs.net.*
2. Bates, F. S.; Fredrickson, G. H. *PHYSICS TODAY* **1999,** 52, (2), 32.
3. Leibler, L. *Macromolecules (Washington, DC, United States)* **1980,** 13, 1602.
4. Bates, F. S.; Fredrickson, G. H. *Annu. Rev. Phys. Chem.* **1990,** 41, 525.

5. Peters, R. D.; Yang, X. M.; Wang, Q.; de Pablo, J. J.; Nealey, P. F. *J. Vac. Sci. Technol. B* **2000,** 18, (6), 3530-3534

6. Segalman, R. A.; Yokoyama, H.; Kramer, E. *J., Adv. Mater.* **2001,** 13, (15), 1152-1155.

7. Han, E.; Stuen, K. O.; La, Y.; Nealey, P. F.; P., G. *Macromolecules* **2008,** 41, 9090-9097.

8. Wuts, P. G. M.; Greene, T. W. *Wiley-Interscience, New York* **2007**, 250- 253.

9. Fréchet, J. M. J.; Eichler, E.; Ito, H.; Willson, C. G. *Polymer* **1983,** 24, (8), 995-1000.

10. Fahey, J.; Conley, W.; Brunsvold, B.; Yang, D.; Moreau, W.; Jordhamo, G.; Pratt, S.; Crockatt, D.; Hefferon, G.; Wood, R. *Proc. SPIE* **1995,** 2438, 125-142.

11. Cheng, J.; Lawson, R. A.; Yeh, W.-M.; Tolbert, L. M.; Henderson, C. L. *Proc. of SPIE* **2011,** 7972, 79722I.

CHAPTER 4

PS-B-PAA AS A HIGH χ POLYMER FOR DIRECTED SELF-ASSEMBLY

4.1 Introduction

As Moore's law predicts, the rate for the semiconductor industry to produce smaller, faster, and denser microelectronic systems, is governed by the ability to create scaled high resolution patterns on substrates of electronic materials.[1] Standard photolithography is becoming increasingly difficult and expensive for the manufacturing of sub-30-nm patterns as it approaches the diffraction limit. Electron-beam lithography is able to push the feature sizes down to sub 10 nm,[2] but it is not suitable for large-scale production because of its high cost and low throughput. The demand for high resolution patterning has made researchers move to an alternative patterning method – block copolymer lithography.[3, 4] Block copolymers undergo microphase separation into periodic domains of sub-30 nm length scales.

Even a diblock copolymer can form lamellar, gyroidal, cylindrical, and spherical microsturctures by tuning the relative composition of the two blocks **(Figure 1).**[5] Because self-assembled block copolymers hardly achieve inherent long range order and the pattern geometries are relatively simple, researchers have used chemically[6] or topographically[7] patterned substrates, combined with thermal or solvent annealing, to direct the assembly of the microdomains to desired patterns.

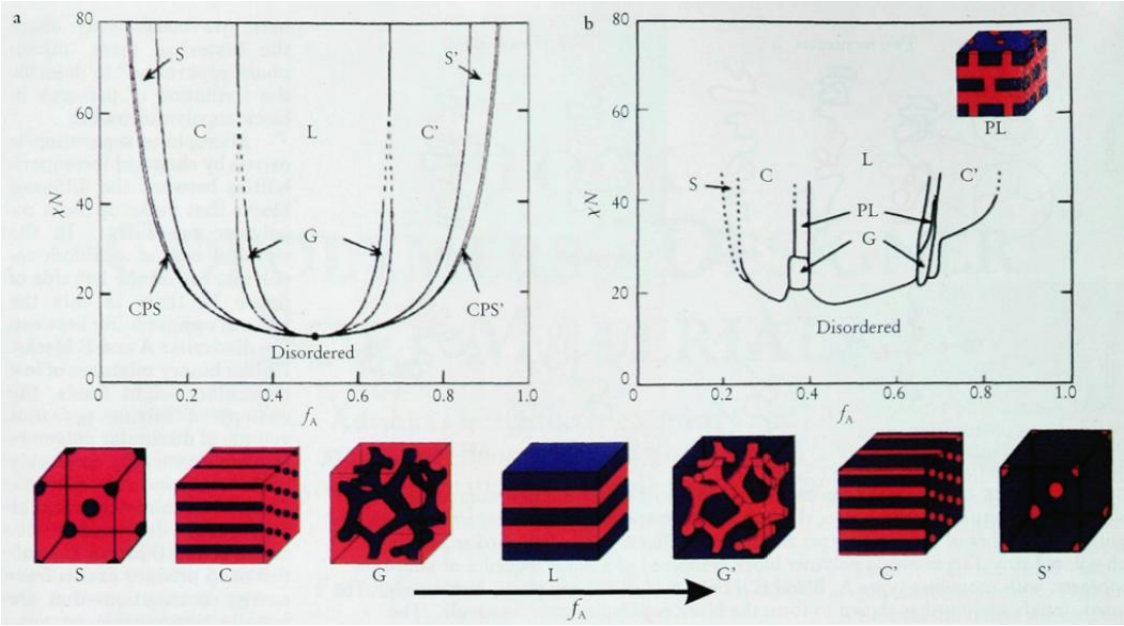

Figure 4.1. PHASE DIAGRAM for linear AB diblock copolymers. a: Self-consistent mean-field theory predicts four equilibrium morphologies: spherical (S), cylindrical (C), gyroid (G) and lamellar (L), depending on the composition f and combination parameter χN.[5]

4.1.1. High χ Block Copolymer for Smaller Feature Sizes

The propensity of the blocks to phase separate depends on the thermodynamic driving forces for such phase separation which are often characterized by the Flory Huggins interaction parameter (χ). When the enthalpic energy gains produced by phase separation of the blocks are sufficiently large as to overcome the entropic driving force to mix the blocks, micro-phase separation occurs, giving rise to a large number of nanostructured phases that depend on the relative volume fractions of the two phases. The condition at which such micro-phase separation occurs is characterized by **Equation 4.1**,[5] where χ is the Flory Huggins interaction parameter, and N is the degree of

polymerization. For block copolymer with compositions near 50:50 volume fractions of the two blocks, lamellar phase separated patterns form. The pitch of such lamellar patterns in the strong segregation limit has been found to be proportional to the statistical segment length (a), Flory Huggins interaction parameter (χ), and the degree of polymerization (N) as shown in **Equation 4.2**.[5]

$$\chi N = 10.4 \tag{4.1}$$

$$\lambda \approx 1.03 a \chi_{AB}^{1/6} N^{2/3} \tag{4.2}$$

The goal lithographically is to utilize this natural tendency of block copolymers to phase separate on length scales dictated by the polymer chain dimensions themselves to form and align small self-assembled patterns on lithographically made guiding patterns to achieve pitch reduction of the primary lithographic pattern. Such processes are commonly referred to as directed self-assembly (DSA). Currently the most widely studied block copolymer (BCP) for such DSA is poly(styrene)-block-poly(methyl methacrylate) or PS-b-PMMA. PS-b-PMMA possesses a modest χ value of only approximately 0.04, which translates into a minimum practical DSA pitch for such materials of ca. 20 nm.[8] The goal in this work has been to develop higher χ polymers and the associated processes required to achieve DSA at higher resolution pitch multiplication from primary lithographic patterns. One such overarching strategy has been to explore the use of poly(acid) blocks in place of the poly(methyl methacrylate) block in PS-b-PMMA. In this paper, the PMMA block from PS-b-PMMA has been replaced with poly(acrylic acid) to produce a block copolymer with a substantially higher χ value.

Since the domain size of the resulting block copolymer pattern is related directly to the degree of polymerization (N), in general N should be as small as possible to achieve the minimum feature size and pitch for a given block copolymer. Combining the

observed lamellar domain size scaling in **Equation 4.2** with the requirement for microphase separation shown in **Equation 4.1**, it is possible to estimate the minimum pitch that can be achieved for a block copolymer as a function of χ. **Figure 4.2** shows the result of such a calculation for a case where the polymer statistical segment length is assumed to be a constant 0.7 nm (i.e. a value that is reasonable for PS-b-PMMA). For PS-b-PMMA, which possesses a χ of approximately 0.4,[8] this equates to a minimum pitch in DSA of between 15 nm and 20 nm. To robustly achieve pitches smaller than 20 nm from DSA, alternative polymers beyond PS-b-PMMA with higher χ values are needed.

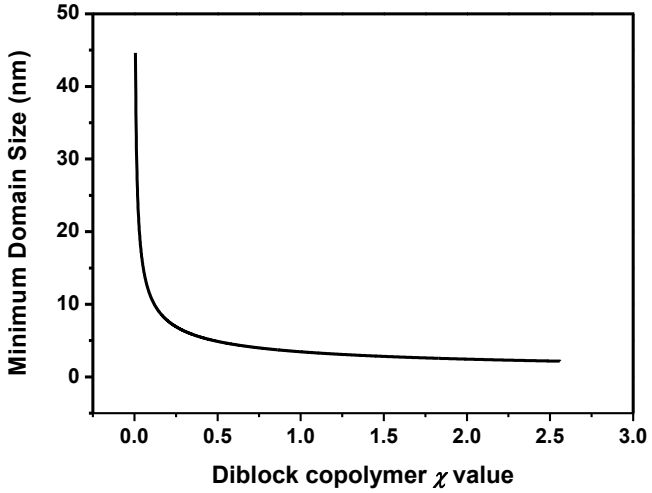

Figure 4.2. Minimum achievable pitch in 1: 1 line: space patterns formed from DSA as a function of block copolymer χ value (assume a = 0.7 nm for all polymer χ values).

4.1.2. Polystyrene-b-polyacid as High χ Block Copolymer

We have proposed a series of block copolymers which are composed of polystyrene and another block with hydrogen bonding motif, like polyacid, polyphenol or polyalcohol **(Figure 3).**

To achieve higher χ polymers for DSA, we are evaluating the polystyrene-b-polyacid polymer design. The carboxylic acid residue is capable of hydrogen bonding, and such hydrogen bonding should provide strong self interaction which would contribute to a high χ value for the block copolymer. Additionally, polystyrene-b-polyacid in particular possesses several key features:

1. Sufficiently high plasma etch contrast to allow for selective block removal: The etch rates of poly(styrene), poly(methyl methacrylate), and poly(acrylic acid) can be roughly compared according to their Ohnishi parameter,[9] a popular model for estimating the relative etch rates of hydrocarbon polymers. According to this relationship, the etch rate of a polymer in a plasma is proportional to $N_T/(N_C-N_O)$, where N_T is the total number of atoms, N_C is the number of carbon atoms, and N_O is the number of oxygen atoms. The etch rates of the three polymer mentioned earlier are estimated to follow the trend: poly(acrylic acid) > poly(methyl methacrylate) > poly(styrene). Since etch processes have already been successfully developed and demonstrated for removing the PMMA block from microphase separated PS-b-PMMA patterns, this same etch technology can be leveraged to produce even better block removal results for PS-b-PAA polymers.

2. Compatibility with current chemical epitaxy process: Like the PS-b-PMMA block copolymer system, the PS-b-PAA system provides a hydrophobic PS block and a hydrophilic polyacid block. Although they may require some retuning of optimal compositions, it is anticipated that PS-b-PAA based DSA processes can reuse the same types of chemoepitaxial guiding layers as those developed for PS-b-PMMA.

3. Moderate T_g: T_g of PS and PAA are both ~ 105 °C, while T_g of PMAA (228 °C) is too high for thermal process. Thus, PS-b-PAA is more promising for use in thermal annealing.

4. Simple to make by controlled living polymerization: PS-b-PAA with controlled molecular weight (Mw) and low polydispersity (PDI) have been successfully synthesized via controlled living polymerization techniques (e.g. atom transfer radical polymerization (ATRP)[10]) of their corresponding esters.

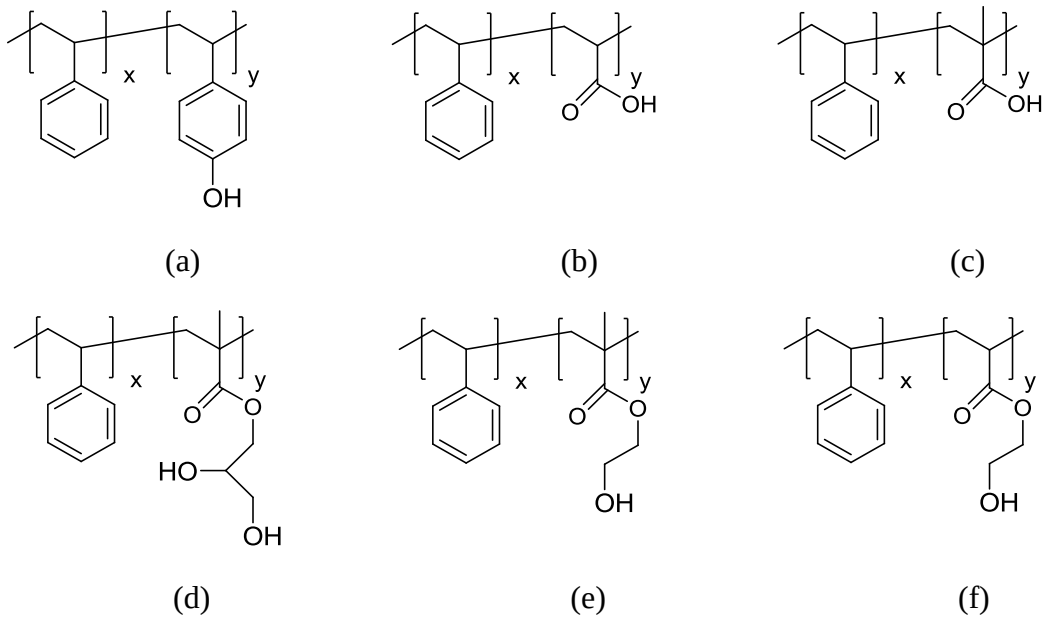

Figure 4.3. Examples of block copolymers which are composed of polystyrene and another block with hydrogen bonding motif, (a) is polystyrene-b-polyphenol, (b) and (c) are polystyrene-b-poly(carboxylic acid), (d), (e) and (f) are polystyrene-b-polyalcohol.

4.1.3. Define the Neutral Substrate for Polystyrene-b-polyacid:

PHOST-iPOC-MA was studied as the first generation photodefinable guiding layer in our group[11]. It is formulated with 5 wt% TPS-SbF_6 (with respect to polymer) and

20 mol% AIBN (relative to MA). The substrate surface energy could be subtly tuned: crosslinked substrate was exposed to gradient dose to achieve gradient deprotection level **(Figure 4).** The more deprotected phenol groups render a more hydrophilic substrate. Optimal dose was determined by checking the annealed BCP film quality. The surface water contact angle could be from 68 ^{o} to 85 ^{o}.

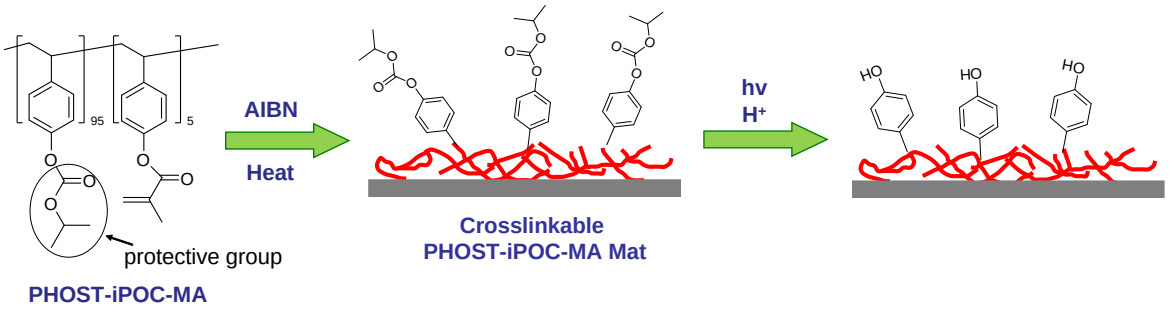

Figure 4.4. Scheme of tuning surface energy by PHOST-iPOC-MA

4.2 Experimental

4.2.1 Materials and Instruments

Materials

Unless otherwise noted, all reagents and solvents were purchased from Sigma-Aldrich, TCI America, or Alfa-Aesar and used as received. Styrene and t-butyl acrylate were dried over CaH_2, passed through a neutral alumina column to remove inhibitor. CuCl was made from reduction of $CuCl_2$ by Na_2SO_3 in HCl solution, precipitated and then washed by diethyl ether and absolute ethanol, dried in vacuum oven at 50 ^{o}C

overnight. ATRP catalysts 4,4'-di(5- nonyl)-2,2'-bipyridine (dNbpy) and N,N,N',N',N''-pentamethyldiethylenetriamine (PMDETA), initiator (1-chloroethyl)benzene (PECl) were used as received. ATRP solvents methyl ethyl ketone (MEK) was dried over K_2CO_3, distilled; isopropanol (IPA) was dried over CaH_2, distilled.

Measurements

A Varian Mercury Vx 300 was used to collect NMR. Molecular weight and PDI of the polymers were estimated by gel permeation chromatography (GPC), using a Waters 1515 isocratic pump coupled to a Waters 2489 UV detector with THF as the elution solvent. All GPC measurements were carried out at a flow rate of 0.3 mL/min at 35 ^{o}C, and calibrated using narrow molecular weight polystyrene standards. Fourier transform infrared (FTIR) spectroscopy was performed using a Bruker Vertex 80v with a Hyperion microscope attachment on KBr pellet. Grazing angle infrared (GIR) spectroscopy of the PS-b-PAA films was performed on gold coated Si wafer. Film thicknesses were measured using an M-2000 spectroscopic ellipsometer (J.A. Woolam, Inc.) over the wavelength range of 350 to 1000 nm using a Cauchy layer to model the resist film. The morphologies of PS-b-PAA films were imaged using a Carl Zeiss Ultra60 SEM with 1 keV acceleration voltage. The size of the self-assembled PS-b-PAA structures were measured with 2D Fast Fourier Transform (FFT) by using Gwyddion software.

4.2.2. Synthesis of symmetric PS-b-PAA via ATRP and Hydrolysis

PS-b-PAA was synthesized with controlled Mw and PDI via ATRP and hydrolysis. The synthetic scheme is shown in Figure 4.

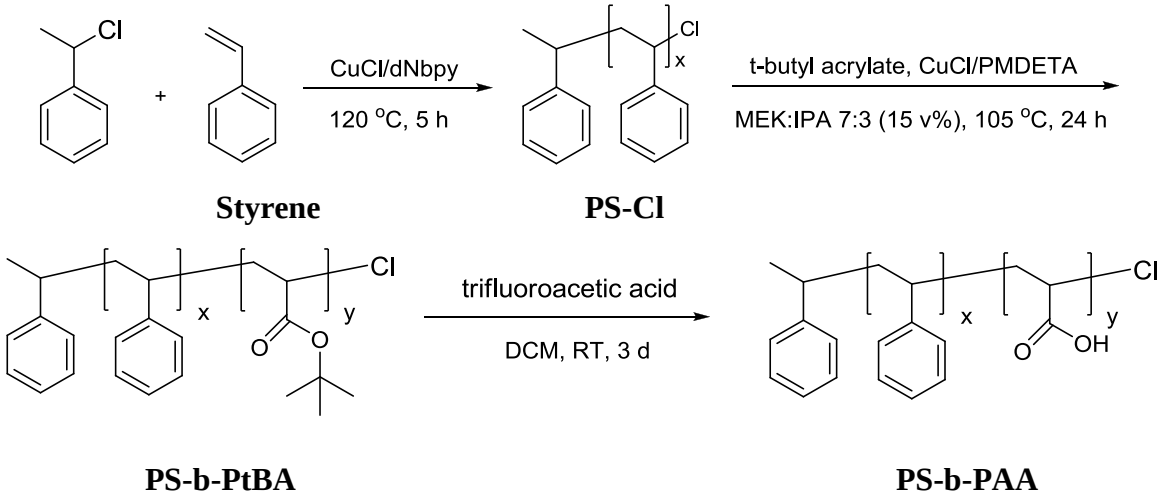

Figure 4.5. Synthetic scheme of PS-b-PAA

4.2.2.1 Synthesis of Macroinitiator PS-Cl

In a 50 mL schlenk flask, styrene (15 mL, 130.9 mmol), CuCl (115 mg, 1.2 mmol), dNbpy (973 mg, 2.4 mmol), PECl (0.158 mL, 1.2 mmol) were added. After three cycles of freeze-pump-thaw to remove oxygen, the schlenk flask was back-filled with dry N_2. The solution was sonicated to completely dissolve the catalyst, which turned brown after sonication. The flask was placed in an oil bath, heated at 130 ℃. After 5 hours, the solution was highly viscous. The polymerization was quenched by placing the flask in an ice bath and exposing the solution to the air. The solution was diluted by

dichloromethane and filtered through a neutral alumina column to remove the catalyst. The polymer solution was then rotary evaporated precipitated into a 10-fold excess of MeOH. After drying under vacuum overnight, 8.4 g white solid was obtained. GPC analysis shows that Mn = 8,000 g/mol, PDI = 1.16 **(Figure 4.6).**

4.2.2.2 Synthesis of PS-b-PtBA.

In a 25 mL schlenk flask, PS-Cl (8,000 g/mol, 2.29 g, 0.3 mmol), t-butyl acrylate (5mL, 34.4 mmol), MEK/IPA (7:3, 15 volume %) were added and allowed to stir until the PS-Cl is completely dissolved. Then CuCl (55 mg, 0.5 mmol), PMDETA (0.144 mL, 6.9 mmol) were added. The solution turned light green after the catalyst complex was formed. After three cycles of freeze-pump-thaw to remove oxygen, the schlenk flask was back-filled with dry N_2. The flask was placed in an oil bath, heated at 105 ℃. After 24 hours, the solution was highly viscous. The polymerization was quenched by placing the flask in an ice bath and exposing the solution to the air. The solution was diluted by dichloromethane and filtered through a neutral alumina column to remove the catalyst. The polymer solution was then rotary evaporated and precipitated into a 10-fold excess of MeOH/H_2O (1:1). After drying under vacuum overnight, 5.1 g white solid was obtained. GPC analysis shows that Mn = 20, 500 g/mol, PDI = 1.38. ^{1}H NMR analysis was performed in $CDCl_3$, shown in **Figure 4.7 (a)**. Two broad resonance peaks at δ = 6.5 ppm and δ =7.1 ppm stand for aromatic protons of the polystyrene. Resonances for poly t-butyl acrylate are at δ = 2.3 and 1.9 ppm for backbone protons, along with a sharp singlet corresponding to the t-butyl group at δ = 1.5 ppm. The composition calculated from ^{1}H NMR is PS-b-PtBA (8, 000 - 14, 000 g/mol), which shows high agreement with the GPC result **(Figure 4.6).**

4.2.2.3 Hydrolysis of PS-b-PtBA.

PS-b-PtBA (2 g) was dissolved in dichloromethane and trifluoroacetic acid (TFA, 10 mL) was added. This mixture was then stirred at room temperature for 3 days. The resulting polystyrene-b-poly(acrylic acid) precipitated out from the reaction solution. The solid was filtered, washed with dichloromethane. After drying under vacuum overnight, 0.9 g white solid was obtained. ^{1}H NMR analysis was performed in DMSO-d_6, shown in **Figure 4.7 (b).** The disappearance of t-butyl group resonance peak suggests the complete hydrolysis of PtBA block. FTIR analysis **(Figure 4.8)** also confirms the formation of PAA by showing the broad absorbance peak from 2800 to 3600 cm^{-1}, and the carbonyl peak is broadened as expected. Thus, block copolymer PS-b-PAA (8, 000 - 8, 000 g/mol, PDI = 1.38) was synthesized and ready for further self-assembly study.

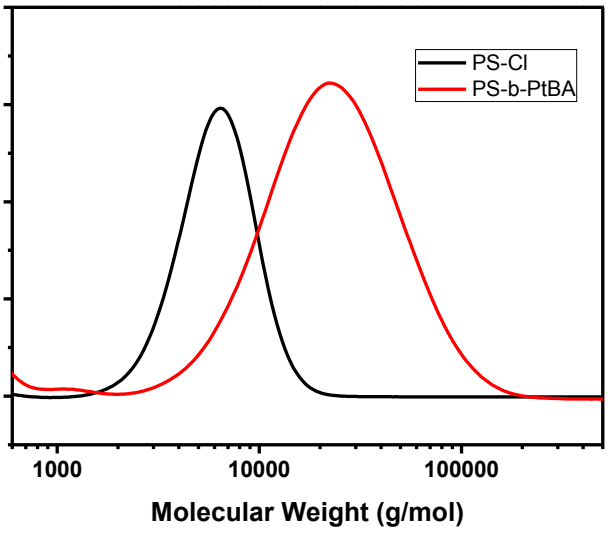

Figure 4.6. GPC curves of PS-Cl and PS-b-PtBA.

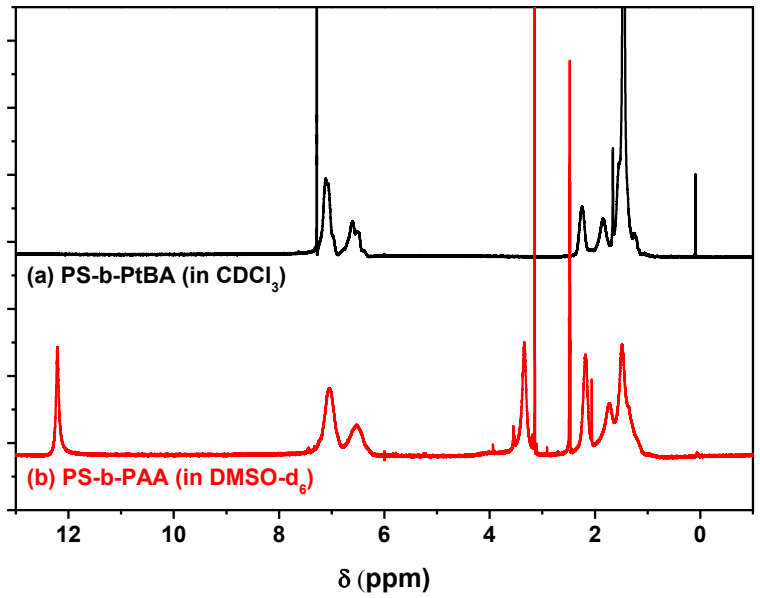

Figure 4.7. ^{1}H NMR results of (a) PS-b-PtBA and (b) PS-b-PAA.

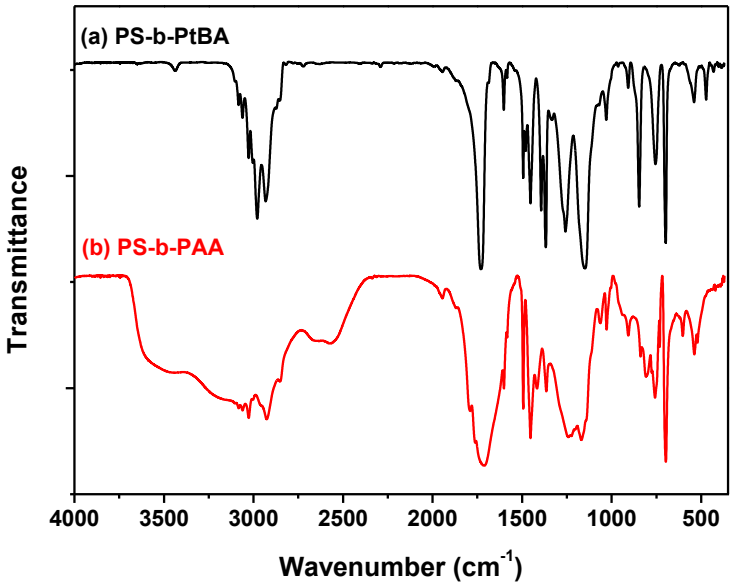

Figure 4.8. FTIR results of (a) PS-b-PtBA and (b) PS-b-PAA.

4.2.3 Fabrication of Neutral Underlayer for PS-b-PAA.

A multi-component blended system was made using PHOST-iPOC-MA with 5 wt% TPS-SbF_6 (with respect to polymer) and 20 mol% AIBN (relative to MA). The solids were dissolved in PGMEA to make a homogeneous solution. After spin-coating of this material onto clean silicon wafers, the films were N_2 gun dried without heat to prevent the decomposition of AIBN. The coated wafers were then placed in a sealed chamber and flushed with N_2 for 10 min to remove any oxygen. The chamber was then heated to 250 ℃ for 10 min to crosslink the methacrylate functional groups via thermal radical generation from the AIBN. A gradient DUV exposure with a dose range from 0 to 100 mJ/cm^2 was applied to the crosslinked PHOST-iPOC-MA film. Immediately after the exposure, the film was baked at 170 ℃ for 2 minutes to drive the deprotection of the secondary carbonate protecting groups and produce hydroxystyrene units. After exposure and PEB, the film was sonicated in PGMEA for 10 min to remove any uncrosslinked polymer and any residues from the deprotection reactions.

4.2.4 Fabrication of PS Brush Underlayer for PS-b-PAA

The Si wafer with a layer of native SiO_2 (~ 2 nm) was thoroughly washed by acetone, methanol and isopropanol. Then it was cleaned with O_2 plasma for 30 min. PS-OH (Mw=5200 g/mol, PDI=1.16) was spin-coated from a 3 wt% PGMEA solution at 2000 rpm onto the Si wafer. The sample was heated at 200 ^oC for 24 h, under vacuum. Then the sample was immersed in PGMEA solution, sonicated for 10 min to remove the excess amount of PS. Contact angle of the PS brush film is ~ 93 ^{o}.

4.2.5 Thermal Annealing of PS-b-PAA

A 45 nm PS-b-PAA film on PS brush was also fabricated for thermal annealing use. The sample was heated at different temperatures for varied amount of time, under N_2 flow. The resulting PS-b-PAA film was imaged by SEM.

4.2.6 Solvent Annealing of PS-b-PAA

PS-b-PAA was spin-coated from a 0.5 wt % THF solution at 2000 rpm onto the DUV exposed PHOST-iPOC-MA underlayer or PS brush, resulting in a 40 to 45 nm block copolymer film. The film was then exposed to acetone vapor for 3 hours in a closed jar. After the acetone vapor annealing, the sample was dried by vacuum.

4.3 Results and Discussion

Both of solvent annealing and thermal annealing of PS-b-PAA thin films were explored. Dramatically different self-assembly behaviors of PS-b-PAA were observed by using these two annealing methods. A series of characterization experiments, including morphology inspection, spectroscopy, and thermal measurements were conducted to help understand these behaviors. It has been shown that PS-b-PAA is an interesting material which possesses versatility in self-assembly applications. Also, the χ value of PS-b-PAA was estimated, which is substantially larger than PS-b-PMMA. It is a very promising material for high resolution DSA.

4.3.1 Solvent Annealing Behavior of PS-b-PAA

In the solvent annealing process, unlike thermal annealing, many annealing condition variables have to be taken into consideration, such as the solvent type, vapor pressure of the solvent, and annealing time, etc. We are able to optimize the solvent annealing process to get desired phase separation of PS-b-PAA films. Three solvents annealing methods, solvent selection and estimation of χ value of PS-b-PAA based on solvent annealing will be discussed.

4.3.1.1 Solvent Annealing Methods

The solvent annealing was performed in the presence of solvent vapor which penetrated into the block copolymer thin film and swelled the polymer to increase the mobility of the polymer chains. In this way, the T_g of the polymer would be decreased to a certain degree. The self-assembly of the block copolymer into ordered structures would be facilitated by the solvent absorption. However, the solvent annealing of polymers are often problematic. Previously, a closed flask was used to provide solvent vapor environment for block copolymer films to self-assemble in a few hours, see **Figure 4.9**. However, if the solvent is fully saturated, the solvent vapor is easily condensed on the cold Si wafer, which causes dewetting of the block copolymer film. Partial vapor pressure or just saturated vapor pressure could fix this problem. Another problem is the drying of the block copolymer film, when taking the sample out from the flask, the film is still wetted by the solvent, which contacts the moisture in air immediately. This might lead to dewetting of the film as well (could see this change by eye) or water bubble condensation on the film.

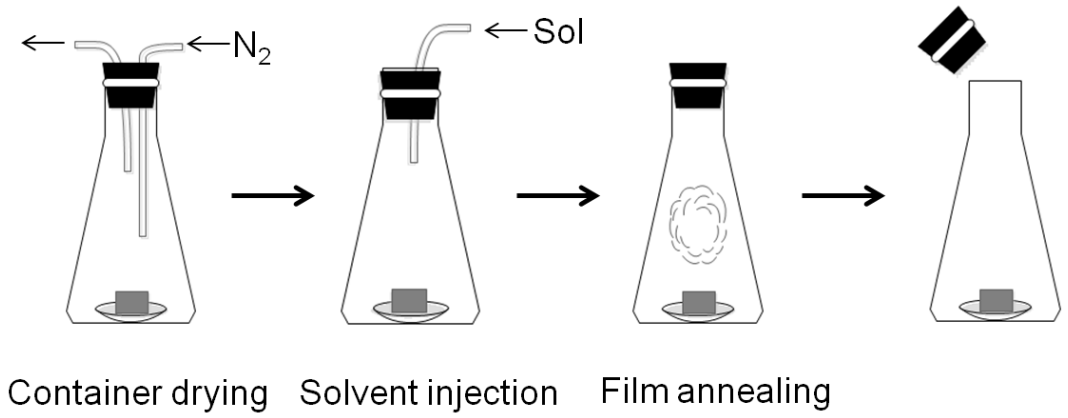

Figure 4.9. First generation solvent annealing method.

In a new attempt, the second generation annealing method **(Figure 4.10),** we introduced an extra step of N_2 flow after the annealing but before opening the flask, which is indicated in the green rectangle. This step would blow away the solvent vapor and dry the film. So, even though the film contacted the humid air immediately after opening the flask, the polymer was not mobile, dewetting would not happen. However, if the N_2 flow is not completely dry, during the "drying" step, the annealing solvent in the film is fast evaporated, which substantially cools down the film. Any moisture in the N_2 flow would condense on the cold wafer, leaving micro wafer drops on the film, see **Figure 4.11**.

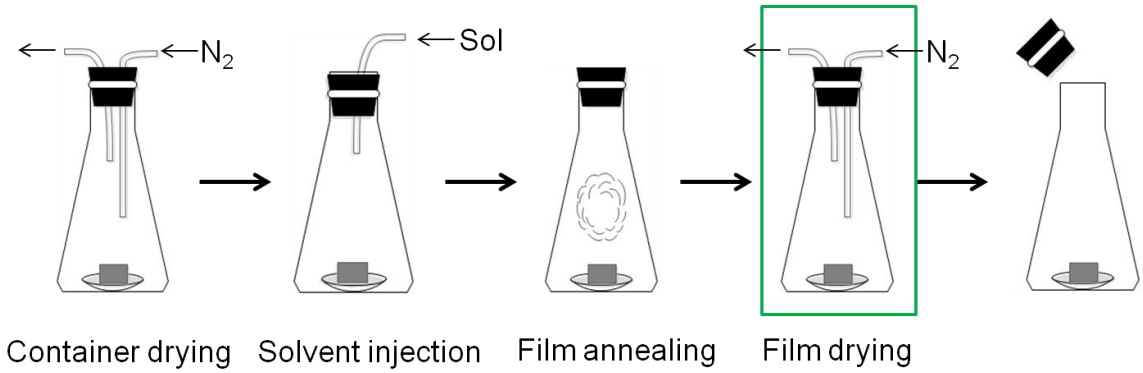

Figure 4.10. Second generation solvent annealing method.

Figure 4.11 shows a comparison between good result and bad result from solvent annealing of PS-b-PAA (8k-b-8k) films. When PS-b-PAA is annealed properly by solvent vapor, a smooth film could be obtained without dewetting or water bubbles formation. However, when the annealing is out of control, bad result is seen. The water bubble formation is the biggest environmental defect, which deforms the film significantly.

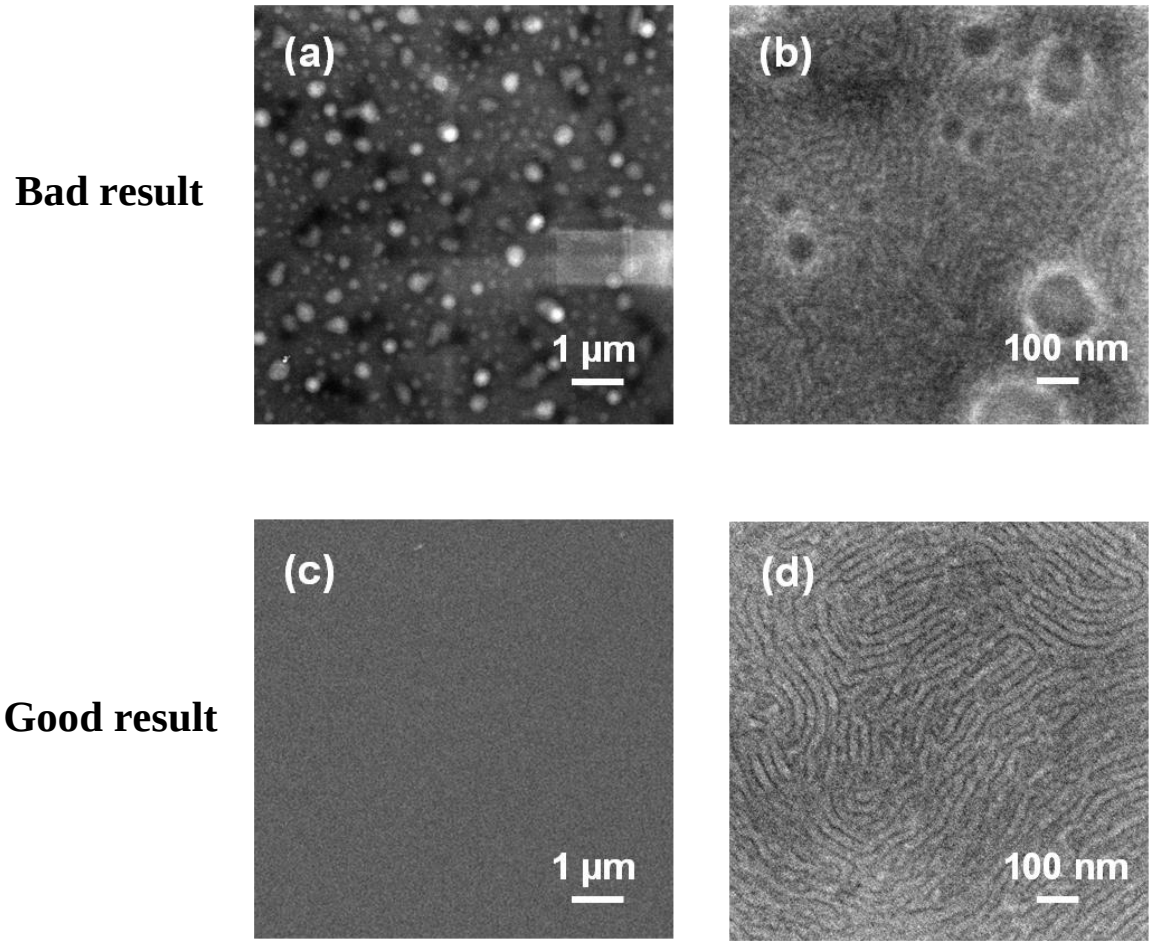

Figure 4.11. Comparison between good result and bad result obtained from solvent annealing of PS-b-PAA (8k-b-8k). (a) and (c) are zoom out SEM images, (c) and (d) are zoom in SEM images.

After understanding the problems associated with solvent annealing, we introduced a third generation of solvent annealing method. Herein, we use vacuum pump, instead of N_2 flow, to dry the container before annealing and to remove the solvent after annealing, see **Figure 4.12**. By using the vacuum pump, no solvent or moisture residue would be left on the polymer film. Thus, the film is truly "dried". Reproducible good film annealing results could be obtained, see **Figure 4.11**.

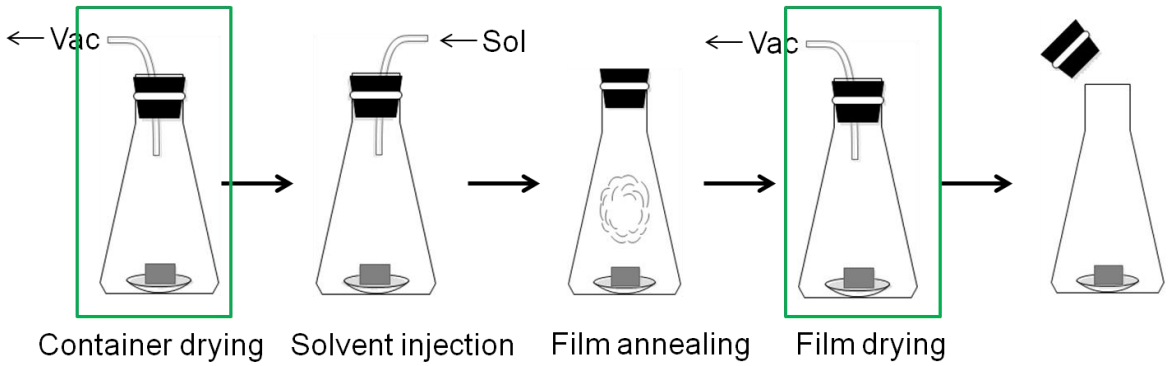

Figure 4.12. Third generation solvent annealing method.

4.3.1.2 Solvent Selection

The impact of different solvents on the self-assembly behavior was also discovered. Long range ordered lamellar structures were obtained with pure acetone annealing. However, disordered and porous structures were obtained with ethyl acetate annealing, see **Figure 4.13**.

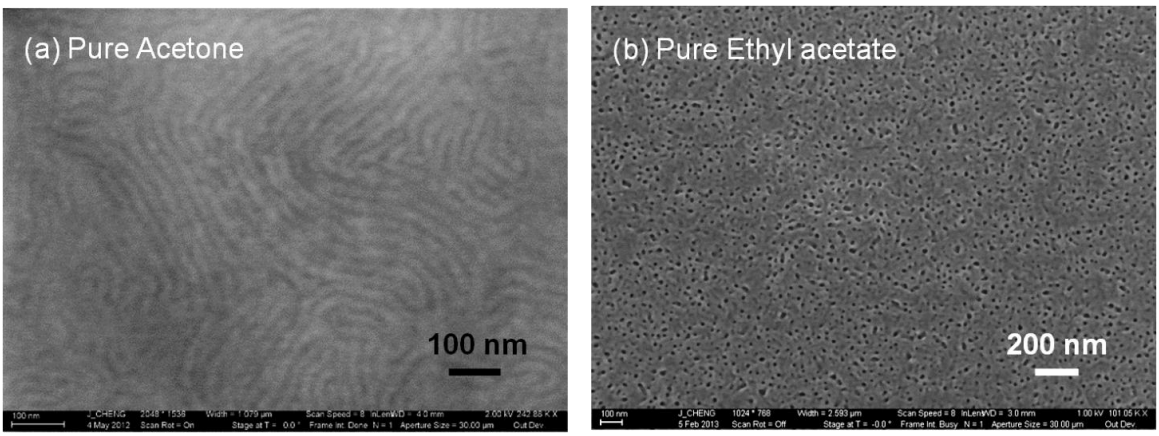

Figure 4.13. PS-b-PAA films annealed by (a) pure acetone, (b) pure ethyl acetate.

Water was also used as an annealing solvent. By using water, the annealing setup could be simpler. One does not need to worry about the atmosphere humid air because water is a co-solvent, which is in excessive amount already. No before and after solvent removal or purging was performed and robust film could be obtained, see **Figure 4.14**.

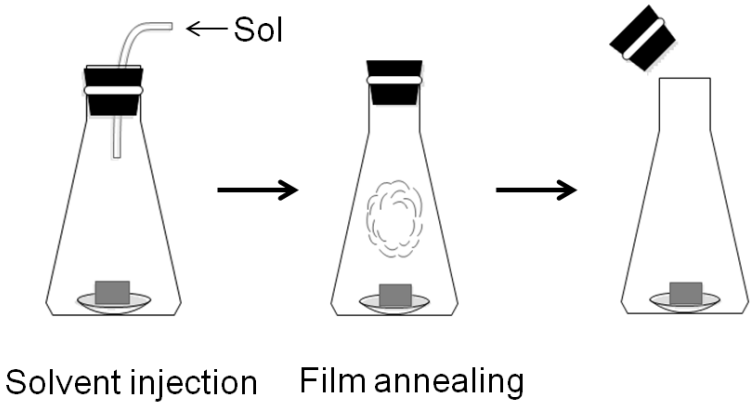

Figure 4.14. Water as co-solvent annealing method.

When water is added into the container as a co-solvent, however, a preferential solvent absorption will be achieved. Since water is more preferential to the hydrophilic

PAA block, the PAA will be more swollen by water. Thus, the volume fraction of PAA block would be greatly changed due to the preferential absorption of water. The structure of the microphase is changed accordingly. When adding water into acetone and ethyl acetate annealing system, cylindrical morphology was seen, see **Figure 4.15**.

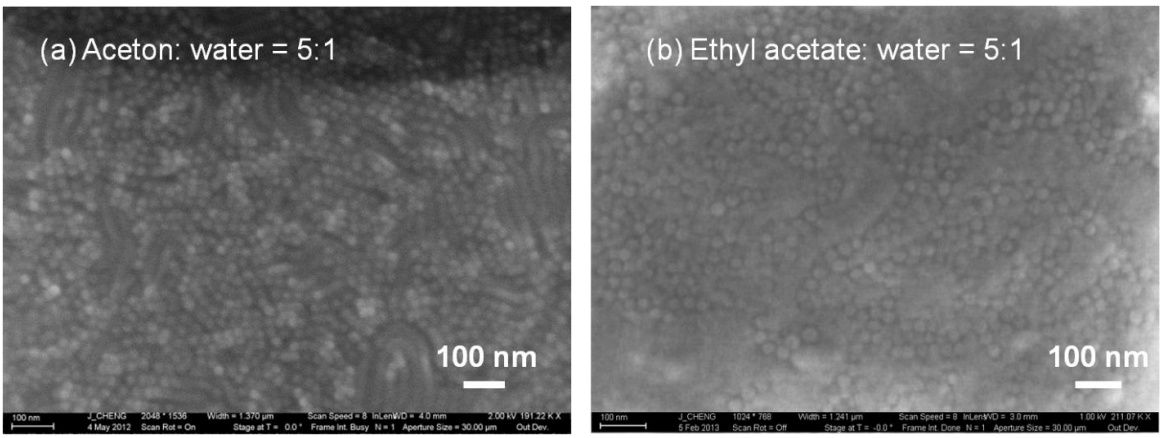

Figure 4.15. PS-b-PAA films annealed by (a) acetone: water 5:1, (b) ethyl acetate: water 5:1.

4.3.2 χ Value Estimation of PS-b-PAA from Solvent Annealing

The PS-b-PAA (8, 000 - 8, 000 g/mol, PDI = 1.38) synthesized from ATRP and subsequent hydrolysis maintains good control of Mw and PDI. The photo-definable substrate PHOST-iPOC-MA is capable of providing a gradient of surface energies to subtly tune the interaction with the top lamella forming PS-b-PAA. Acetone vapor annealed PS-b-PAA clearly shows microphase separation, which forms 30 nm pitch size lamella (L_0 = 30 nm, as shown in **Figure 4.16**).

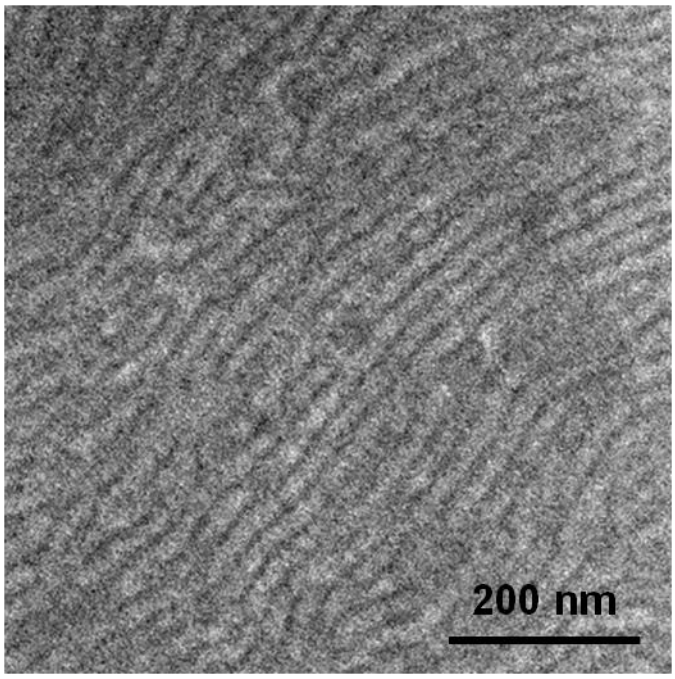

Figure 4.16. Lamellar morphology of PS-b-PAA after acetone vapor annealing on PS brush.

When comparing our PS_{8000}-b-PAA_{8000} ($L_{0,1}$ = 30 nm, N_1 = 188) with a reported PS_{37000}-b-$PMMA_{37000}$[12] ($L_{0,2}$ = 40 nm, N_2 = 725, $\chi_2 = \chi_{PS\text{-}b\text{-}PMMA}$ = 0.038), we may use **Equation 4.2** to roughly estimate χ value for PS-b-PAA (assume a_{PAA}, a_{PS}, and a_{PMMA} are similar). Then we get:

$$\frac{30}{40} = \frac{L_{0,1}}{L_{0,2}} = \frac{\chi_1^{1/6} N_1^{2/3}}{\chi_2^{1/6} N_2^{2/3}} = \frac{\chi_1^{1/6} 188^{2/3}}{(0.038^{1/6} 725^{2/3})}$$

$$\chi_{PS\text{-}b\text{-}PAA} = \chi_1 = 1.49$$

Even the rough estimation has proven that PS-b-PAA is a superior material than PS-b-PMMA. It also has much greater χ while still maintains high etch contrast and

potential for chemical epitaxy. These advancing features make PS-b-PAA a promising material for sub-20 nm DSA.

4.3.2 Thermal Annealing Behavior of PS-b-PAA

Polystyrene-block-poly(acrylic acid) (PS-b-PAA), as an amphiphilic block copolymer, has been widely used in the self-assembly study. The distinguished features between the two blocks have made it applicable in fabricating many nanostructures, such as micelles or aggregates, in selective solvents, being used as carriers for microdevices and chemicals.[13-16] PS-b-PAA self-assembled patterns in thin films, have been used as templates or scaffolds for pattern transfer.[17-21] We are mostly interested in the application of block copolymers as masks/templates for pattern transfer, as the DSA (directed self-assembly) of block copolymers has become a promising technique for next generation nanolithography.[22-24]

However, among those studies, PS-b-PAA films were mostly self-assembled in its chemically pristine state, e.g. by using solvent annealing at relative low temperatures that won't change the chemical structures of PS-b-PAA.[17-19] Even though the thermally treated PS-b-PAA film was used as template as well and the anhydride formed after heating was further reacted to bring new functions to the surface, the thermal behavior of PS-b-PAA film regarding the morphological and chemical evolution has not yet been well related and understood.[20, 21]

Herein, we would relate the thermal chemistry of PS-b-PAA film to the thermal morphology change. A symmetric PS-b-PAA, which self-assembles into lamellar

morphology, was made into thin film and thermally annealed. The size of the lamellae decreases upon ongoing thermal treatment. Those thermal behaviors are further explored and understood by DSC, GIR, and GPC characterization.

4.3.2.1 Thermal Behavior of PS-b-PAA

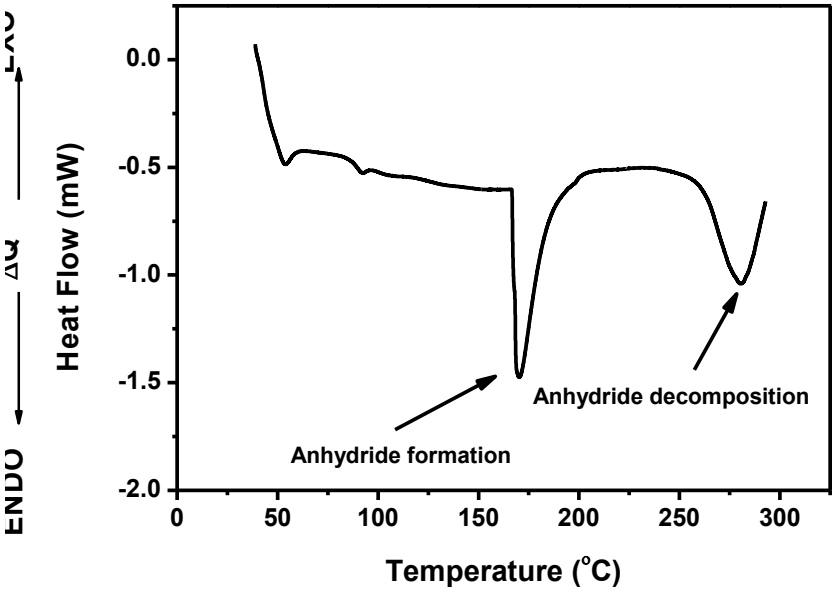

Figure 4.17. MDSC of PS-b-PAA solid.

To study the thermal behavior of PS-b-PAA, the polymer solid was heated with Modulated Differential Scanning Calorimetry (MDSC), see **Figure 4.17**. The MDSC spectra help better understand the thermal reactions in PS-b-PAA film. Clearly, in the MDSC graph, there are two endo-thermal peaks from 40 ^{o}C to 300 ^{o}C heating range. The sharp one at ~ 170 ^{o}C indicates the anhydride formation inner- or inter-molecularly between PAA chains, while the relatively broad on at ~ 280 ^{o}C indicates the anhydride decomposition.[25] As an example of the thermal reaction path, **Figure 4.18** shows the

inner-molecular anhydride formation and decomposition.[26] At an early heating stage, two carboxylic acids lose one H_2O molecule and crosslink to form an anhydride. As the heating goes on, the anhydride will lose a CO_2 molecule to form a ketone. The ketone further decomposes and loses a CO molecule upon heating. Thus, the chemical structures of the PS-b-PAA film are changing gradually when it is thermally annealed.

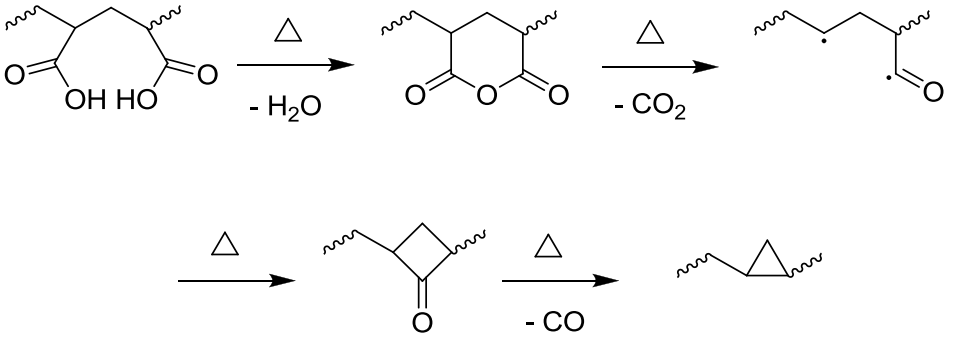

Figure 4.18. Reaction path of anhydride formation and decomposition.

4.3.2.2 Thermal Evolution of PS-b-PAA Self-assembly

Since the T_g for both PS and PAA are ~ 105 ℃, the PAA block starts to crosslink to form anhydrides at ~ 170 ℃. We would like to select an annealing condition that would allow a smooth yet efficient morphology evolution. Three temperatures, 120 ℃, 140 ℃ and 160 ℃, which were within 105 ℃ to 170 ℃ process window, were chosen as annealing temperatures.

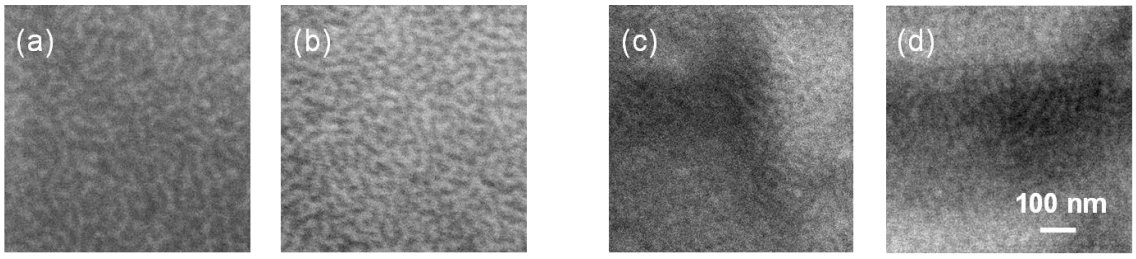

Figure 4.19. SEM images of PS-b-PAA phase-separation after (a) annealing at 120 ℃ for 1h; (b) annealing at 120 ℃ for 23h; (c) annealing at 140 ℃ for 1h; (d) annealing at 140 ℃ for 23h.

When the PS-b-PAA was annealed at 120 ℃ and 140 ℃, however, short and irregular lamellar structures were obtained, which indicates poor phase separation due to slow diffusion of the polymer chain at those annealing temperatures, see **Figure 4.19**. When annealed at 160 ℃, which was well above the T_g of the block copolymer, the diffusion of PS-b-PAA was more facilitated by increasing the mobility of the polymer chain. Thus, the PS-b-PAA was prone to self-assemble into well-defined morphology, the long range ordered and more regular lamellar structure. The size of the lamellar structure was decreasing as the thermal annealing continued at 160 ℃, e.g. when annealed 10 min, 43.5 nm lamella was obtained, however surprisingly, after annealing for 6 h, the size shrank to 35.0 nm, as shown in **Figure 4.20**. The origin of this size change was further investigated by GIR and GPC.

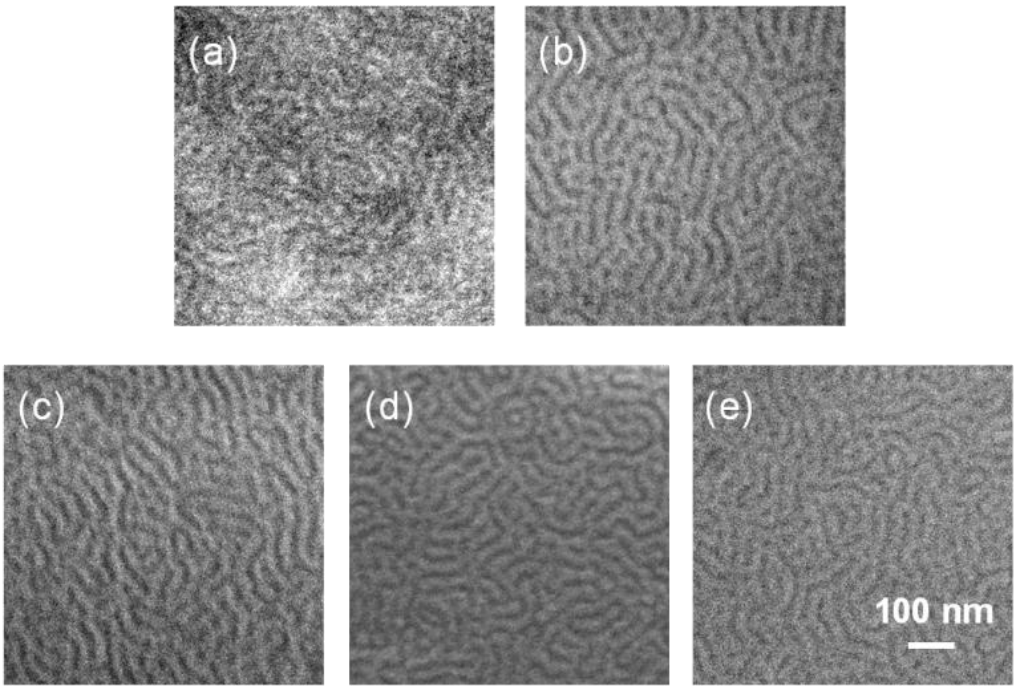

Figure 4.20. SEM images of PS-b-PAA phase-separation after (a) annealing at 160 ℃ for 10 min; (b) 30 min; (c) 1 h; (d) 2 h; (e) 6 h.

4.3.2.3 Investigation of PS-b-PAA Thermal Self-assembly

To study the chemical change within the PS-b-PAA film, GIR was taken on the films which were heated at the condition same to the annealing experiment. Those films were annealed on gold coated Si wafer and cooled down to room temperature before the GIR measurement. The IR spectra in **Figure 4.21** clearly shows chemical evolution of the film with gradual disappearance of the carboxylic acid absorption peaks and appearance of the anhydride absorption peaks.[27] All of the IR spectra were normalized to a reference peak at 702 cm^{-1}, which indicates monosubstituted aromatic C-H bending. The characteristic absorption at 1265 cm^{-1} and 1184 cm^{-1} indicate C-O stretching coupled

with O-H in-plane bending, at 1716 cm^{-1} indicates C=O stretch of COOH. The intensities of those peaks were decreasing as the film was annealed longer. The characteristic absorption at 1763 cm^{-1} and 1808 cm^{-1} indicate symmetric and asymmetric C=O coupled stretch of anhydride, at 1053 cm^{-1} indicates C-CO-O-CO-C stretch. They appeared stronger as the thermal annealing was proceeding in the first 2 h, however, they went weaker after the first 2 h, which suggested the decomposition of anhydride.

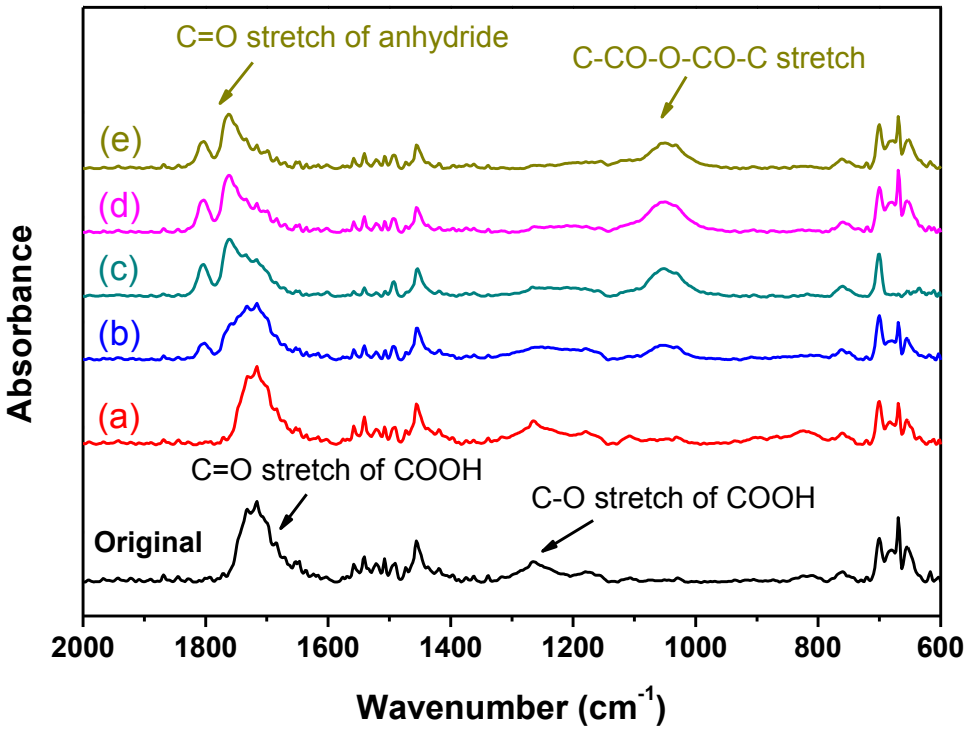

Figure 4.21. Grazing angle infrared spectroscopy of PS-b-PAA films on gold coated Si wafer in its original form and after (a) annealing at 160 ℃ for 10 min; (b) 30 min; (c) 1 h; (d) 2 h; (e) 6 h under N_2 flow.

The evolving peak at 1808 cm^{-1}, which stands for the asymmetric C=O coupled stretch of anhydride, was used to monitor the anhydride formation during thermal annealing. As shown in **Figure 4.22**, during the thermal annealing period of the first 2 h (in the red area), the anhydride was formed continuously, as the intensity at1808 cm^{-1} was increasing. However, the further annealing rendered decomposition of the anhydride (in the blue area), as the intensity at1808 cm^{-1} started to decrease. The pitch size decreased continuously.

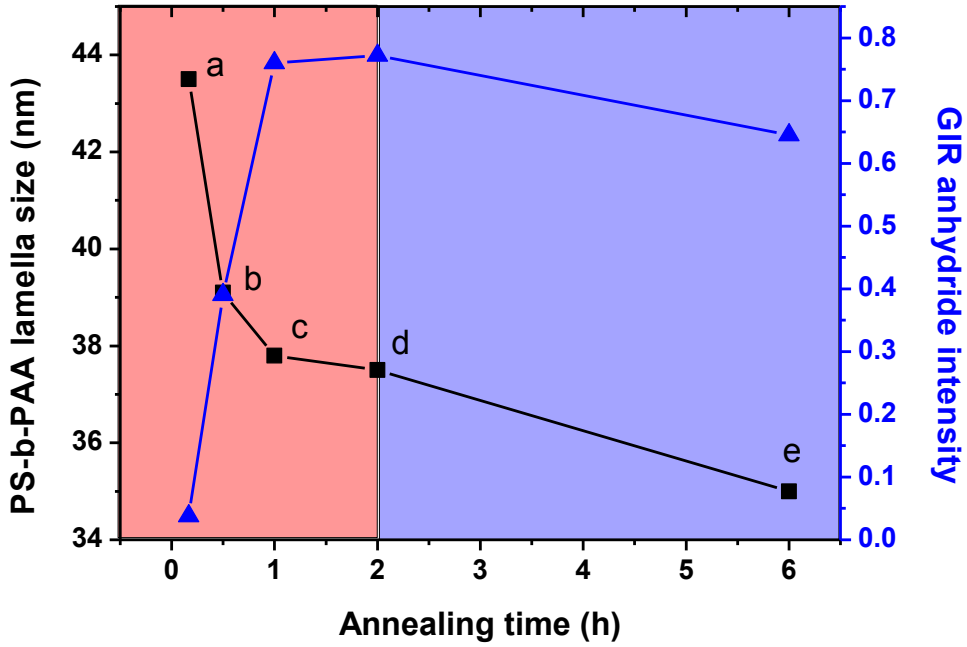

Figure 4.22. Comparison of PS-b-PAA lamella size (black square) and GIR anhydride intensity (blue triangle) change upon thermal annealing. Red area indicates anhydride formation stage, while blue are indicates anhydride decomposition stage.

According to **Euqation 4.2**, the pitch size of the block copolymer is related to the Flory-Huggins parameter χ. χ is proportional to the repulsive interaction between the blocks. A larger χ means a stronger repulsive interaction. For the PS-b-PAA block copolymer in this paper, the carboxylic functional group in PAA block evolved into anhydride, ketone and so on during thermal annealing. **Figure 4.23** shows the water contact angle change upon thermal annealing.

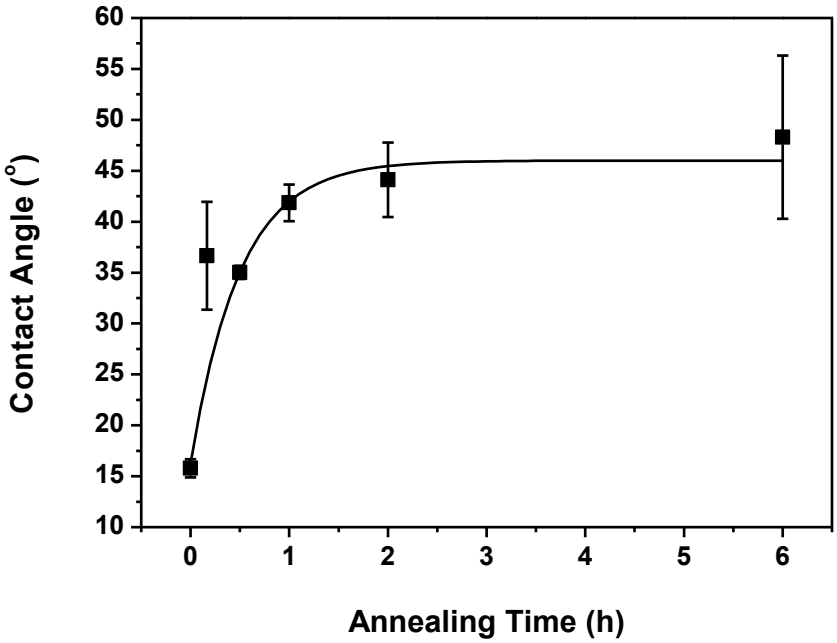

Figure 2.23. Contact angle of water on the thermally annealed films.

The water contact angle shows an exponential increased when the thermal annealing proceeded, which fits into **Equation 4.3** (where **CA** is the water contact angle, **t** is the annealing time). The increase of the contact angle suggested that the surface became more hydrophobic. The oxygen loss from the thermal reaction lead to the

formation of less hydrophilic polymer, which was more energetically similar to PS. Thus, the two blocks were less repulsive, which indicated that the χ value was getting smaller. This explains that the pitch size was smaller upon heating.

$$\mathrm{CA} = 46 - 29.76\mathrm{e}^{-2\mathrm{t}} \quad (3)$$

4.3.3 Comparison of PS-b-PAA Solvent and Thermal Self-assembly

The pitch of PS-b-PAA increases dramatically after thermal annealing and poor phase separation morphology was obtained, see **Figure 4.24**. For the solvent annealing, a pitch size of 30.0 nm was measured (**Figure 4.24.a**), however, after the thermal annealing, the pitch size increased to 43.0 nm (**Figure 4.24.b**), which is almost 1.5 times of the solvent annealing pitch size. Further investigation is needed to better understand this behavior.

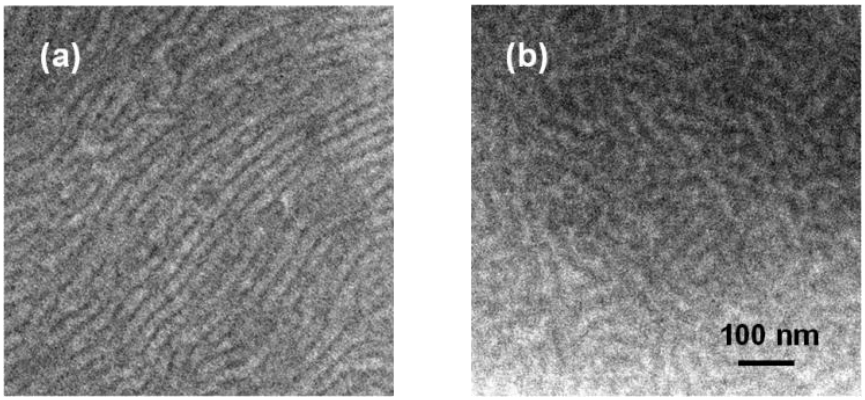

Figure 4.24. SEM of PS-b-PAA lamella after solvent annealing (a) and thermal annealing (b).

Besides the MDSC measurement, GPC was also used to study the thermal crosslinking of PS-b-PAA. After thermal annealing, the PS-b-PAA film was washed off by THF, which was used in GPC measurement. The GPC of thermally annealed PS-b-PAA film was compared with the GPC of the original PS-b-PAA solid, see **Figure 4.25**. It is found that from the GPC of thermally annealed PS-b-PAA, the "original" pristine polymer shows a narrow elution peak at ~ 12.8 min. However, there is a broad "bump" at earlier elution time, ~ 10.6 minute, which indicates a small portion of higher Mw polymer. The GPC reveals that inter-molecular anhydride forms during thermal treatment. According to **Euqation 4.2**,[5] polymerization degree N plays an important role to the phase separated pitch size. After thermal annealing, the inter-molecular anhydride formation leads to higher Mw polymer chain, the effective N is increased. The domain size is increased accordingly.

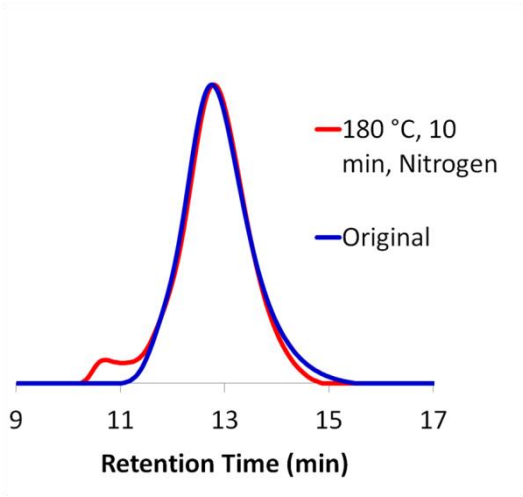

Figure 4.25. GPC curves of original PS-b-PAA solid (blue) and thermally annealed PS-b-PAA film (red).

4.4 Conclusion

High χ block copolymer is desired for DSA of smaller feature size and reduced defectivity. Polystyrene-b-polyacid is a good candidate for DSA due to its hydrogen-bonding interactions. PS-b-PAA (8, 000 - 8, 000 g/mol, PDI = 1.38) was successfully synthesized via ATRP with controlled Mw and PDI. The PS-b-PAA was acetone vapor annealed to form 30.0 nm pitch size lamella. Initial estimate for the χ of PS-b-PAA was 1.49, which is much greater than PS-b-PMMA. PS-b-PAA undergoes thermal reaction to form anhydride, ketone, and alkane sequentially. The χ value of PS-b-PAA decreases upon thermal annealing. As a result of χ change, the pitch size of the self-assembled PS-b-PAA lamella decreases. A large pitch size window from 43.5 nm to 35.0 nm could be obtained within 6 h thermal annealing at 160 ℃. The size of the same PS-b-PAA polymer is tunable by varying the annealing time. Also, the chemical structure change after thermal annealing, like the anhydride formation, could be further utilized to decorate the surface chemistry by reacting with certain reagents, e.g. amine containing chemicals. The thermal behavior of PS-b-PAA was well studied and related to the morphology evolution.

4.5 References

1. *Excerpts from A Conversation with Gordon Moore: Moore's Law. Video Transcripts. Intel Museum.*

2. Miyazaki, T.; Hayashi, K.; Kobayashi, K.; Kuba, Y.; Ohyi, H.; Obara, T.; Mizuta, O.; Murayama, N.; Tanaka, N.; Kawamura, Y.; Uemoto, H. *J. Vac. Sci. Technol. B* **2008,** 26, 2611.

3. Cheng, J. Y.; Ross, C. A.; Chan, V. Z.-H.; Thomas, E. L.; Lammertink, R. G. H.; Vancso, G. J. *Adv. Mater.* **2001,** 13, 1174.

4. M. Park, C.; Harrison; Chaikin, P. M.; Register, R. A.; Adamson, D. H. *Science* **1997,** 276, 1401.

5. Bates, F. S.; Fredrickson, G. H. *PHYSICS TODAY* **1999,** 52, (2), 32.

6. Peters, R. D.; Yang, X. M.; Wang, Q.; de Pablo, J. J.; Nealey, P. F. *J. Vac. Sci. Technol. B* **2000,** 18, (6), 3530-3534

7. Segalman, R. A.; Yokoyama, H.; Kramer, E. *J., Adv. Mater.* **2001,** 13, (15), 1152-1155.

8. Russell, T. P.; Hjelm, R. P.; Seeger, P. A. *Macromolecules* **1990,** 23, (3), 890-893.

9. Gokan, H.; Esho, S.; Ohnishi, Y. *Journal of the Electrochemical Society* **1983,** 130, 143-146.

10. Davis, K. A.; Charleux, B.; Matyjaszewski, K. **2000,** 38, 2274-2283.

11. Cheng, J.; Lawson, R. A.; Yeh, W.-M.; Tolbert, L. M.; Henderson, C. L. *Proc. of SPIE* **2011,** 7972, 79722I.

12. Liu, C.-C.; Han, E.; Onses, M. S.; Thode, C. J.; Ji, S.; Gopalan, P.; Nealey, P. F. *Macromolecules* **2011,** 44, 1876-1885.

13. Hwang, W.; Choi, J.-H.; Kim, T. H.; Sung, J.; Myoung, J.-M.; Choi, D.-G.; Sohn, B.-H.; Lee, S. S.; Kim, D. H.; Park, C. *Chem. Mater.* **2008,** 20, 6041–6047.

14. Kang, Y.; Taton, T. A. *J. AM. CHEM. SOC.* **2003,** 125, 5650-5651.

15. Kang, Y.; Taton, T. A. *Angew. Chem.* **2005,** 117, 413 –416.

16. Kim, B.-S.; Taton, T. A. *Langmuir* **2007,** 23, 2198-2202.

17. Li, L.; Zhong, Y.; Li, J.; Gong, J.; Ben, Y.; Xu, J.; Chen, X.; Ma, Z. *Journal of Colloid and Interface Science* **2010,** 342, 192–197.

18. Min, E.; Wong, K. H.; Stenzel, M. H. *Adv. Mater.* **2008,** 20, 3550–3556.

19. Wang, C.; Mao, Y.; Wang, D.; Qu, Q.; Yang, G.; Hu, X. *J. Mater. Chem.* **2008,** 18, 683–690.

20. Kim, S. M.; Ku, S. J.; Kim, J.-B. *Nanotechnology* **2010,** 21, 235302.

21. Kim, S. M.; Ku, S. J.; Kim, J.-B. *Macromolecular Research* **2011,** 19, (9), 891-896.

22. Kim, H.-C.; Hinsberg, W. D. *J. Vac. Sci. Technol. A* **2008,** 26, (6), 1369-1382.

23. Liu, C.-C.; Nealey, P. F.; Raub, A. K.; Hakeem, P. J.; Brueck, S. R. J.; Han, E.; Gopalan, P. *J. Vac. Sci. Technol. B* **2010,** 28, (6), C6B30-C6B34.

24. Cheng, J. Y.; Sanders, D. P.; Truong, H. D.; Harrer, S.; Friz, A.; Holmes, S.; Colburn, M.; Hinsberg, W. D. *ACS Nano* **2010,** 4 (8), 4815–4823.

25. McNeill, I. C.; Sadeghiet, S. M. T. *Polymer Degradation and Stability* **1990,** 29, 233-246.

26. Maurer, J. J.; Eustace, D. J.; Ratcliffet, C. T. *Macromolecules* **1987,** 20, 196-202.

27. Dong, J.; Ozaki, Y.; Nakashima, K. *Macromolecules* **1997,** 30, 1111-1117.

CHAPTER 5

PS-B-PHEMA AS A HIGH χ POLYMER FOR DIRECTED SELF-ASSEMBLY

5.1 Introduction

Directed self-assembly (DSA) of block copolymers, as an alternative lithographic method, is promising for production of sub-20nm pitch patterns. PS-b-PMMA, as a DSA polymer, has been demonstrated to pattern large area regular structures with low defectivity. However, PS-b-PMMA is limited to 17 nm patterning due to its small χ value (0.038).[1] We are inventing a series of new block copolymer materials with high χ values for sub-20 nm pitch patterning. These materials should be also suitable for industrial processing, which means that they should have high etch contrast in order to easily remove one of the blocks, and they should have high thermal stability to stand the harsh thermal processing, like thermal annealing of block copolymers to facilitate self-assembly. We have proposed a series of block copolymers A-b-B which are composed of polystyrene A and another block B with a hydrogen bonding motif, see **Figure 5.1**, such as a polyacid, polyphenol or polyalcohol. It is expected that the hydrogen bonding would provide strong self interaction within B block, thus the repulsive interaction between A and B blocks would be intensified, which would contribute to a high χ value. In this work, polystyrene-b-polyalcohol block copolymer as potential high χ DSA material using has been explored.

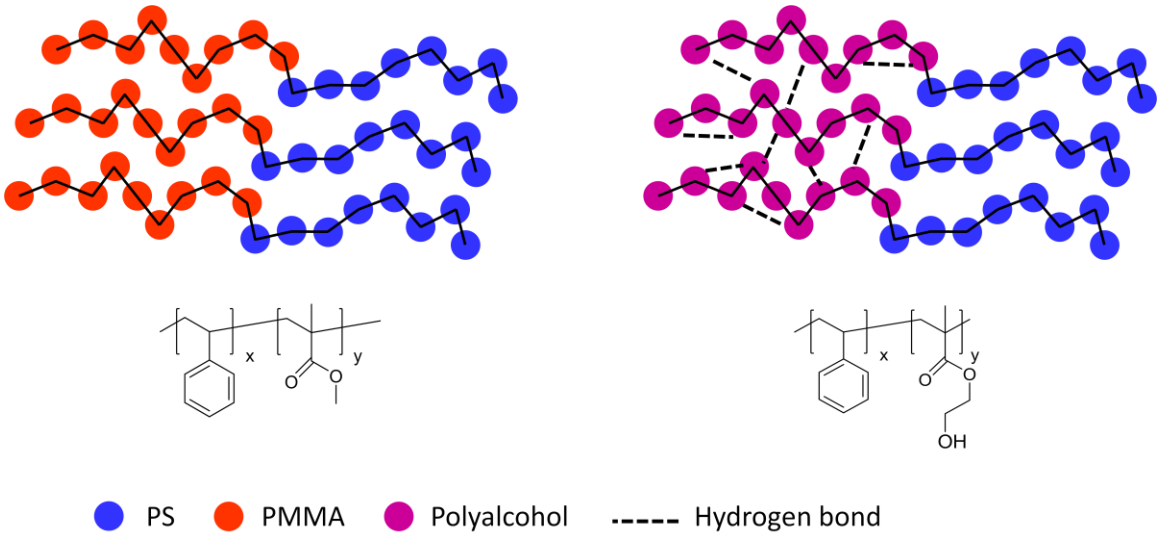

Figure 5.1. Comparison between PS-b-PMMA and hydrogen-bond containing PS-b-PHEMA.

5.1.1 Hydrogen-bonding Containing Block Copolymer

The microphase separation of block copolymers takes place when the product χN, where χ is the Flory-Huggins interaction and N is number of monomers in the diblock copolymer, is greater than 10.5 (**Equation 5.1**). The higher χN is, the easier block copolymers will microphase separate. According to **Equation 5.2**[2] below (here λ is the domain size of one block, a is the kuhn segment length, N is degree of polymerization), the minimum domain size of the microphase separated structure is more related to N. In order to have phase separation at a small N to give small domain size, the χ value should be big enough to keep χN>10. The current widely studied PS-b-PMMA system only has a modest χ value as 0.038,[1] witch limits its patterning resolution at ~ 17 nm. A high χ block copolymer is highly desired for higher resolution, e.g., sub-20 nm patterning.

$$\chi N = 10.4 \qquad (5.1)$$

$$\lambda \approx 1.03 a \chi_{AB}^{1/6} N^{2/3} \quad (5.2)$$

5.1.2 Polystyrene-b-polyalcohol as High χ Block Copolymer

Our previous study with poly(styrene)-block-polyacid copolymers has introduced PS-b-PAA as a high χ block copolymer. It is processable with solvent annealing. As we are interested in the industry-friendly thermal processing, we looked at the thermal behavior of PS-b-PAA as well. Literature has shown that PAA undergoes thermal crosslinking at ~ 170 ^{o}C through anhydride formation.[3] While the T_g for PS and PAA are both ~ 105 ^{o}C, a higher heating temperature is required for thermal annealing. Those facts lead to a narrow thermal annealing window for PS-b-PAA. The decomposition of PAA might take place when the polymer film is thermally annealed, from whitch poor phase separation might result. Industrial fabrication would require block copolymers that could be rapidly annealed at relatively high temperatures to generate patterns. Thus, a new polymer based on the hydrogen-bonding containing system is desired. Literature reports have shown that PHEMA is more thermally stable than PAA. PHEMA is stable up to 320 ^{o}C (see a comparison in **Figure 5.2**).[4] Based on the higher thermal stability of alcohols over acids, we decided to study PS-b-PHEMA as a candidate for thermal annealing.

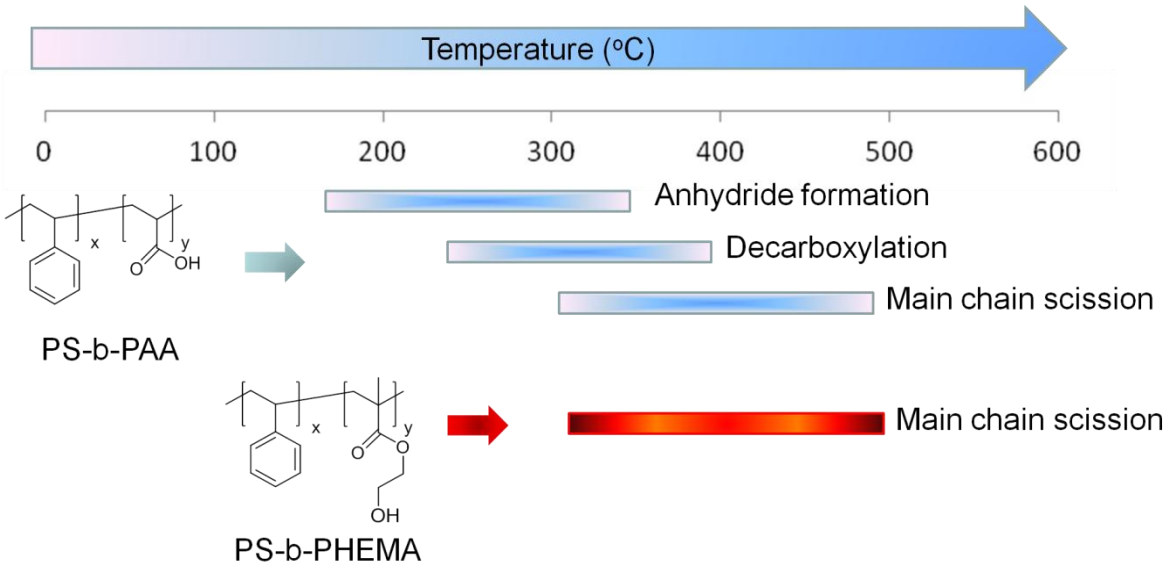

Figure 5.2. Comparison of thermal reaction path between PS-b-PMMA and PS-b-PHEMA.

5.2 Experimental

5.2.1 Materials and Instruments

Materials

Unless otherwise noted, all reagents and solvents used were purchased from Sigma-Aldrich, TCI America, or Alfa-Aesar, and used as received. Styrene and 2-hydroxyethyl methacrylate (HEMA) were passed through neutral alumina columns to remove inhibitors. CuCl was made from reduction of $CuCl_2$ by Na_2SO_3 in HCl solution, precipitated and washed by diethyl ether and absolute ethanol, dried in vacuum oven at

50 ^{o}C overnight. ATRP catalysts 4,4'-di(5- nonyl)-2,2'-bipyridine (dNbpy) and initiator ethyl 2-bromoisobutyrate (EBiB) were used as received.

Instruments

A Varian Mercury Vx 300 was used to record NMR spectra. Molecular weights and PDIs of the polymers were estimated by gel permeation chromatography (GPC), using a Waters 1515 isocratic pump coupled to a Waters 2489 UV detector with THF as the elution solvent. All GPC measurements were carried out at a flow rate of 0.3 mL/min at 35 ^{o}C, and calibrated using narrow molecular weight polystyrene standards. Film thicknesses were measured using a M-2000 spectroscopic ellipsometer (J.A. Woolam, Inc.) over the wavelength range of 350 to 1000 nm using a Cauchy layer to model the film. Fourier transform infrared (FTIR) spectroscopy was done using a Bruker Vertex 80v with a Hyperion microscope attachment on KBr pellet. The self-assembled block copolymer films were imaged using a Carl Zeiss Ultra60 SEM with 1 keV acceleration voltage.

5.2.2 Synthesis of Symmetric PS-b-PHEMA via ATRP and Hydrolysis

Matyjaszewski has reported the synthesis of PHEMA and its block copolymers with controlled Mw and PDI from ATRP.[5] It was suggested that PHEMA with desired Mw and low PDI could be obtained from ATRP of PHEMA-TMS (trimethylsilyl group protected HEMA monomer) and subsequent hydrolysis. A synthesis route of PS-b-PHEMA was proposed similarly, as shown in **Figure 5.2**. Here we use a more stable protective group tert-butyl trimethylsilyl (TBS) to protect the HEMA monomer.[6] A block copolymer PS-b-PHEMA (5, 500 - 5, 400 g/mol, PDI = 1.31) was successfully synthesized and fully characterized by GPC, NMR and FTIR.

5.2.2.1 Synthesis of Protected Monomer HEMA-TBS:

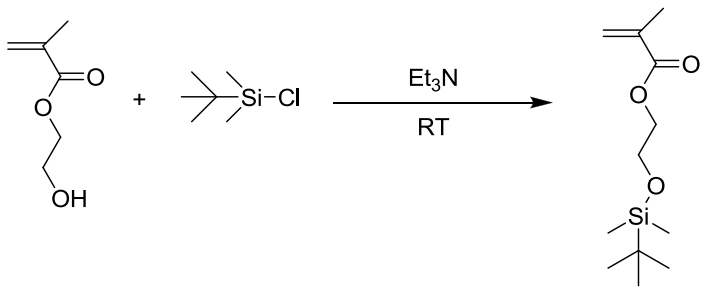

HEMA **HEMA-TBS**

Scheme 5.3. Synthesis route for HEMA-TBS.

In a 150 mL Schlenk flask, 2-hydroxyethyl methacrylate (HEMA monomer, 10 mL, 82.5 mmol), triethylamine (Et_3N, 14.9 mL, 107.2 mmol), dichloromethane (80 mL) were added and stirred for 10 min. *tert*-Butyl dimethylsilyl chloride (TBS-Cl, 14.9 g, 98.9 mmol) was added. The solution was stirred for 24 h at room temperature. It was washed twice with 3% HCl solution, three times with DI water, extracted with dichloromethane, dried over anhydrous $MgSO_4$, and dried using a rotary evaporator. This produced HEMA-TBS as a yellow liquid (8.6 mL, 86%). The spectral data were: ^{1}H-NMR (300 MHz, $CDCl_3$) δ (ppm) 0.06 (s, 6H), 0.88 (s, 9H), 1.94 (m, 3H), 3.85 (tt, 4H), 4.22 (tt, 4H), 5.56 (m, 1H), 6.12 (m, 1H).

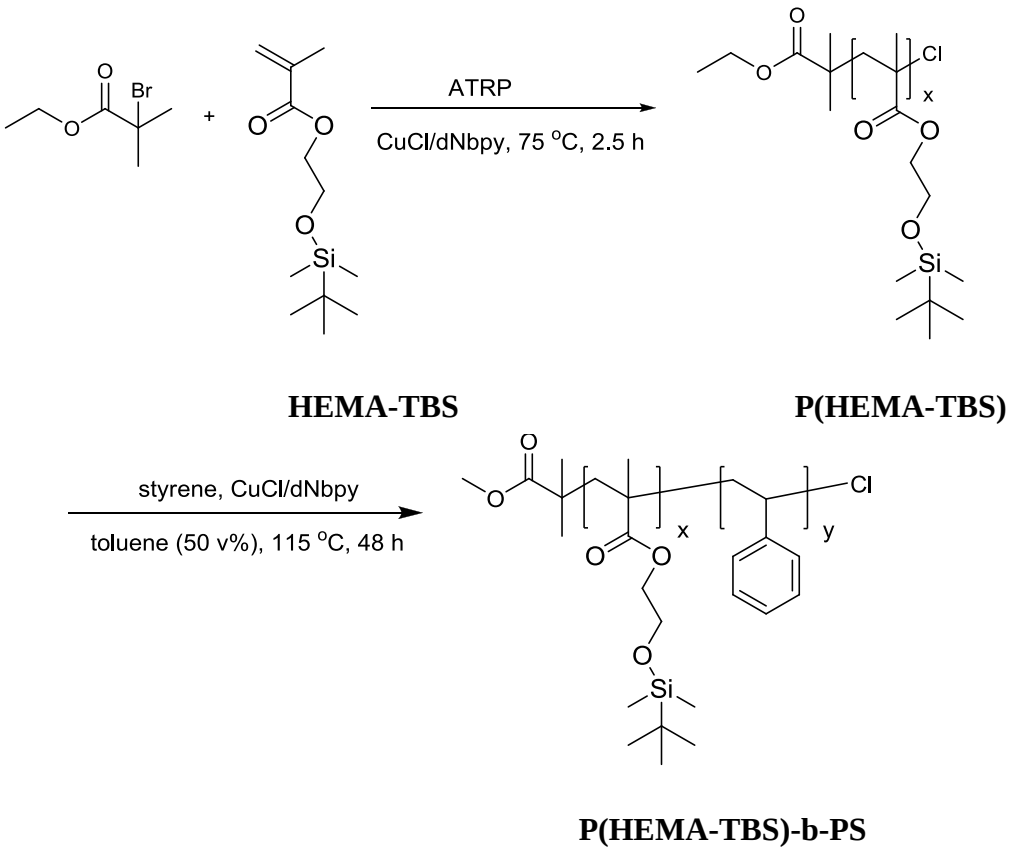

Figure 5.4. Synthesis route for P(HEMA-TBS)-b-PS.

5.2.2.2 Synthesis of Macroinitiator P(HEMA-TBS)-Cl

In a 50 mL Schlenk flask, HEMA-TBS (2 mL), CuCl (18 mg, 1.9 mmol), dNbpy (155 mg, 3.8 mmol), EBiB (27.7 μl, 36.9 mmol) were added. After three cycles of freeze-pump-thaw to remove oxygen, the flask was back-filled with dry N_2. The flask was placed in an oil bath and heated at 75 ^oC. After 2 hours, the solution was highly viscous. The polymerization was quenched by placing the flask in an ice bath and exposing the solution to the air. The solution was diluted with dichloromethane and filtered through a neutral alumina column to remove the catalyst. The clean polymer solution was rotary evaporated to remove the solvent. After drying under vacuum overnight, 1.6 g colorless

solid was obtained. GPC analysis showed that Mn = 10,500 g/mol, PDI = 1.28, see **Figure 5.5**.

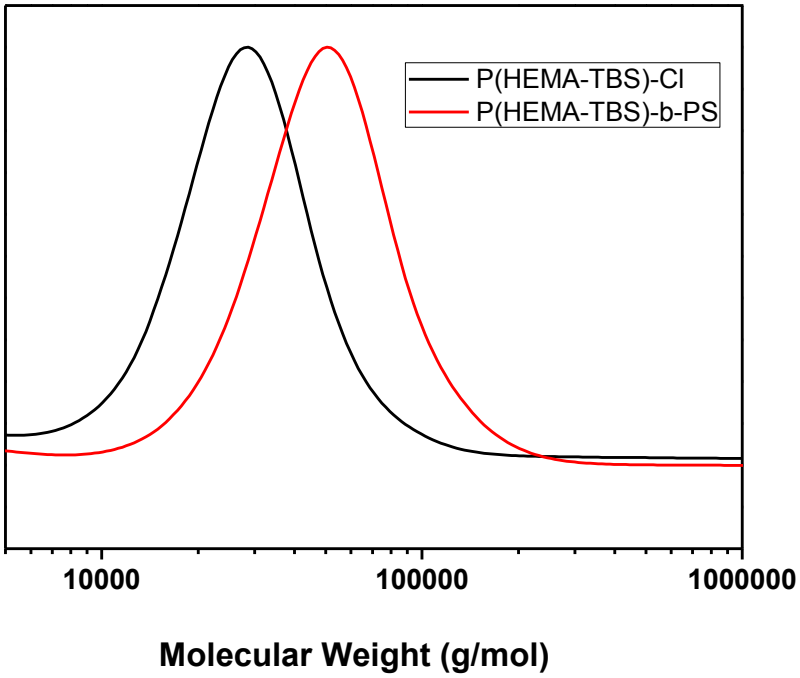

Figure 5.5. GPC curves of P(HEMA-TBS)-Cl and P(HEMA-TBS)-b-PS.

5.2.2.3 Synthesis of P(HEMA-TBS)-b-PS

In a 25 mL Schlenk flask, P(HEMA-TBS)-Cl (10,500 g/mol, 1.16 g), styrene (0.7 mL, 6.1 mmol), toluene (2 mL) were added and allowed to stir until the polymer is completely dissolved. CuCl (32 mg, 0.3 mmol) and dNbpy (286 mg, 0.7 mmol) were added. After three cycles of freeze-pump-thaw to remove oxygen, the Schlenk flask was back-filled with dry N_2. The flask was placed in an oil bath, heated at 125 ^{o}C. After 24 hours, the solution was highly viscous. The polymerization was quenched by placing the flask in an ice bath and exposing the solution to the air. The solution was diluted by

dichloromethane and filtered through a neutral alumina column to remove the catalyst. The polymer solution was rotary evaporated and precipitated into a 10-fold excess of MeOH/H_2O (1:1). After drying under vacuum overnight, 1.4 g colorless solid was obtained. GPC analysis shows that Mn = 14, 000 g/mol, PDI = 1.31. ^{1}H NMR analysis was performed in $CDCl_3$. PS has two broad resonance peaks of aromatic protons at δ = 6.5 ppm and δ =7.1 ppm. P(HEMA-TBS) has absorptions for protons on the ethyl chain at δ = 4.0 and 3.8, along with two sharp singlets corresponding to the t-butyl group at δ = 0.9 ppm and methyl group attached to Si at δ = 0.1 ppm. The composition calculated from ^{1}H NMR (in $CDCl_3$, **Figure 5.6a**) is P(HEMA-TBS)-b-PS (10, 500 - 5, 400 g/mol), which shows high agreement with the GPC result **(Figure 5.5)**.

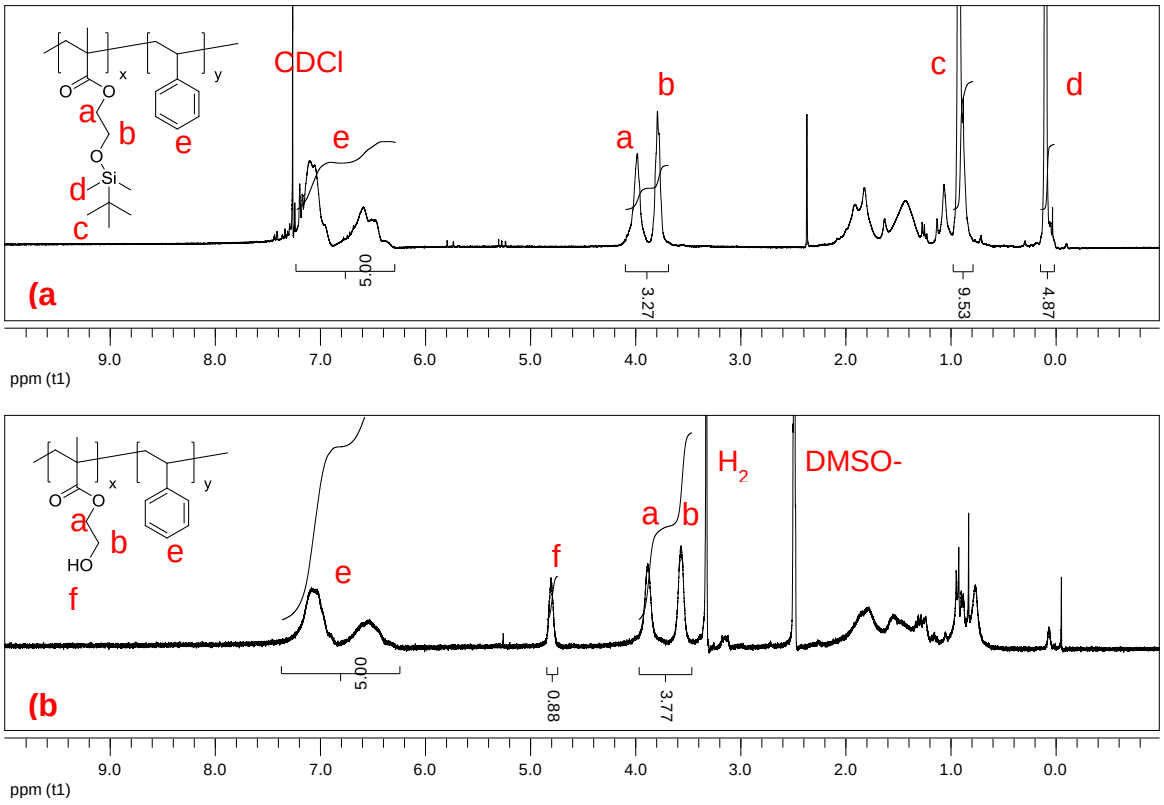

Figure 5.6. ^{1}H NMR of P(HEMA-TBS)-Cl and P(HEMA-TBS)-b-PS.

5.2.2.4 Deprotection of P(HEMA-TBS)-b-PS

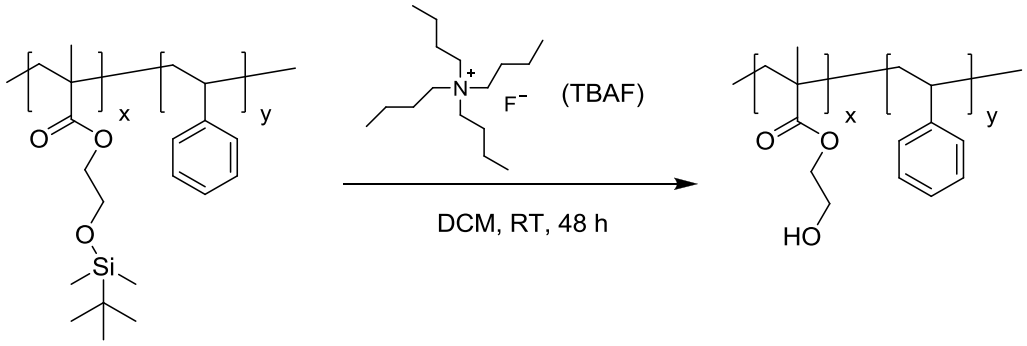

P(HEMA-TBS)-b-PS **PHEMA-b-PS**

Figure 5.7. Deprotection route for P(HEMA-TBS)-b-PS.

As shown in **Figure 5.7**, P(HEMA-TBS)-b-PS (1.2 g) was dissolved in dichloromethane and tetra-n-butylammonium fluoride (TBAF, 5 mL) was added.[6] This mixture was stirred at room temperature for 2 days. The resulting solution was thoroughly washed with DI water 3 times and concentrated by rotary evaporator. The polymer solution was dropped into a 10-fold excess of cold hexane and a colorless solid precipitated. The precipitate was dried under vacuum overnight to yield 0.7 g of a colorless solid. ^{1}H NMR analysis (see **Figure 5.6b**) was performed in DMSO-d_6. The disappearance of resonance peaks of the *t*-butyl group and methyl groups attached to Si suggested the complete removal of TBS protective group. FTIR analysis (**Figure 5.8**) also confirmed the formation of PHEMA by showing the broad absorbance peak from 2800 to 3600 cm^{-1}, and the carbonyl peak is broadened as expected. Thus, block copolymer PS-b-PHEMA (5, 500 - 5, 400 g/mol, PDI = 1.31) was synthesized and ready for further self-assembly study.

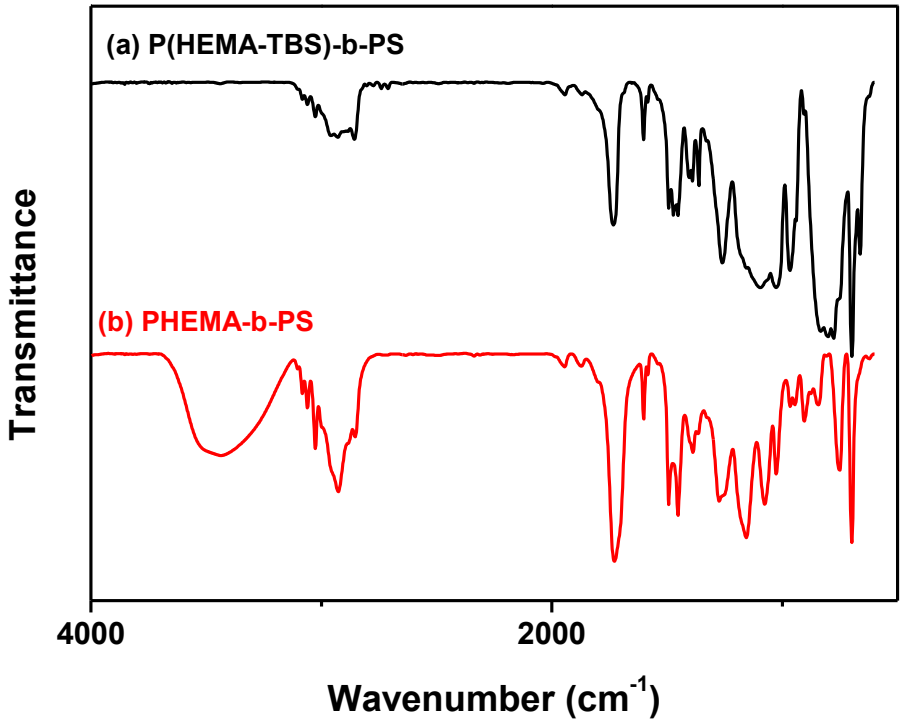

Figure 5.8. FTIR results of P(HEMA-TBS)-b-PS and PHEMA-b-PS.

5.2.3 Neutral Underlayer Selection for PS-b-PHEMA

PHOST-iPOC-MA was studied as the first generation directly photodefinable guiding layer in our group.[7] We have reported the use of PHOST-iPOC-MA as tunable neutral underlayer for PS-b-PAA self-assembly elsewhere.[8] The substrate surface energy was finely tuned by gradient DUV exposure. The block copolymer was deposited on these substrate films. After annealing, SEM imaging was used to screen the optimal condition for neutral underlayer on which perpendicular lamella was formed.

5.2.4 Thermal Annealing of PS-b-PHEMA

After DUV treatment, PS-b-PHEMA was spin-coated from a 0.3 wt % THF solution at 2000 rpm onto the PHOST-iPOC-MA underlayer, resulting in a 40 nm film. The film was heated at 180 ^{o}C for 10 min under N_2 flow. The film was imaged by SEM.

5.2.5 Solvent Annealing of PS-b-PAA

PS-b-PHMA was spin-coated from a 0.5 wt % THF solution at 2000 rpm onto the DUV exposed PHOST-iPOC-MA underlayer, resulting in a 40 to 45 nm block copolymer film. The film was exposed to dry ethyl acetate vapor for 6 hours in a closed jar (0.5 mL ethyl acetate in 250 mL jar). After the solvent vapor annealing, the sample was dried under vacuum.

5.3 Results and Discussion

Block copolymer PS-b-PHEMA (5, 500 - 5, 400 g/mol, PDI = 1.31) was synthesized via ATRP. It was fully characterized by NMR, FTIR and GPC. The photo-definable substrate PHOST-iPOC-MA treated with certain DUV dose window could provide equal surface energy to PS and PHEMA and used as neutral underlay for the solvent and thermal annealing. Both of solvent annealing and thermal annealing of PS-b-PHEMA thin films were explored. In contrast to the results obtained from PS-b-PAA annealing, both of the solvent annealing and thermal annealing of PS-b-PHEMA gave similar results.

5.3.1 Solvent Annealing Behavior of PS-b-PHEMA

Ethyl acetate was used as solvent for PS-b-PHMEA solvent annealing. Long range ordered lamellar morphology was obtained, see **Figure 5.9**. The pitch size of PS-b-PHEMA after solvent annealing was calculated by 2D FFT as 19 nm.

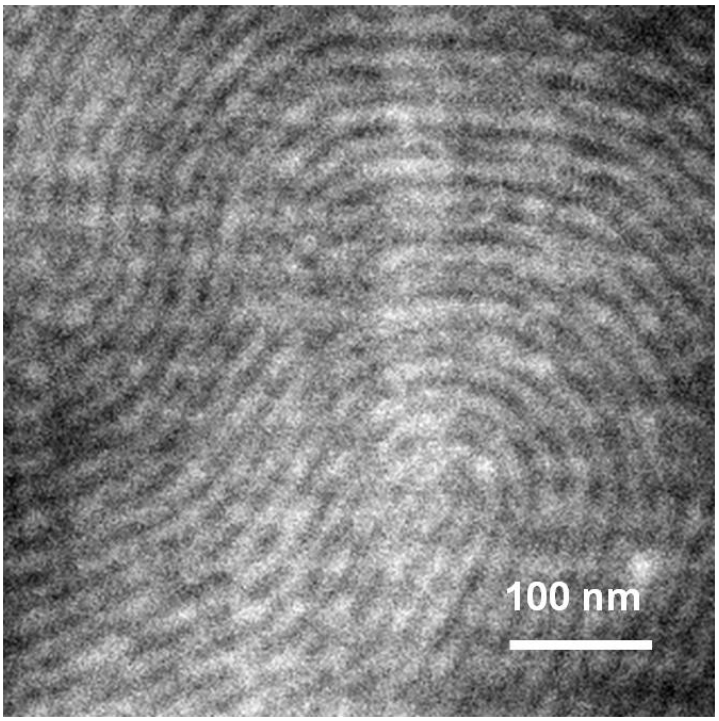

Figure 5.9. Lamella morphology of PS-b-PHEMA after solvent annealing.

5.3.2 Thermal Annealing Behavior of PS-b-PHEMA

The thermal property of PS-b-PHEMA was evaluated by using MDSC, see **Figure 5.10**. PS-b-PHEMA was stable during the heating period, which was from 50 to 300 ℃. The high thermal stability is suitable for a fast thermal annealing process.

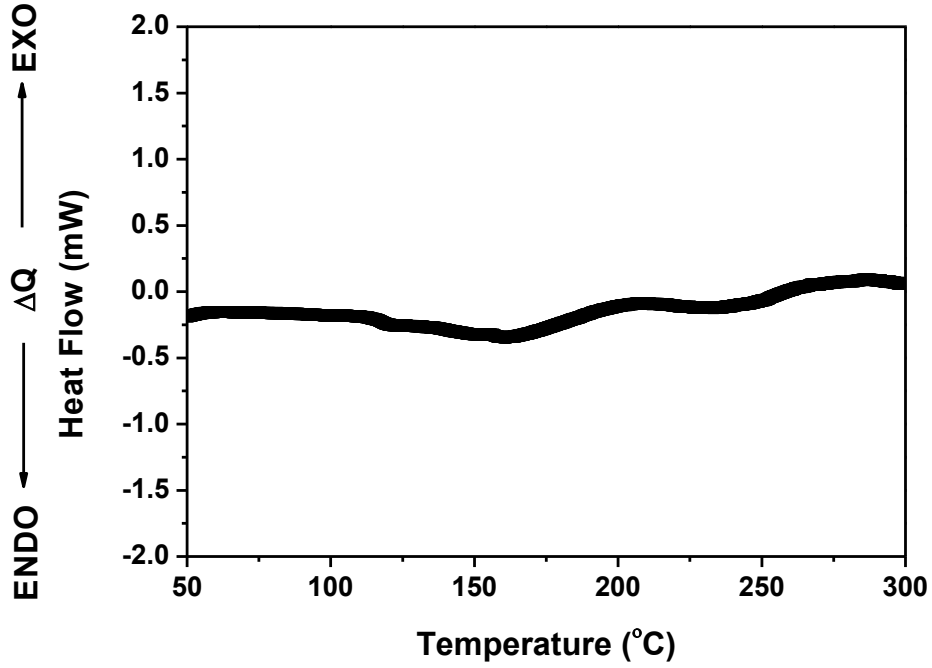

Figure 5.10. Modulated DSC of PS-b-PHEMA.

With only a fast thermal annealing (180 °C for 10 min under N_2 flow) the block copolymer film was able to self-assemble into long range ordered lamella structure with pitch size as low as 15 nm (L_0 = 15 nm, as shown in **Figure 5.11**, the inset is the 2D FFT analysis). In contrast to the thermal annealing result from PS-b-PAA (30 nm pitch by using solvent annealing, 43 nm pitch by using thermal annealing), the pitch size of PS-b-PHEMA obtained from both annealing methods are consistent. The solvent annealing pitch size is a bit larger, which might be due to the solvent swelling of the polymer.

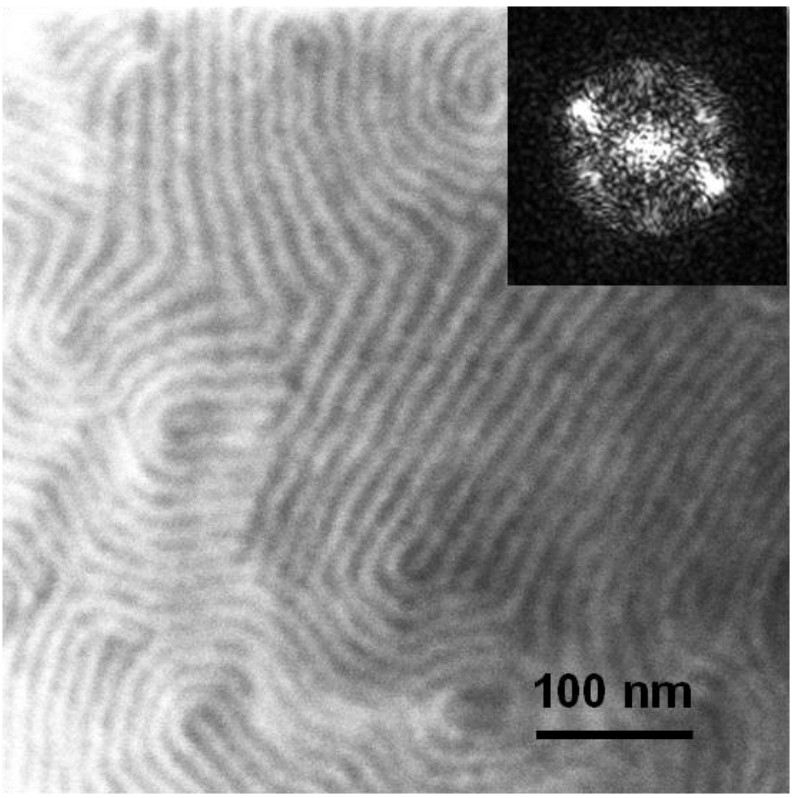

Figure 5.11. Lamellar morphology of PS-b-PHEMA after thermal annealing, the inset 2D FFT was used for pitch size calculation.

When comparing our PS_{5500}-b-$PHEMA_{5400}$ ($L_{0,1}$ = 15 nm, N_1 = 95) with a reported PS_{37000}-b-$PMMA_{37000}$[9] ($L_{0,2}$ = 40 nm, N_2 = 725, $\chi_2 = \chi_{PS\text{-}b\text{-}PMMA}$ = 0.038), we may use **Equation 5.2** to roughly estimate χ value for PS-b-PHEMA (assume a_{PHEMA}, a_{PS}, and a_{PMMA} are similar). we get:

$$\frac{15}{40} = \frac{L_{0,1}}{L_{0,2}} = \frac{\chi_1^{1/6} N_1^{2/3}}{\chi_2^{1/6} N_2^{2/3}} = \frac{\chi_1^{1/6} 95^{2/3}}{0.038^{1/6} \times 725^{2/3}}$$

$$\chi_{PS\text{-}b\text{-}PHEMA} = \chi_1 = 0.37$$

The rough estimation gave a χ value of PS-b-PHEMA about 10 times of PS-b-PMMA. A 15 nm lamellar structure was obtained. This polymer is also expected to have similar etch contrast to PS-b-PMMA and PS-b-PAA by using Ohnishi parameter calculation.[10] Future work would focus on the study of etch transfer on the 15 nm pitch scale by using PS-b-PHEMA.

5.4 Conclusion

PS-b-PHEMA is a suitable block polymer for the industry-friendly thermal annealing process. Similar to PS-b-PAA, PS-b-PHEMA is a hydrogen-bond containing block copolymer. The hydrogen-bond induced network within PHEMA block would strengthen the self association of PHEMA chains, thus helping to increase the χ value. PS-b-PHEMA with controlled Mw and PDI (5, 500 - 5, 400 g/mol, PDI = 1.31) was synthesized by ATRP and fully characterized. This block copolymer forms 15 nm pitch size lamella by using thermal annealing. A rough estimation for the χ of PS-b-PHEMA was 0.37, which is about 10 times of PS-b-PMMA.

5.5 References

1. Russell, T. P.; Hjelm, R. P.; Seeger, P. A. *Macromolecules* **1990,** 23, (3), 890-893.

2. Bates, F. S.; Fredrickson, G. H. *PHYSICS TODAY* **1999,** 52, (2), 32.

3. McNeill, I. C.; Sadeghiet, S. M. T. *Polymer Degradation and Stability* **1990,** 29, 233-246.

4. Caykara, T.; Ozyurek, C.; Kantoglu, O.; Erdogan, B. *Polymer Degradation and Stability* **2003,** 80, 339-343.

5. Beers, K. L.; Boo, S.; Gaynor, S. G.; Matyjaszewski, K. *Macromolecules* **1999,** 32, 5772-5776

6. Green, T. W.; Wuts, P. G. M. *Wiley-Interscience, New York,* **1999**, 127-141, 708-711.

7. Cheng, J.; Lawson, R. A.; Yeh, W.-M.; Tolbert, L. M.; Henderson, C. L. *Proc. of SPIE* **2011,** 7972, 79722I.

8. Cheng, J.; Lawson, R. A.; Yeh, W.-M.; Jarnagin, N. D.; Peters, A.; Tolbert, L. M.; Henderson, C. L. *Proc. of SPIE* **2012,** 8323, 83232R.

9. Liu, C.-C.; Han, E.; Onses, M. S.; Thode, C. J.; Ji, S.; Gopalan, P.; Nealey, P. F. *Macromolecules* **2011,** 44, 1876-1885.

10. Gokan, H.; Esho, S.; Ohnishi, Y. *Journal of the Electrochemical Society* **1983,** 130, 143-146.

CHAPTER 6

LATERAL PACKING SYSTEM: PS-UREA-UREA-PS

6.1 Introduction

Self-complementary hydrogen-bonding urea groups have been incorporated into polymer chains to form strong and directional interactions, which could strongly affect the mechanical properties and the morphology of the polymer. Versteegen *et al.* produced pTHF (PTMO) -U_2 with exactly two urea groups at the center of the polymer chain which form long and uniform hard blocks.[1] These urea groups packed laterally, so the polymer material possessed interesting elastomeric properties. Kim *et al.* synthesized amphiphilic block copolymer poly(ethylene glycol)-poly(l-lactide)(PEG – PLA) which incorporates urea – benzamide or thiourea – benzamide motifs at the interface of the two blocks.[2] Both of the motifs are capable of strong anisotropic hydrogen-bonding interactions which transforms the morphology of diblock copolymers from spherical to nanotubular morphologies. Vora *et al.* blends PS-$(Urea)_4$-PS with symmetric PS-b-PMMA.[3] The urea groups are stable under lithographic conditions and the polymer doesn't show macroseparation at high molecular weights like the homopolymer PS does. Srivinas *et al.* conducted coarse-grain molecular dynamics simulations on model poly(ethyleneoxide)-poly(ethylethylene) (PEO-PEE) lamellae.[4] Their simulation results show that both increasing χ and adding strong specific interactions at the block interface can help smooth lines of patterns, while the former shows more dramatic change. Another significance of the urea block is its ease for synthesis and the convenience of controlling the number of urea groups introduced into a polymer chain. Thus, the urea "connection node" could be a

very promising candidate for improving LER of directed-assembled block copolymers in a lithographic process.

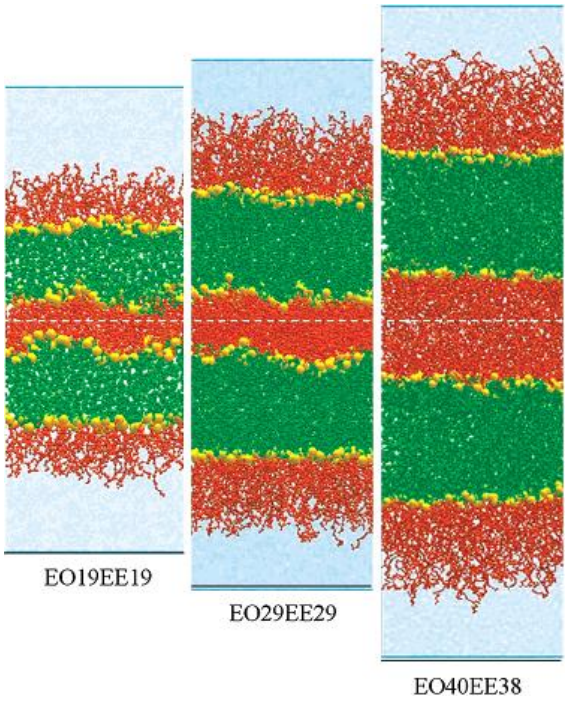

Figure 6.1. CG simulations: Configurations of $EO_{19}EE_{19}$, $EO_{29}EE_{29}$, and $EO_{40}EE_{38}$ double bilayer systems. Red and green particles represent EO and EE units, respectively, while the interface units are shown as large yellow spheres. The water is drawn in translucent blue for clarity. The dashed line represents the midpoint of the corresponding central bilayer. The scale bars (thick black lines) each correspond to 12 nm.[4]

As mentioned above, LER and LWR are key features for lithographic performance. A significant concern of LER has also been placed on block copolymer lithography. Block copolymers have shown self-healing capabilities for correcting small defects in surface patterns of chemically patterned substrates.[5, 6] However, the inherent

quality of the block copolymers, as well as the process that transfers that pattern onto the substrate, has its own physical and chemical limitations, which might coarsen the resulting structure. **Figure 6.1** shows a coarse-grain simulation on configurations of poly(ethyleneoxide)-poly(ethylethylene) (PEO-PEE). This offers a theoretical insight into the interface of domains, which is coarse due to the poor registration between the two blocks.[4] Therefore, further design on modification of block copolymer structure is needed to fix this problem.

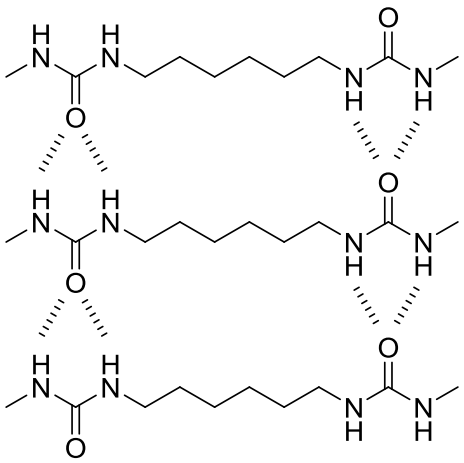

Figure 6.2. Lateral packing effect of Bis- Urea group.

In a symmetric PS-b-PMMA block copolymer, if a "urea connection node" is placed at the interface within the two blocks of polymer, which offers non-covalently lateral packing effect, the interface between the self-assembled two lamellar domains is expected to be smoother, see **Figure 6.2**. As a result of the laterally packing effect, interfacial penetration of blocks might be "blocked".[3] So, self-assembly of symmetric PS-b-PMMA will be better stabilized and registered, see **Figure 6.3**.

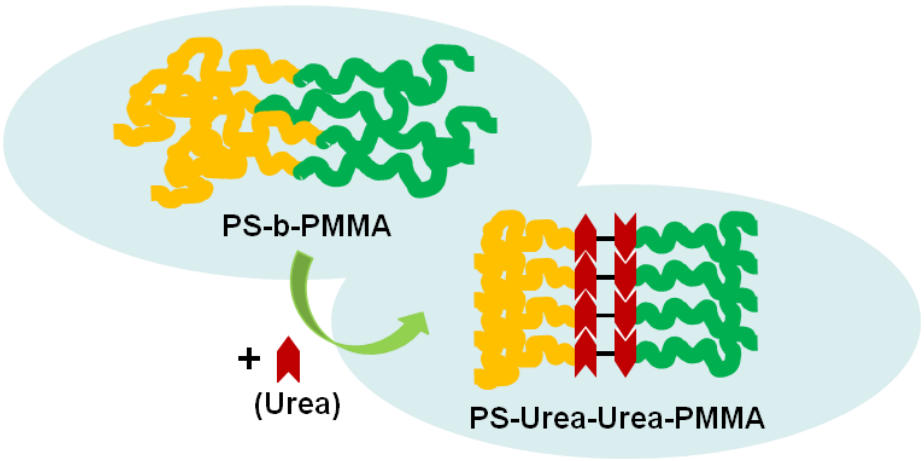

Figure 6.3. Comparison between PS-b-PMMA and PS-Urea-Urea-PMMA.

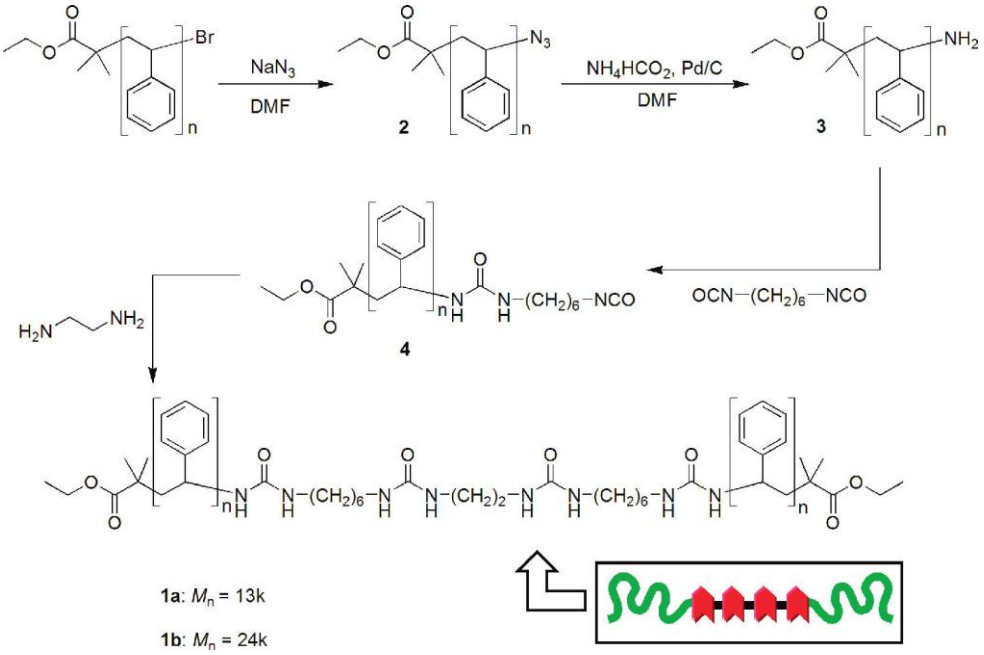

Figure 6.4. Synthesis route of PS-(Urea)$_4$-PS through a convergent method by Vora *et al.*[3]

First, we are interested in exploring a robust synthetic method for the center urea blocks functionalized polymer. PS-Urea-Urea-PS was used as a model target. Vora *et al.* synthesized PS-$(Urea)_4$-PS through a convergent method, see **Figure 6.4**.[3] However, this method was problematic as indicated by the GPC of the product PS-$(Urea)_4$-PS, see **Figure 6.5**. The final product was not clean, which means that the precursor PS-Urea-NCO did not couple completely. There was still a shoulder peak of PS-Urea-NCO in this GPC curve. Assuming that the stoichiometry and chemicals loading were correct, there are a couple of possible reasons that the final product PS-$(Urea)_4$-PS was not monodisperse: (a) the coupling reaction was too slow, so that the conversion within given amount of time was low; (b) the isocyanate end group (NCO) of the precursor PS-Urea-NCO, which is reactive towards a series of nucleophiles such as alcohol, amine and water, was very unstable. Finally, part of the NCO functional group might decompose before the coupling reaction.

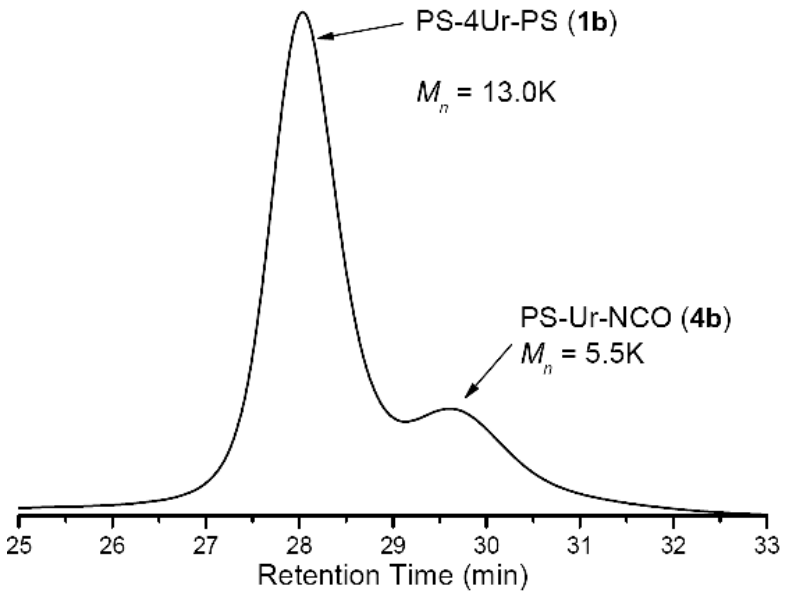

Figure 6.5. GPC trace for tetra-urea polymer PS-$(Urea)_4$-PS, cited from Vora *et al.*'s paper. [3]

Therefore, we were looking for a more robust method to make center urea-decorated polymers with controlled Mw and PDI. We proposed two synthetic routes. The first route was very similar to what was used in Vora *et al.*'s paper,[3] in which the urea functional block was formed through isocyanate and amine coupling, see **Figure 6.6**. In this route, PS-Cl (Mn = 7400 g/mol, PDI =1.14) was synthesized from ATRP with controlled Mw and PDI. Then it was converted to PS-N_3 and reduced to PS-NH_2. Two PS-NH_2 chains were coupled by a diisocyanate linker, such as hexamethylene diisocyanate. This reaction was monitored by GPC to study the reaction rate. However, the first synthesis route, which was very similar to the one that Vora *et al.*paper described, was very unsuccessful. The reaction only produced ~ 40% conversion after 30 days, which will be shown later.

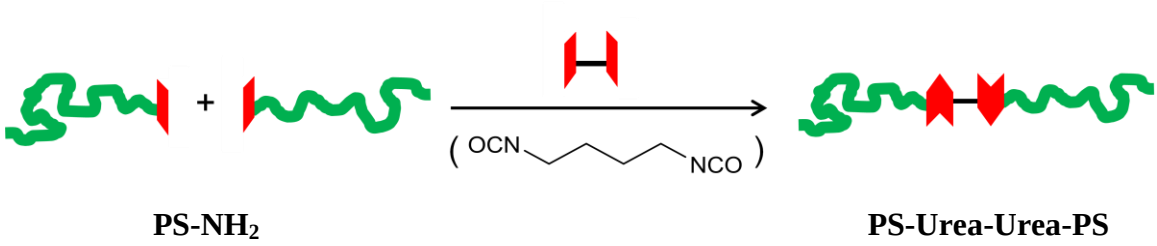

Figure 6.6. Synthesis of PS-Urea-Urea-PS through isocyanate and amine coupling.

Therefore, a second synthetic method was introduced using "click" chemistry, see **Figure 6.7**.[7, 8] "Click" chemistry has shown high efficiency on polymer chain coupling to make di-block copolymers. In this route, two PS-N_3 (Mn = 7400 g/mol, PDI =1.14) chains were coupled by a dialkyne functionalized bis-Urea linker. The synthesis was very successful, showing ~ 60% conversion after 24 h. Those two synthetic methods shown above will be compared in this chapter. "Click" chemistry will be used as an efficient method to synthesize monodisperse PS-Urea-Urea-PMMA.

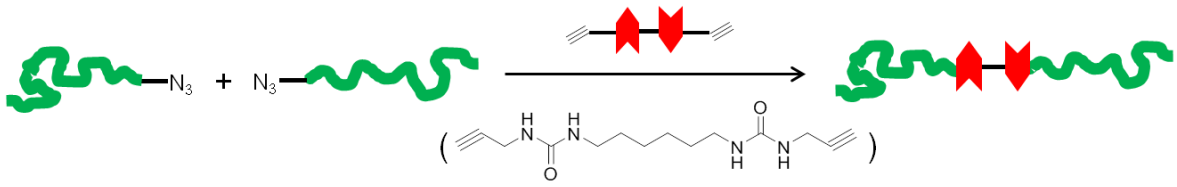

PS-N_3 **PS-Urea-Urea-PS**

Figure 6.7. Synthesis of PS-Urea-Urea-PS through "click" chemistry.

6.2 Experimental

6.2.1 Materials and Instruments

Materials

Unless otherwise noted, all reagents and solvents were purchased from Sigma-Aldrich, TCI America, or Alfa-Aesar and used as received. Styrene was dried over CaH_2 and passed through a neutral alumina column to remove inhibitor. CuCl was made by reduction of $CuCl_2$ by Na_2SO_3 in HCl solution, precipitated with and washed by diethyl ether and absolute ethanol, and dried in vacuum oven at 50 ^oC overnight. ATRP catalysts 4,4'-di(5- nonyl)-2,2'-bipyridine (dNbpy), initiator (1-chloroethyl)benzene (PECl) were used as received.

Measurements

A Varian Mercury Vx 300 was used to collect NMR. Molecular weight and PDI of the polymers were estimated by gel permeation chromatography (GPC), using a

Waters 1515 isocratic pump coupled to a Waters 2489 UV detector with THF as the elution solvent. All GPC measurements were carried out at a flow rate of 0.3 mL/min at 35 ^{o}C, and calibrated using narrow molecular weight polystyrene standards. Fourier transform infrared (FTIR) spectroscopy was performed using a Bruker Vertex 80v with a Hyperion microscope attachment on KBr pellet.

6.2.2 Modification of PS Chain End

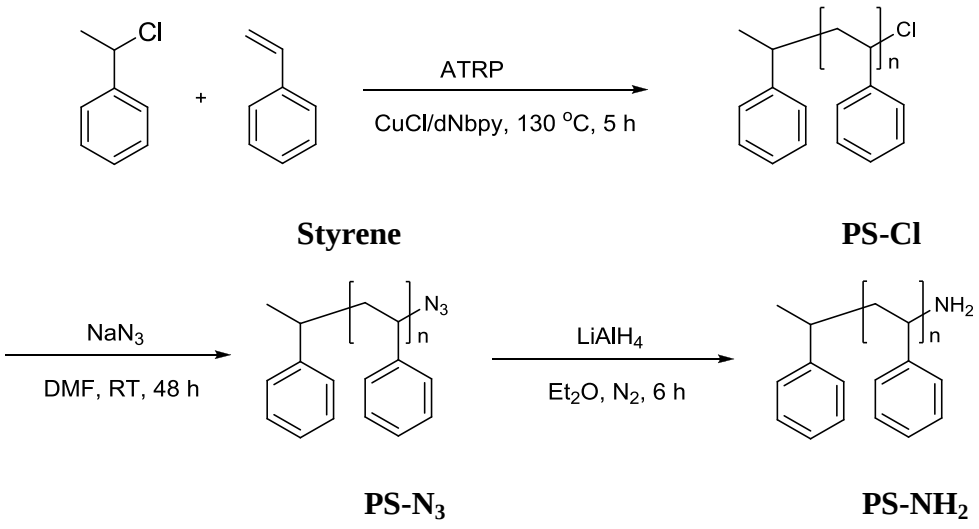

Figure 6.8. Synthesis of PS-NH_2 by PS chain end modification.

The PS chain end was functionalized with chloride functional group after ATRP of the styrene monomer. Then it was replaced by azide group and reduced to amine. The PS-NH_2 with different molecular weights were synthesized, which included ~ 16k, 7.4k and 3.5k. They were used as precursors for PS-Urea-Urea-PS synthesis.

6.2.2.1 Synthesis of PS-Cl

In a 50 mL Schlenk flask, styrene (15 mL, 130.9 mmol), CuCl (181 mg, 1.9 mmol), dNbpy (161 mg, 3.90 mmol), PECl (0.248 mL, 1.9 mmol) were added. After three cycles of freeze-pump-thaw to remove oxygen, the Schlenk flask was back-filled with dry N_2. The solution was sonicated to completely dissolve the catalyst, which turned brown after sonication. The flask was placed in an oil bath and heated at 130 ℃. After 5 hours, the solution was highly viscous. The reaction was quenched by placing the flask in an ice bath and exposing the solution to the air. The solution was diluted with dichloromethane and filtered through a neutral alumina column to remove the catalyst. The polymer solution was rotary evaporated and precipitated into a 10-fold excess of MeOH. After drying under vacuum overnight, 10.6 g of colorless solid was obtained. GPC analysis showed that Mn = 7,400 g/mol, PDI = 1.14 **(Figure 6.9)**. ^{1}H NMR (in $CDCl_3$) showed that the methine proton geminal to the chloride group had a chemical shift at 4.40 ppm, see **Figure 6.11a**.

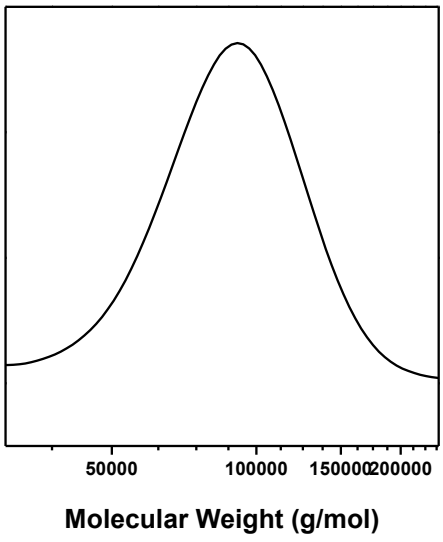

Figure 6.9. GPC curve of PS-Cl (Mn = 7,400 g/mol, PDI = 1.14).

6.2.2.2 Synthesis of PS-N_3

In a 250 mL round bottom flask, PS-Cl (Mn = 7,400 g/mol, 2g, 0.27 mmol), NaN_3 (928 mg, 13.5 mmol), 40 mL dry DMF were added. The reaction mixture was stirred at room temperature for 48 h. 40 mL DCM was added and the solution was washed with DI water 3X to remove the sodium salt and DMF. The organic layer was rotary evaporated and precipitated with a 10-fold excess of MeOH. After drying under vacuum overnight, 1.8 g colorless solid was obtained. ^{1}H NMR (in $CDCl_3$) showed that the methine proton that was geminal to the azide group had a chemical shift at 3.95 ppm, see **Figure 6.11b**. FTIR result suggested that the azide group had a strong absorption peak at 2096 cm-1, see **Figure 6.10**.

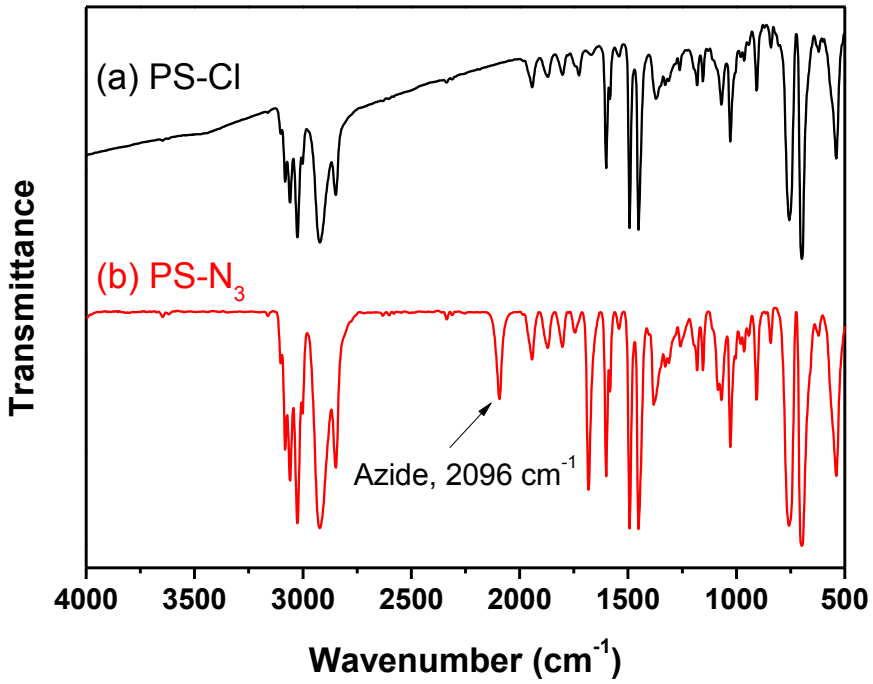

Figure 6.10. FTIR of (a) PS-Cl and (b) PS-N_3.

6.2.2.3 Synthesis of PS-NH_2

In a 250 mL round bottom flask, PS-N_3 (Mn = 7,400 g/mol, 1.5 g, 0.20 mmol), $LiAlH_4$ (385 mg, 10 mmol), 40 mL dry diethyl ether were added. The reaction mixture was stirred at 40 ℃ under N_2 for 6 h. 21 mL 1% NaOH aqueous solution was added to quench the reaction. The reaction mixture was filtered. The filtrate was concentrated and precipitated into a 10-fold excess of MeOH. After drying under vacuum overnight, 1.2 g of a colorless solid was obtained. ^{1}H NMR (in $CDCl_3$) showed that the methine proton geminal to the azide group at 3.95 ppm completely disappeared, see **Figure 6.11c**, in good agreement with the literature, see **Figure 6.12**.[9]

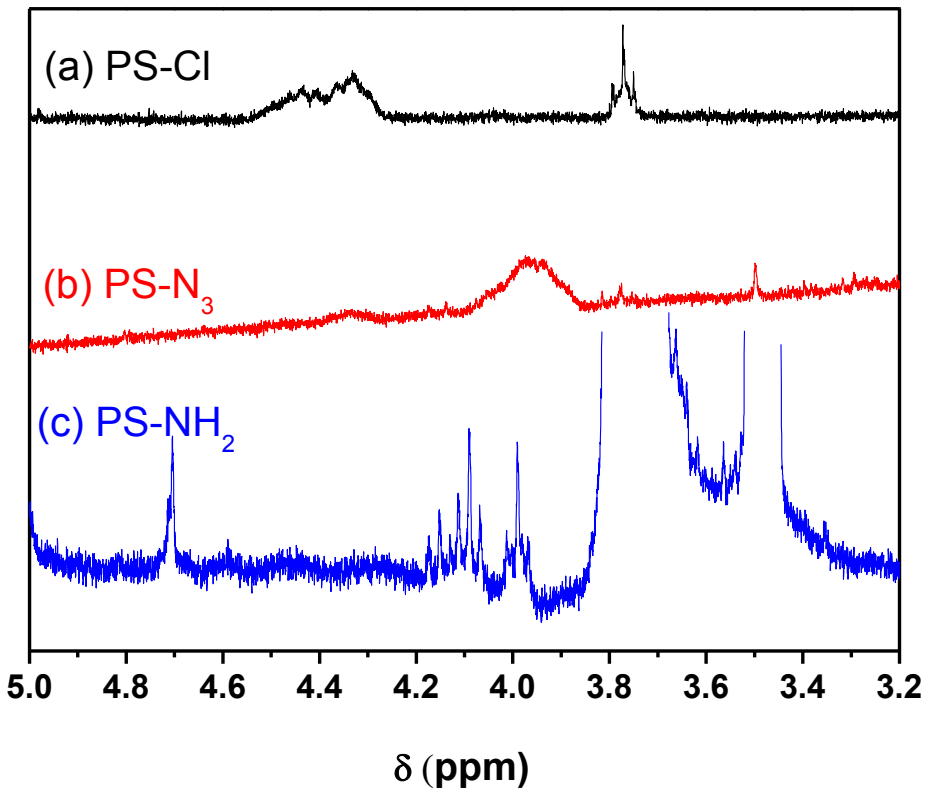

Figure 6.11. 1H ^{1}H NMR of the methine proton that is geminal to the end group of PS-Cl, PS-N_3 and PS-NH_2.

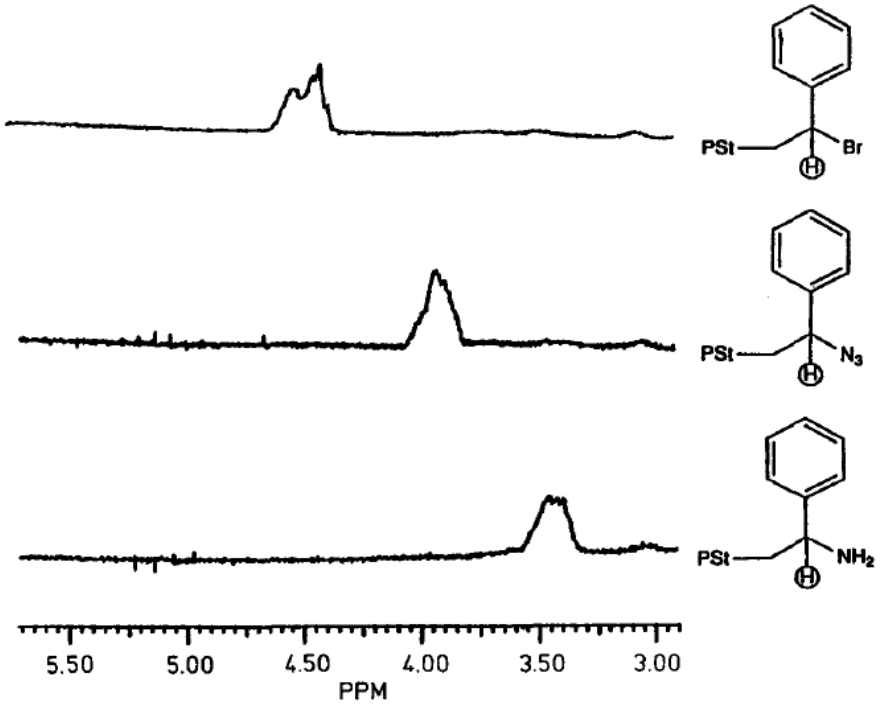

Figure 6.12. ^{1}H NMR spectra of geminal protons of polystyrene with bromo, azido and amino end groups.[9]

6.2.3 Synthesis of PS-Urea-Urea-PS through Isocyanate and Amine Coupling

In a 25 mL round bottom flask, PS-NH_2 (Mn = 7,400 g/mol, 145 mg, 2 eqiv.), hexamethylene diisocyanate (HDI, 1.6 mg, 1 eqiv.), 5 mL dry THF were added. The reaction mixture was stirred at room temperature. ~ 100 μl aliquots of the reaction solution were taken out for GPC analysis after 7, 20 and 30 days.

6.2.4 Synthesis of CH-Urea-Urea-CH Linker

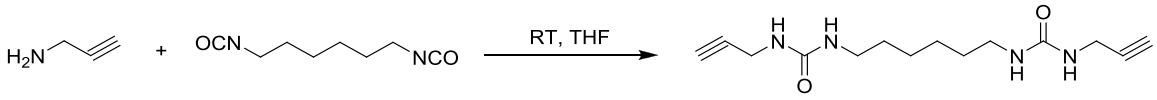

CH-Urea-Urea-CH

Figure 6.13. Synthesis of CH-Urea-Urea-CH linker

To a solution mixture of propargyl amine (172 mg, 2.5 eqiv.) and 50 mL dry THF in a 100 mL round bottom flask, hexamethylene diisocyanate (210 mg, 1 eqiv.) in a 10 mL dry THF solution was slowly added. A colorless solid was immediately precipitated. The solid was collected by filtering the reaction mixture, washed by THF and dried under vacuum.

6.2.5 Synthesis of PS-Urea-Urea-PS through Click Chemistry

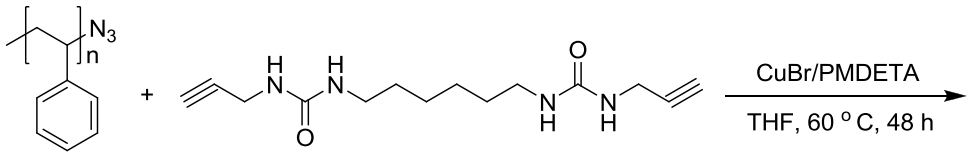

PS-N_3 **CH-Urea-Urea-CH**

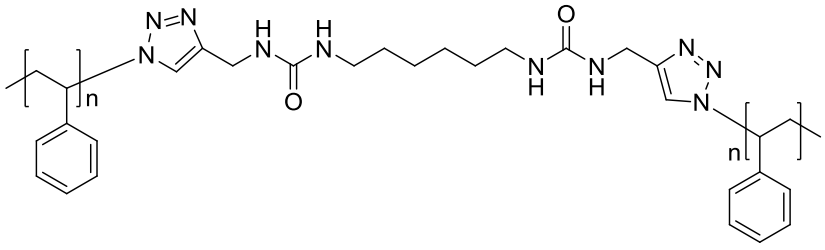

PS-Urea-Urea-PS

Figure 6.14. Synthesis of PS-Urea-Urea-PS through click chemistry.

In a 25 mL Schlenk flask, PS-N_3 (4,500 g/mol, PDI =1.18, 1.0 g, 0.2 mmol), CH-Urea-Urea-CH (31 mg, 0.1 mmol), dry THF (10 mL) were added and allowed to stir until the PS was completely dissolved. CuBr (96 mg, 0.6 mmol), PMDETA (0.139 mL, 0.6 mmol) were added. The solution turned light green after the catalyst complex was formed, and the CH-Urea-Urea-CH slowly dissolved in the THF solution. After three cycles of freeze-pump-thaw to remove oxygen, the Schlenk flask was back-filled with dry N_2. The flask was placed in an oil bath, heated at 60 ℃. After 48 hours, the solution was highly viscous. The reaction was quenched by placing the flask in an ice bath and exposing the solution to the air. The solution was diluted by dichloromethane and filtered through a neutral alumina column to remove the catalyst. The polymer solution was rotary evaporated and precipitated into a 10-fold excess of MeOH/H_2O (1:1). After drying under vacuum overnight, 0.8 g colorless solid was obtained. GPC analysis of the product shows that Mn = 74, 00 g/mol, PDI = 1.24, see **Figure 6.19**.

6.3 Results and Discussion

The center hydrogen bonding facilitated urea linker might bring a smoother interface for the block copolymer phase separation. A robust and controlled synthesis method is needed to produce monodisperse polymer. In this chapter, two different synthetic approaches of PS-Urea-Urea-PS were introduced and compared.

First, a synthetic method based on amine and isocyanate coupling, as shown in **Figure 6.6**, which is quite similar to the reported method in Vora *et al* paper,[3] was performed and characterized by GPC analysis. After the coupling reaction started, about 100 μl of the reaction solution was taken out for GPC analysis at 7, 20 and 30 days.

Figure 6.15 shows the GPC analysis of these three samples. The experimental GPC curve was fitted into two peaks, one of which was the reactant, another was the coupling product PS-Urea-Urea-PS. By integrating the areas of the GPC fit peaks, the conversion could be calculated. The reaction reached ~ 40% conversion after 30 days.

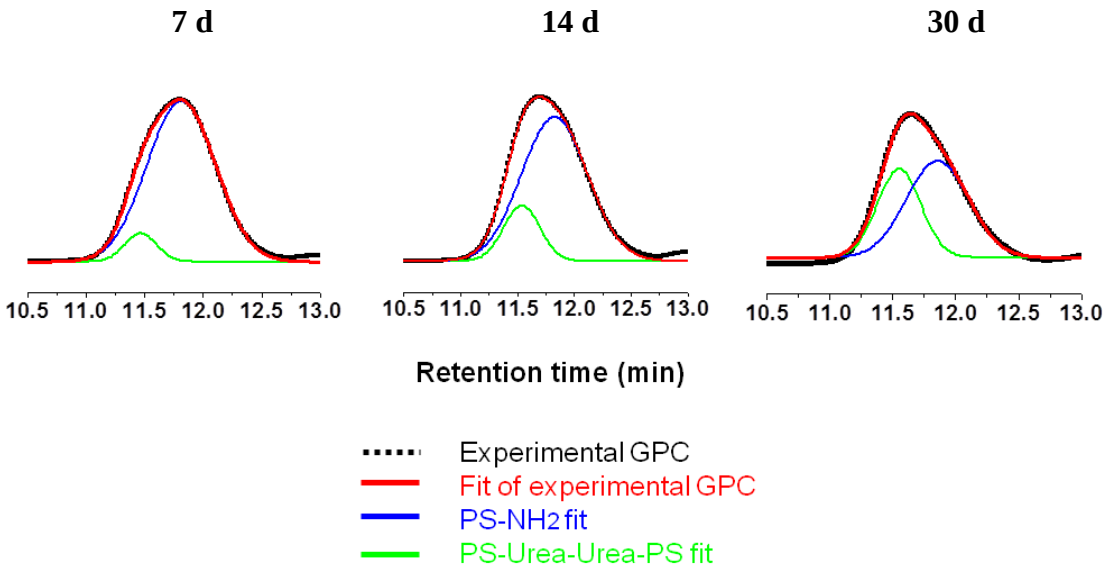

Figure 6.15. GPC analysis of the PS-NH_2 and diisocyanate coupling at 7, 20 and 30 days.

We also have studied different reaction conditions as a combination of solvent and catalyst. Due to the fact that PS_{7000}-NH_2 coupling by HDI was slow (reach conversion ~ 40% after 30 days, in THF), reaction rate optimization was needed. PS_{16000}-NH_2 was chosen for coupling tests. Three sets of reaction conditions were chosen: (1) in DMF, (2) in DMF with 25 eq. TEA (triethylamine), and (3) in THF with 25 eq. TEA. All were performed with same concentration at room temperature. DMF was chosen as a weak base to catalyze and dissolve PS_{16000}-NH_2, while TEA acted as a stronger base catalyst. GPC analysis was again used to calculate the reaction conversion after 2 and 17 days, see **Figure 6.16**. The concentration of PS_{16000}-NH_2 was used to indicate the reaction

conversion. The results under condition (1) and (2) showed minor differences, (3) was faster than (1) and (2).

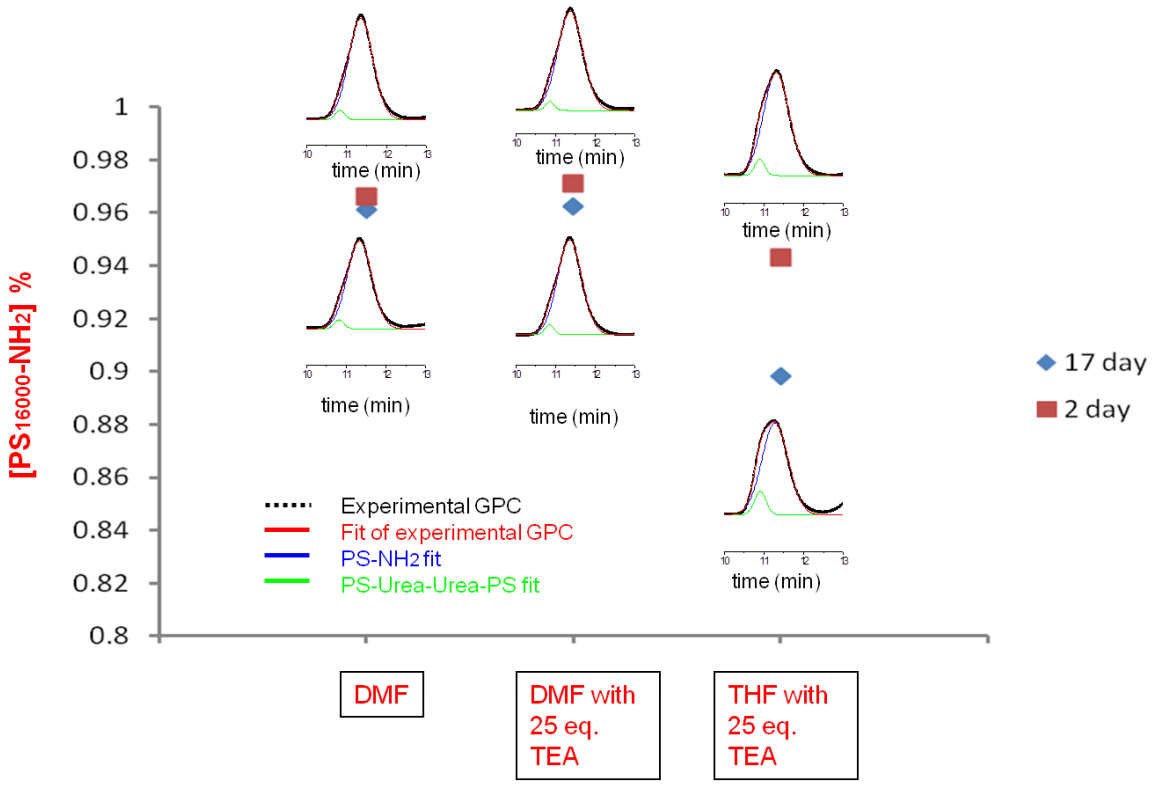

Figure 6.16. GPC analysis of the PS_{16000}-NH_2 and diisocyanate coupling at 2 and 17 days under different reaction conditions: (1) in DMF, (2) in DMF with 25 eq. TEA (triethylamine), and (3) in THF with 25 eq. TEA.

While the addition of the catalyst didn't accelerate the coupling reaction, the solvent showed different effects, which might be due to the fact that THF was a better solvent than DMF for PS (see the solubility parameter chart in **Figure 6.17**, the solubility parameter of THF is closer to PS). However, all of them were significantly slow which might not be favorable for material synthesis. Thus, this synthetic approach based on PS-NH_2 and HDI coupling was difficult and inconvenient to get low PDI block-copolymer as

the reaction was too slow. So, it was unsuitable to synthesize lithographic A-Urea$_n$-B block copolymers, which required excellent monodispersity.

	PS	DMF	THF
Solubility parameter ($J^{1/2}/cm^{3/2}$)	18.5	24.7	19.5

Figure 6.17. Solubility parameters of PS, DMF and THF.

Based on the concern mentioned above, a convenient synthetic approach based on "click" chemistry for A-Urea$_n$-B block copolymer was proposed, as shown in **Figure 6.7**, which might also show better qualification for lithographic requirement. Again, the PS_{7000}-N_3 was used in the synthesis; it was coupled with a bis-urea functionalized di-alkyne CH-Urea-Urea-CH. Two reaction conditions were used, which are shown in **Figure 6.18**.

	PS-N_3:CuBr:PMDETA	Solvent	Conversion by GPC
A	1:1:1	THF	0.05
B	1:3:3	THF	0.58

Figure 6.18. Reaction conditions and results for "click" chemistry.

For a same 24 h reaction time, when the **Condition A** was used, the loading ratio between PS-N_3:CuBr:PMDETA was 1:1:1, which was the same as conventional "click" chemistry condition. However, the reaction conversion was ~ 5%, which was almost negligible. After realizing the fact that the urea linker CH-Urea-Urea-CH was hardly soluble in organic solvents even THF due to the strong H-bonding association, more CuBr/PMDETA catalyst was loaded and the loading ratio between PS-N_3:CuBr:PMDETA was 1:3:3. The nitrogen containing CH-Urea-Urea-CH coordinated to the CuBr, like PMDETA and more examples shown in **Figure 6.19** formed a complex. Thus, the CH-Urea-Urea-CH became soluble after more catalyst was added, as observed experimentally. In this way, the reaction solution became homogeneous and was allowed to proceed smoothly. The reaction convention was ~ 58%, as shown by GPC analysis in **Figure 6.20**. Thus the "click" chemistry was selected as an efficient way to synthesize center Urea functionalized block copolymer.

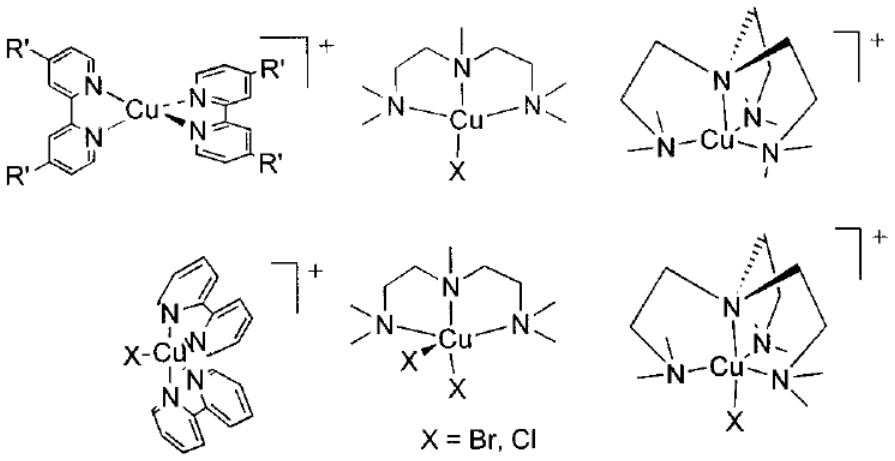

Figure 6.19. Catalyst complex used in ATRP.

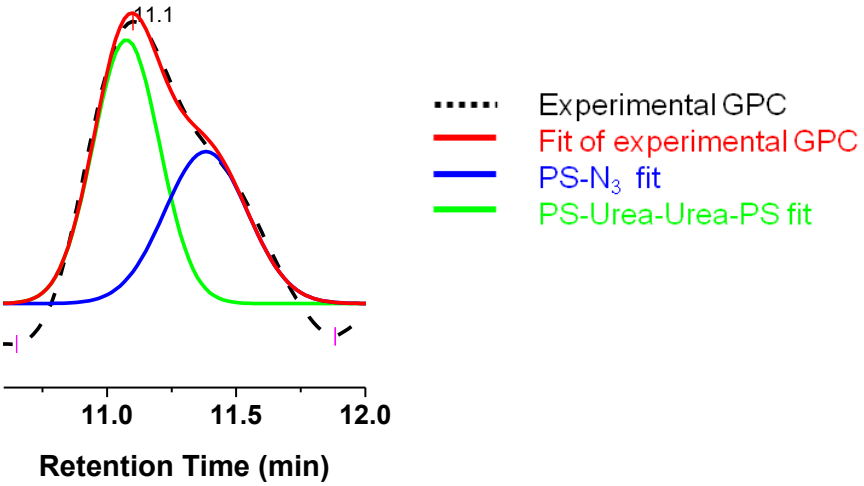

Figure 6.20. GPC analysis of PS-N3 and CH-Urea-Urea-CH coupling by "click" chemistry, loading ratio of PS-N_3:CuBr:PMDETA was 1:3:3.

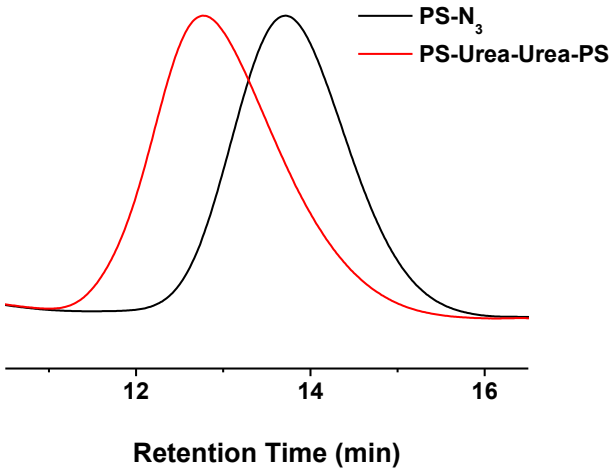

Figure 6.21. GPC analysis of PS-N_3 (4, 500 g/mol, PDI = 1.18) and CH-Urea-Urea-CH coupling by "click" chemistry to synthesize PS-Urea-Urea-PS (7, 400 g/mol, PDI = 1.24).

Figure 6.21. shows GPC analysis of PS-N_3 (4, 500 g/mol, PDI = 1.18) and CH-Urea-Urea-CH coupling by "click" chemistry to synthesize PS-Urea-Urea-PS (7, 400 g/mol, PDI = 1.24). As compared to the result from Vora *et al.*[3] paper in **Figure 6.5**, which showed ineffective coupling of PS with a close Mw of 5.5 k, our result is more promising to synthesize center Urea functionalized block copolymers. A synthetic process for PS-Urea-Urea-PMMA was also proposed, see **Figure 6.22**.

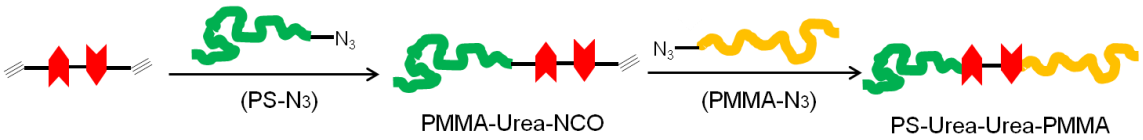

Figure 6.22. Synthetic process for PS-Urea-Urea-PMMA by using "click" chemistry.

6.4 Conclusion

Self-complementary hydrogen-bonding urea groups have shown application in facilitating the self-assembly of polymers. This strong and directional interaction can form "hard blocks" if the ureas are placed at the center of polymers to prevent the penetration of polymer chains. In this chapter, we compared two synthetic methods to make PS-Urea-Urea-PS. PS-NH_2 chains were coupled by a diisocyanate linker, which was similar to a published paper,[3] however, only low reaction conversion was obtained. When two PS-N_3 chains were coupled by a dialkyne functionalized bis-urea linker through "click" chemistry, ~ 60% conversion was obtained after 24 h reaction with the same Mw polymer precursor. "Click" chemistry will be used for synthesis of PS-Urea-Urea-PMMA.

6.5 References

1. Versteegen, R. M.; Kleppinger, R.; Sijbesma, R. P.; Meijer, E. W. *Macromolecules (Washington, DC, United States)* 2006, 39, 772-783.

2. Kim, S. H.; Nederberg, F.; Jakobs, R.; Tan, J. P. K.; Fukushima, K.; Nelson, A.; Meijer, E. W.; Yang, Y. Y.; Hedrick, J. L. *Angew. Chem. Int. Ed.* 2009, 48, 4508 - 4512.

3. Vora, A.; Zhao, B.; To, D.; Cheng, J. Y.; Nelson, A. *Macromolecules (Washington, DC, United States)* 43, (3), 1199-1202.

4. Srinivas, G.; Swope, W. C.; Pitera, J. W. *Journal of Physical Chemistry B* 2007, 111, (49), 13734-13742.

5. Cheng, J. Y.; Rettner, C. T.; Sanders, D. P.; Kim, H. C.; Hinsberg, W. D. *Adv. Mater.* 2008, 20, 3155–3158.

6. Daoulas, K. C.; Muller, M.; Stoykovich, M. P.; Kang, H.; de Pablo; J., J.; Nealey, P. F. *Langmuir* 2008, 24, 1284–1295.

7. Moses, J. E.; Moorhouse, A. D. *Chem. Soc. Rev.* 2007, 36, 1249–1262.

8. Golas, P. L.; Matyjaszewski, K. *Chem. Soc. Rev.* 2010, 39, 1338–1354.

9. Matyjaszewski, K.; Nakagawa, Y.; Gaynor, S. G. *Macromol. Rapid Commun.* 1997, 18, 1057-1064.

10. Matyjaszewski, K.; Xia, J. *Chem. Rev.* 2001, 101, 2921-2990.

11. Gololobov, Y. G. *Tetrahedron* 1981, 37, (437).

12. Zhao, Y.; Sivaniah, E.; Hashimoto, T. *Macromolecules (Washington, DC, United States)* 2008, 41, (24), 9948-9951.

13. Park, S.-M.; Park, O.-H.; Cheng, J. Y.; Rettner, C. T.; Kim, H.-C. *Nanotechnology* 2008, 19, (45), 455304/1-455304/6.

14. *Excerpts from A Conversation with Gordon Moore: Moore's Law. Video Transcripts. Intel Museum.*

15. Miyazaki, T.; Hayashi, K.; Kobayashi, K.; Kuba, Y.; Ohyi, H.; Obara, T.; Mizuta, O.; Murayama, N.; Tanaka, N.; Kawamura, Y.; Uemoto, H. *J. Vac. Sci. Technol. B* 2008, 26, 2611.

16. Cheng, J. Y.; Ross, C. A.; Chan, V. Z.-H.; Thomas, E. L.; Lammertink, R. G. H.; Vancso, G. J. *Adv. Mater.* 2001, 13, 1174.

17. M. Park, C.; Harrison; Chaikin, P. M.; Register, R. A.; Adamson, D. H. *Science* 1997, 276, 1401.

18. Bates, F. S.; Fredrickson, G. H. *PHYSICS TODAY* 1999, 52, (2), 32.

19. Leibler, L. *Macromolecules (Washington, DC, United States)* 1980, 13, 1602.

20. Bates, F. S.; Fredrickson, G. H. *Annu. Rev. Phys. Chem.* 1990, 41, 525.

21. Peters, R. D.; Yang, X. M.; Wang, Q.; de Pablo, J. J.; Nealey, P. F. *J. Vac. Sci. Technol. B* 2000, 18, (6), 3530-3534

22. Segalman, R. A.; Yokoyama, H.; Kramer, E. *J., Adv. Mater.* 2001, 13, (15), 1152-1155.

CHAPTER 7

SUMMARY AND RECOMMENDATIONS FOR FUTURE WORK

7.1 Summary

This thesis has provided solutions for new materials design used in lithography. Higher resolution patterning is goal of this thesis. Two lithographic techniques are involved in the discussion: the conventional photolithography and block copolymer lithography by using directed self-assembly (DSA) of block copolymers.

Chapter 2 describes the concept of single molecule resists. The previous work on epoxy-based single molecule resists has been reviewed. Acidic groups are introduced to the resist molecules to make them aqueous base soluble, which is more friendly to the industrial manufacturing. DPA-2Ep, which is based on a carboxylic group, however, shows swelling problem during the base development. TPOE-3Ep, on the other hand, maintains good patterning quality in base development without swelling. Also, a new design based on a different epoxide group – the cyclohexene oxide cross linking group is introduced. The resist BHPF-2CHEp based on this functional group has shown a better contrast than the analogues BHPF-2Ep and BHPF-2Ox. Also, a higher resolution is achieved with 15 nm line width.

Chapter 3 describes a 3-step simplified process for DSA by using a photodefinable substrate. A polymer material, PHOST-iPOC-MA, which is derived from a polyhydroxystyrene which is functionalized with isopropyloxycarbonyl (iPOC) group

and methacrylate (MA) group. The iPOC group serves as an energy switchable group which is deprotected after patterning and the substrate surface turns from hydrophobic to hydrophilic. The MA group is crosslinkable while blended with a thermal initiator AIBN and baked. The first generation photodefinable substrates has successfully directed the self-assembly of PS-b-PMMA into lamella structure. Due to the low crosslinking, the substrate has to be thick enough to provide neutral energy to the block copolymer.

Chapter 4 describes a high χ block copolymer polystyrene-b-polyacid. PS-b-PAA (8, 000 - 8, 000 g/mol, PDI = 1.38) is successfully synthesized via ATRP with controlled Mw and PDI. The PS-b-PAA is acetone vapor annealed to form 30.0 nm pitch size lamella. Initial estimate for the χ of PS-b-PAA is 1.49, which is much greater than PS-b-PMMA. PS-b-PAA undergoes thermal reaction to form anhydride, ketone, and alkane sequentially. The χ value of PS-b-PAA decreases upon thermal annealing. As a result of χ change, the pitch size of the self-assembled PS-b-PAA lamella decreases. The size of the same PS-b-PAA polymer is tunable by varying the annealing time. The thermal behavior of PS-b-PAA is well studied and related to the morphology evolution.

Chapter 5 describes PS-b-PHEMA as a suitable block polymer for the industry-friendly thermal annealing process. Similar to PS-b-PAA, PS-b-PHEMA is a hydrogen-bond containing block copolymer. The hydrogen-bond induced network within PHEMA block would strengthen the self association of PHEMA chains, thus helping to increase the χ value. PS-b-PHEMA with controlled Mw and PDI (5, 500 - 5, 400 g/mol, PDI = 1.31) was synthesized by ATRP and fully characterized. This block copolymer forms 15 nm pitch size lamella by using thermal annealing. A rough estimation for the χ of PS-b-PHEMA was 0.37, which is about 10 times of PS-b-PMMA.

Chapter 6 describes the self-complementary hydrogen-bonding urea groups as a center group to be used in facilitating the self-assembly of polymers. In this chapter, we compared two synthetic methods to make PS-Urea-Urea-PS. PS-NH_2 chains were coupled by a diisocyanate linker, which was similar to a published paper,[1] however, only low reaction conversion was obtained. When two PS-N_3 chains were coupled by a dialkyne functionalized bis-urea linker through "click" chemistry, ~ 60% conversion was obtained after 24 h reaction with the same Mw polymer precursor. "Click" chemistry will be used for synthesis of PS-Urea-Urea-PMMA.

7.2 Recommendations for Future Work

The first generation of iPOC group based photodefinable substrate is very promising for DSA. High film remaining is needed to reduce defects observed in the DSA. The NRT could be increased by using more effective crosslinking groups: epoxide and benzocyclobutene crosslinking groups. Epoxides have shown superior film remaining ability in our previous molecular resist study.[2-4] Benzocyclobutene crosslinks thermally without using initiators or catalysts.[5] Thus, as shown in **Figure 7.1**, three designs are listed.

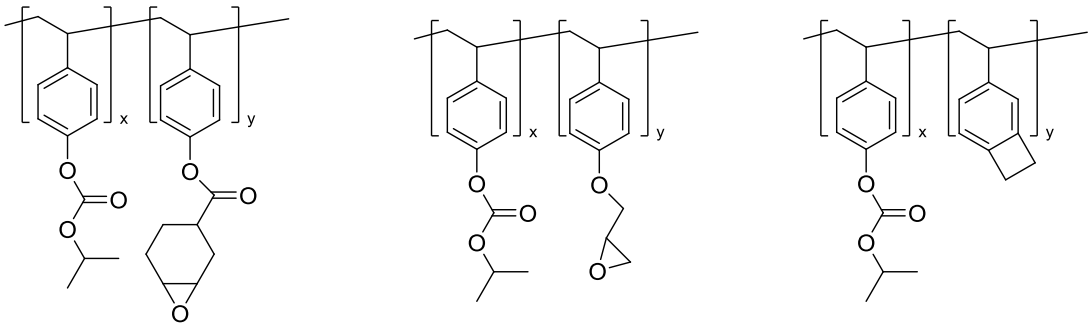

Figure 7.1. New designs for 2nd generation photodefinable substrates.

7.3 References

1. Vora, A.; Zhao, B.; To, D.; Cheng, J. Y.; Nelson, A. *Macromolecules (Washington, DC, United States)* 43, (3), 1199-1202.

2. Lawson, R. A.; Lee, C.-T.; Tolbert, L. M.; Younkin, T. R.; Henderson, C. L. *Microelectronic Engineering* **2009,** 86, 734–737.

3. Lawson, R. A.; Lee, C.-T.; Yueh, W.; Tolbert, L.; Henderson, C. L. *Microelectronic Engineering* **2008,** 85, 959–962.

4. Lawson, R. A.; Noga, D. E.; Younkin, T. R.; Tolbert, L. M.; Henderson, C. L. *J. Vac. Sci. Technol. B* **2009,** 27, 2998.

5. Shin, K.; Drockenmuller, E.; Hawker, C.; Russell, T. *Science* **2005,** 308, (5719), 236-239